UNIVERSITY OF Southampton

University of Southampton Research Repository
ePrints Soton

Copyright © and Moral Rights for this thesis are retained by the author and/or other copyright owners. A copy can be downloaded for personal non-commercial research or study, without prior permission or charge. This thesis cannot be reproduced or quoted extensively from without first obtaining permission in writing from the copyright holder/s. The content must not be changed in any way or sold commercially in any format or medium without the formal permission of the copyright holders.

When referring to this work, full bibliographic details including the author, title, awarding institution and date of the thesis must be given e.g.

AUTHOR (year of submission) "Full thesis title", University of Southampton, name of the University School or Department, PhD Thesis, pagination

http://eprints.soton.ac.uk

UNIVERSITY OF SOUTHAMPTON

A spectroscopic study on some atmospherically relevant reactions with the support of electronic structure calculations

A thesis submitted for the Degree of Master of Philosophy

February 2010

Sonya Beccaceci

SCHOOL OF CHEMISTRY

UNIVERSITY OF SOUTHAMPTON

UNIVERSITY OF SOUTHAMPTON

ABSTRACT

Faculty of Science
School of Chemistry

Master of Philosophy

A spectroscopic study on some atmospherically relevant reactions with the support of electronic structure calculations

by Sonya Beccaceci

The work described in this thesis is a study of the atmospherically relevant reactions of dimethyl sulfide (DMS) with halogen and interhalogen molecules (Cl_2, Br_2, I_2, BrCl and ICl) and ozone with selected alkenes (ethylene, tetramethylethylene and 2-methylpropene). The aim was to investigate the mechanisms of these reactions and identify reaction intermediates.

Infrared matrix isolation spectroscopy and u.v.-photoelectron spectroscopy were used to detect intermediates and products, and *ab initio* calculations were used to facilitate spectral assignments and to provide information on the structure of the molecules studied.

The results confirm and extend previous matrix isolation infrared studies on the DMS/Cl_2 system and also provide vibrational assignment and *ab initio* calculations for the electronic structure of the intermediates present in the related DMS/Br_2, DMS/I_2, DMS/BrCl and DMS/ICl reactions. For all systems, the intermediate is shown to be a van der Waals complex of the type DMS:XY, where XY is a halogen or interhalogen molecule.

The reactions of ozone and alkenes were studied by u.v.-photoelectron spectroscopy. The results follow the general mechanism proposed by Criegee but no Criege intermediate is observed. Reaction mechanisms are presented and discussed for each reaction investigated.

Of great importance is the observation of the first excited state of oxygen (O_2 $a^1\ \Delta_g$) in the reactions of ozone with ethylene and 2-methylpropene which play an important role in the oxidation chemistry of the troposphere.

This thesis is an account of original research performed by the author in the School of Chemistry of the University of Southampton between October 2006 and August 2008. Where findings of other work have been used, due references has been given.

Acknowledgements

I wish to thank Prof. John Dyke and Dr. Steve Ogden for their supervision and guidance during the research time and their assistance in reaching the target.

I thank the people of the PES group that in a way or an other gave contribution to my work: Grant, Otello, Nerina, Fabrizio, Marie, Ed and Alan.

I thank all the friends I met in Southampton for the nice time spent together, my family for always being supportive and Luca for being present and patient during hard time.

I also thank EU Early Stage Research Training Network (SEARCHERS) for financial support without which this work would not have been possible.

Contents

1. Introduction

1.1 Aims of the project

The objectives of this work are to study the reactions between dimethyl sulphide and some halogen and interhalogen molecules in inert gas matrices and the gas-phase, and to investigate the mechanism of the reaction of ozone with some alkenes in the gas-phase using spectroscopic methods.

The first reason for the choice of these reactions was the possibility that they could proceed by formation of reaction intermediates. The study of reaction intermediates has been a long-established field of research in the Southampton PES (PhotoElectron Spectroscopy) group.

In addition to this, the chemistry of dimethyl sulphide, alkenes and ozone has been the subject of increasing investigations, due to their importance in the Earth's atmosphere.

The DMS+halogen studies were carried out by means of ultraviolet photoelectron spectroscopy (PES) and infrared matrix isolation spectroscopy with the support of *ab initio* electronic structure calculations, whereas the ozone+alkene experiments were carried out with u.v.-photoelectron spectroscopy.

This chapter will describe the importance of dimethyl sulphide, ozone and alkenes in atmospheric chemistry. A detailed description of the underlying principles of these spectroscopic techniques and the experimental methods will be given in Chapter 2. Chapter 3 will outline the basic principles of *ab initio* electronic structure calculations and the reasons why their use was of central importance in the outcome of the work.

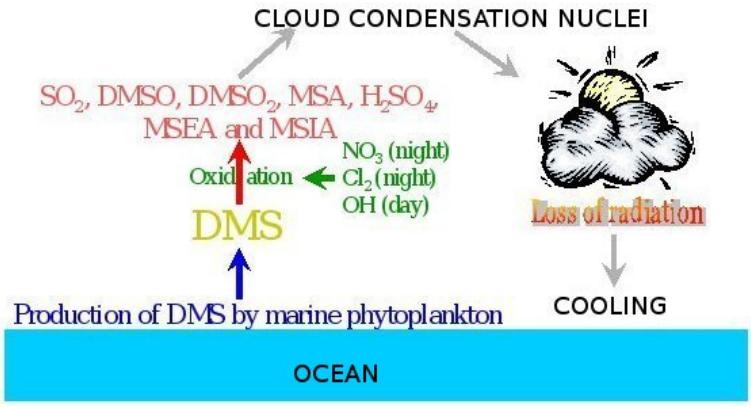

Figure 1.1: *The cyclic CLAW [2] mechanism for the role of DMS in climate control*

1.2 Relevance of work to Atmospheric Chemistry

1.2.1 Dimethyl sulphide

Dimethyl sulphide CH_3SCH_3 (DMS) is an important sulphur-containing species that has natural sources and is considered the main source of sulphur in the Earth's atmosphere [1–3]. It is mainly produced by biodegradation of algae in ocean environments initiated by u.v. radiation from the Sun but it also produced from anthropogenic activities such as paper mills or fishmeal production [4].

Oxidation of DMS leads to aerosol production and cloud formation that play an important role in climate regulation [2]. DMS oxidation products contribute to the formation of cloud condensation nuclei (CCNs) and subsequent reduction of solar radiation reaching the Earth's surface, see Figure 1.1. An increase in DMS production by algae degradation is reflected by a decrease of temperature at the ocean's surface, because more CCNs are produced, and these reduce the UV radiation reaching the ocean surface, which reduces algae degradation; on the other hand, when the amount of DMS, and then CCNs, is reduced, the solar radiation causes an increase of biological activity of the sulphur containing algae and then an increase of DMS production. Such an equilibrium is very delicate and is subject to fluctuations.

The main oxidants of DMS in the atmosphere are thought to be the OH radical during

the day and the NO_3 radical at night [4–7]. However, oxidation of DMS in the troposphere appears to be more rapid than expected; other sink processes have been proposed involving halogen or halogenated radicals such as Br, Cl or BrO [8, 9].

Particular importance must be given to the fact that high amounts of chlorine have been observed in coastal air, either as HCl or Cl_2 produced by sea-salt particles, from algae decomposition or from anthropogenic activities [8, 10]. Also molecular chlorine is produced from heterogeneous reactions of ozone with wet sea-salt which is enhanced by the presence of ferric ions [11]. An investigation of the reactions between DMS and halogens is therefore important.

A study of the DMS+Cl_2 reaction has been made at the University of Southampton using u.v.-photoelectron spectroscopy, indicating that a reaction intermediate is formed in the first step of the reaction, before decomposition occurs to CH_3SCH_2Cl+HCl [12–14]. The derived room temperature rate constant for the DMS + Cl_2 reaction [12] and the estimated night-time levels of DMS and Cl_2 in the Southern Ocean indicate that significant levels of CH_3SCH_2Cl (MDMS) + HCl may build up at night [12]. During the day, CH_3SCH_2Cl will be photolysed to CH_3S and CH_2Cl, and reaction of CH_3S with O_2 and O_3 leads to CH_3SO_2 which will give CH_3 and SO_2 on thermal decomposition. Hence the reaction of DMS and Cl_2 at night leads to enhanced levels of SO_2 during the day, leading to increased acidity of the atmosphere (via H_2SO_4) and cloud formation.

Given the impact that this reaction might have on climate studies, the emphasis of this work was to extend this study to reactions between DMS and other halogen molecules that might be present in the atmosphere (see Figure 1.2).

The direct release of gas-phase molecular bromine into the Earths atmosphere is supported by several laboratory studies [15]. In particular, Hirokawa et al. [16] have demonstrated, in a series of experiments using mass spectrometry as the detection method, that finely divided NaBr salt in the presence of moist ozone is a source of Br_2. Also, in a series of field experiments in North America, it has been shown that acidic aerosol solutions containing HOCl and HOBr, Cl^- and Br^-, can act as sources of Br_2, BrCl and Cl_2 which

are released into the atmosphere [17]. In related work, freezing of acidified sea salt solutions containing halide and nitrite ions has also been identified as atmospheric sources of ICl, IBr and I_2 [18].

Recent data have provided more information about halogen or other chermically mediated air-snow interactions and chemistry [19]. All of these interconnected processes have led to a complex picture of the interplay among gas-phase photochemistry, ice surface chemistry, marine biological processes and reaction on/in aerosols [19]. Figure 1.2 provides a summary of emission of halogens into the atmosphere.

The reactions of DMS and Br_2, I_2, ICl and BrCl were investigated in the gas-phase by u.v.-photolelectron spectroscopy and in inert gas matrices by infrared matrix isolation spectroscopy in order to determine the mechanism of the reactions and if possible to detect and study reaction intermediates.

1.2.2 Alkenes and ozone

Ozone (O_3) plays a significant part in the chemistry of the Earth's atmosphere, even though it is a minor species in terms of abundance [4]. Concentrations are rather variable, but the mixing ratio with respect to the entire atmosphere is a few tenths of a part per million [4]. Atmospheric ozone is mainly concentrated in a layer called the *ozone layer*, about 20 km thick and centred in an altitude range of about 20 - 40 km (see Figure 1.3). Ozone in the stratosphere is mostly produced from ultraviolet rays dissociating molecular oxygen and oxygen atoms then reacting with O_2 to give O_3.

$$O_2 + h\nu \rightarrow O + O \tag{1.1}$$

$$M + O + O_2 \rightarrow O_3 + M \tag{1.2}$$

Several factors contribute to ozone's importance with, perhaps, the outstanding feature being the relationship between the absorption spectrum of ozone and the protection of

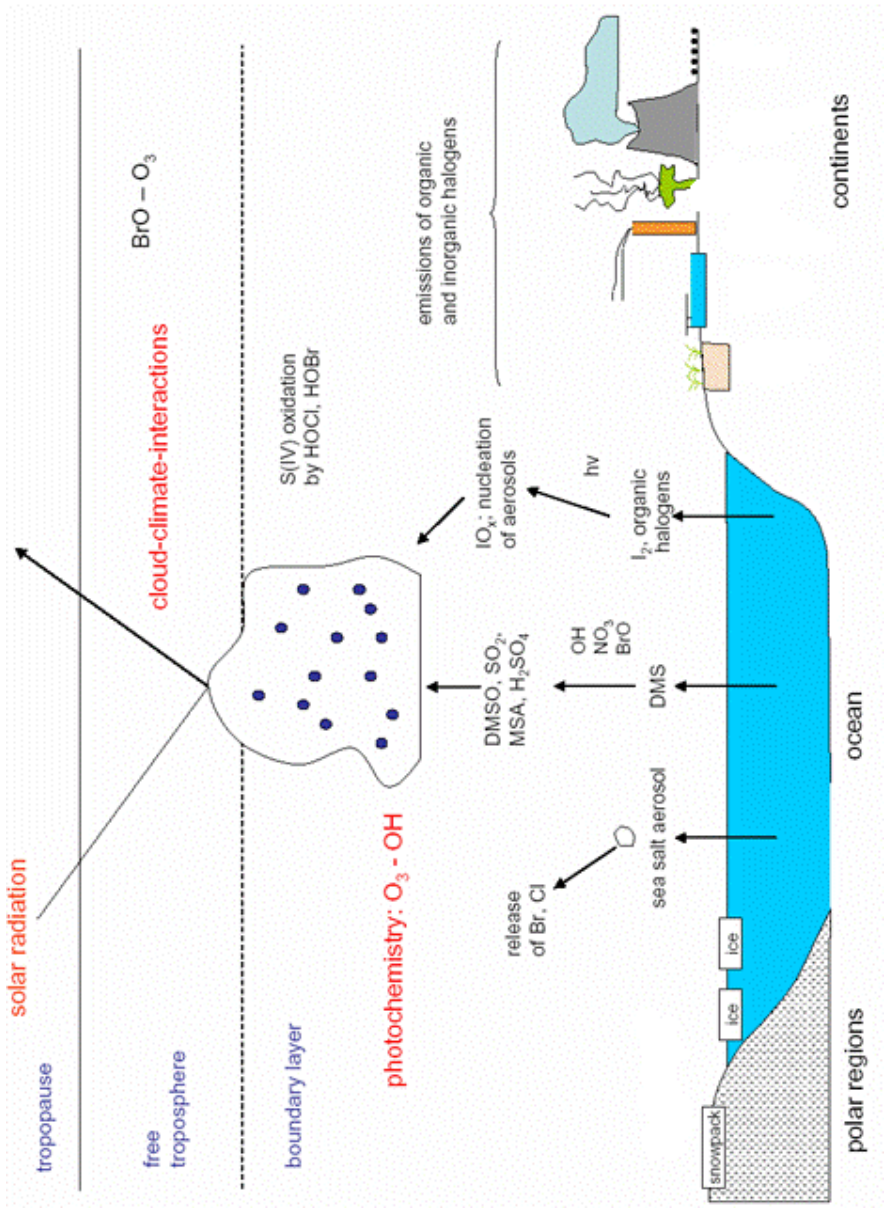

Figure 1.2: *Emission of halogens in the atmosphere: Br_2 and BrCl are emitted from sea salt-laden ice and snowpack in the Artic Ocean region where they can be photolysed yielding Br and Cl atoms [20–23]. Large concentration of I_2 can occur in costal marine boundary layer. A clear correlation of I_2 with tidal state indicates that emissions from exposed macro-algae are responsible [24].*

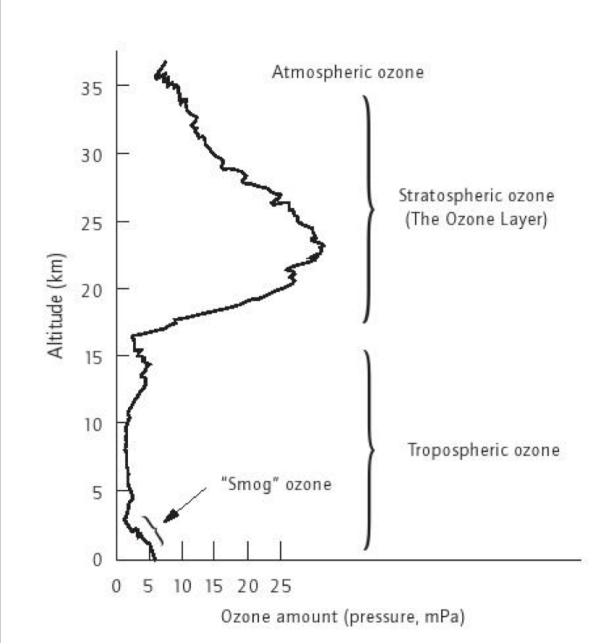

Figure 1.3: *Vertical variation of ozone concentration [25]*

living systems from the full intensity of solar ultraviolet radiation [4].

Low level ozone (or tropospheric ozone) is regarded as a pollutant. It is not emitted directly by car engines or by industrial operations. It is formed by the effect of sunlight on air containing nitrogen oxides (for example NO_2) to produce O atoms that combine with molecular oxygen react to form ozone at the source of the pollution [4].

$$NO_2 \rightarrow NO + O(\lambda \leq 400nm) \tag{1.3}$$

$$O + O_2 + M \rightarrow O_3 + M \tag{1.4}$$

Reactions of volatile organic compounds (VOCs) with (NO_x) also cause the formation of ozone and other oxidants, commonly referred to as "smog" or "ground-level ozone" [26]. Formation of ground - level ozone is not the only harmful consequence of the atmospheric reactions of VOCs. Other oxidants present in smog include hydrogen peroxide, peroxy acetyl nitrate (PAN), organic peroxides, and oxidising radicals such as hydroxyl (OH) [27, 28]. Understanding the atmospheric chemistry of VOCs is central to understanding

the relationship between VOC emissions and these different types of atmosphere pollution.

Of the many volatile organic compounds released to the atmosphere, alkenes exhibit some of the most rapid rates of reaction with the hydroxyl radical and furthermore, reactions between alkenes and ozone have been reported to yield OH as a product [29].

Large quantities of non-methane organic compounds (NMOCs), which include alkenes, are emitted by vegetation [30–33]. NMOCs are also emitted into the troposphere from a variety of anthropogenic sources, including combustion sources, fuel storage and transport, solvent usage, emission from industrial operation, landfills and hazardous waste facilities [32].

Alkenes are an important class of VOCs present in the atmosphere, and chemical reaction is the main removal pathway for alkenes from the atmosphere. The main chemical species that initiate reactions of alkenes in the atmosphere are ozone, the hydroxyl radical and the nitrate radical [26]. As compared with the reactions of both OH and NO_3 with alkenes, the initial rate of the reaction of ozone with an alkene is relatively low; these reactions can, however, become important under regimes where there are high concentrations of alkenes and/or ozone [34].

The mechanism of the reaction between ozone and alkenes was first proposed by Criegee [35, 36] and involves the concerted addition of ozone to form a primary ozononide, which rapidly decomposes to form a vibrationally excited carbonyl oxide (a **Criegee intermediate**) and carbonyl products. The Criegee intermediate can then either be collisionally stabilised by a third body or undergo unimolecular decomposition to products (see Figure 1.4).

The Criegee intermediate mechanism is universally accepted, but no Criegee intermediate has been observed so far in the gas-phase, although some evidence of the primary Criegee intermediate, formaldehyde oxide (CH_2OO), is available from mass spectroscopic experiments involving chlorine-initiated gas-phase oxidation of dimethyl sulfoxide (DMSO) [37].

In this work, reactions of ozone with ethene, tetramethylethylene and 2-methylpropene

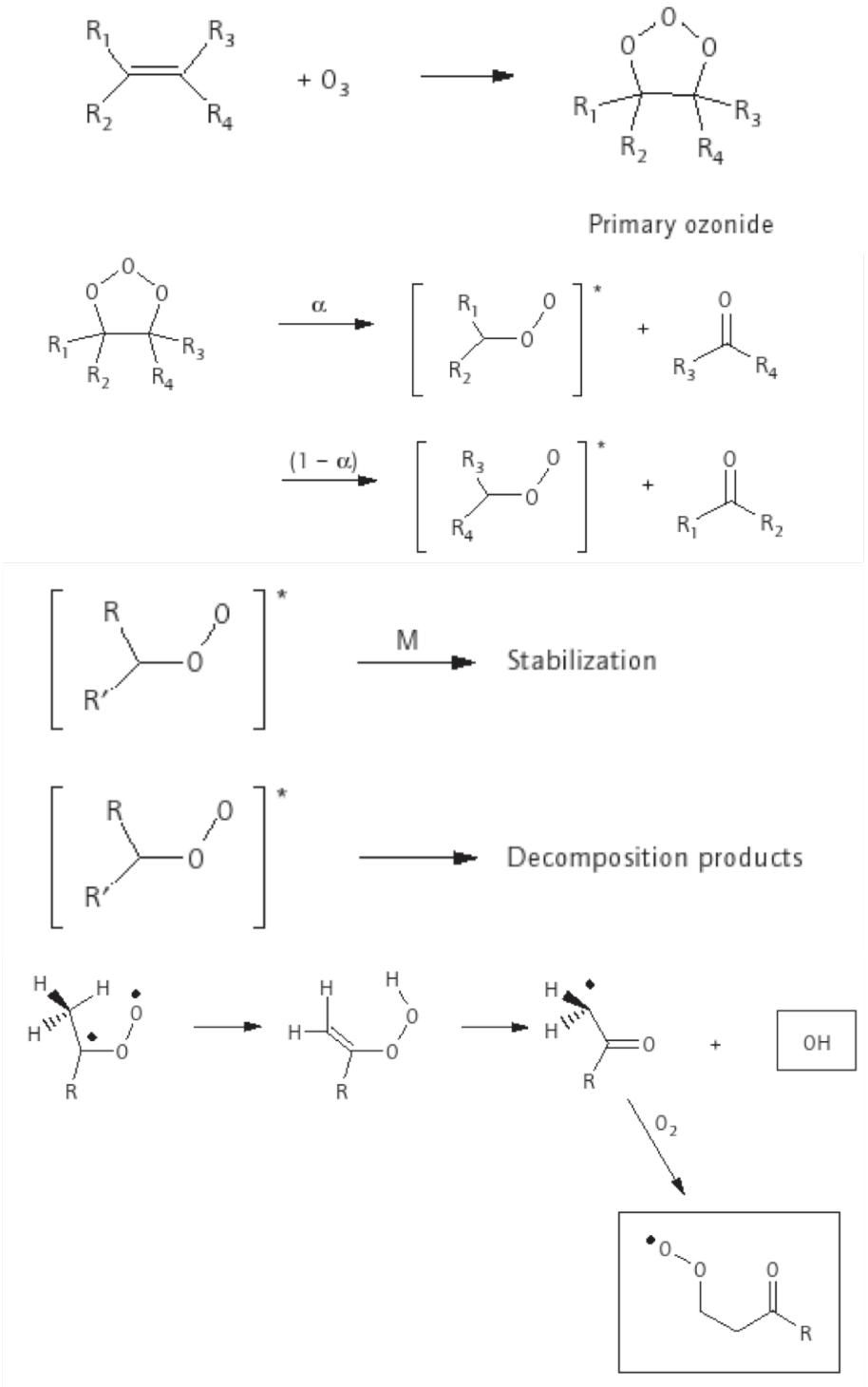

Figure 1.4: *Criegee intermediate mechanism for reaction of an alkene with ozone [34]*

have been investigated by u.v.-photoelectron spectroscopy in order to estimate the branching ratio between channels α and (1 - α), the decomposition pathways of the primamry ozonide and to see if any reaction intermediates can be observed.

2. Experimental methods

2.1 The matrix isolation technique

2.1.1 Principles and characteristics of the method

Matrix isolation [38, 39] is an experimental technique used in chemistry and physics which generally involves a material being trapped within an unreactive matrix. A host matrix is a continuous solid in which guest particles (atoms, molecules, ions, etc.) are embedded. The **guest** is isolated within the **host** matrix (Figure 2.1).

Initially the term "matrix-isolation" was used to describe the placing of a chemical species in any unreactive material, often a polymer or a resin, but more recently it has been used to specifically refer to molecules isolated in low temperature solids.

A typical matrix isolation experiment involves a sample being diluted in the gas-phase with the host material gas, usually a noble gas or nitrogen. This mixture is then deposited on a cold window, often cooled to 10 K or below. The sample may then be studied using various spectroscopic methods.

Matrix isolation has its origins in the first half of the 20th century with experiments

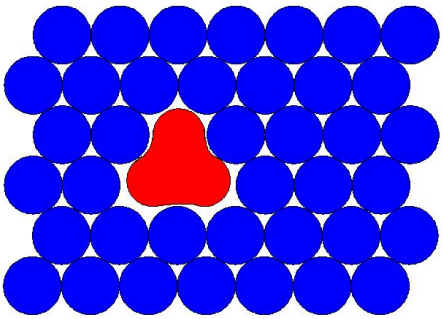

Figure 2.1: *Guest species (in red) isolated in solid host matrix (in blue)*

by photochemists and physicists which involved freezing a sample in a liquefied gas. The earliest matrix isolation experiments involved the freezing of species in transparent, low temperature organic glasses [40, 41]. The modern matrix isolation technique was developed extensively during the 1950s, in particular by Pimentel [38]. He initially used inert gases like xenon and nitrogen as the host material, and he is often said to be *the father of matrix isolation.*

The inert gas plays the role of isolating the sample molecules in the matrix. Elimination of interactions between sample molecules in the matrix, and the cooling of the sample, leads to infrared spectra with much narrower bands than the ones obtained in a high temperature vapour spectrum. As the molecules are trapped at low temperature, the contribution of "hot bands", background radiation and rotational-vibrational structure is almost eliminated. However an effect that must be taken into account is the possible shift of the bands from their gas-phase values due to interactions with the matrix.

The transparent window, onto which the sample is deposited, is usually cooled using compressed helium or similar refrigeration methods. Experiments must be performed under a high vacuum to prevent contaminants from unwanted gases freezing on the cold window. Noble gases such as argon, and also molecular nitrogen, are often used as matrix gases.

Using the matrix isolation technique short-lived, highly-reactive species such as radicals, ions and reaction intermediates may be observed and identified by spectroscopic means. Infrared and visible-ultraviolet spectroscopy are important tools for detecting and studying reaction intermediates in matrices [42, 43].

2.1.2 Matrix isolation apparatus

In this work, an instrument equipped with a CsI deposition window, transparent to infrared radiation, is used [44] (see Figure 2.2). In the experiments, both nitrogen and argon were used as matrix gases. Cryogenic cooling is provided by an Air Products CSW-202 water cooled 'Displex' closed cycle unit, which uses helium as the refrigerant. The

unit consists of two parts, a compressor and an expander module which are connected by flexible, high pressure hoses. The expander is mounted in a high vacuum chamber using a double 'o'-ring seal. The CsI window is mounted at the base of the expander unit to provide a cold deposition surface.

The lower section of the vacuum shroud has two CsI windows to permit the transmission of the infrared beam, which is perpendicular to the direction of the vapour, so the windows are rotated by 90^o after a suitable amount of sample has been deposited on the window: in this way, IR spectra can be obtained.

The vacuum chamber is maintained at low pressure, ca. $1 \cdot 10^{-6}$ mbar, using an Edwards 'Diffstak' unit comprising oil diffusion and rotary pumps, and a liquid nitrogen cooled trap. The vacuum shroud and the cryostat are connected to the sample cell of a Perkin Elmer 983G (5000-180 cm^{-1}) infrared spectrometer. The spectrometer is interfaced to a Perkin Elmer 3600 data station to allow manipulation and storage of experimental data.

The experiments in this work were performed using a flow-tube inlet system (Figure 2.3) similar to that used by Dyke et al. [13]. In this inlet system, the inner tube is movable with respect to the outer tube; DMS and molecular halogens, diluted with the matrix gas, could be introduced into this inlet system (one reagent admitted to the inner tube and the other to the outer tube) and as the inner inlet tube is moved, so the reaction distance (reaction time) from the window could be changed.

2.1.3 Fourier Transform IR spectroscopy

The main component in a Fourier-transform Infrared (FT-IR) spectrometer is the interferometer [45]. The basic components of an idealised Michelson interferometer are shown in Figure 2.4.

In this spectrometer, infrared radiation emitted by a source is directed to a device called the beam splitter, which ideally allows half of the radiation to pass through while it reflects the other half. The reflected part of the beam travels to the fixed mirror **M1** along a distance L. It is reflected there and hits the beam splitter again after a total path

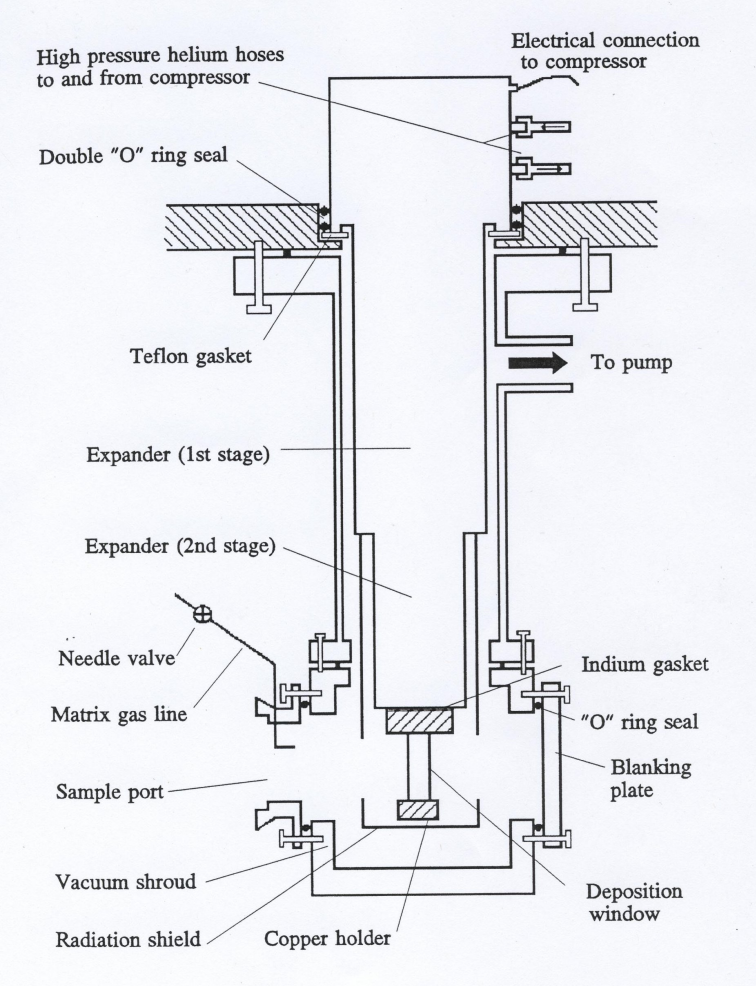

Figure 2.2: *Vertical section scheme of the "Displex" cryogenic cooling unit of the IR matrix isolation spectrometer used in this work*

length of 2L. The same happens to the transmitted part of the beam. However, as the reflecting mirror **M2** for this interferometer arm is not fixed at the same position L but can be moved very precisely back and forth around L by a distance x, the total path length of this beam is accordingly 2·(L+x). Thus when the two halves of the beam recombine again on the beam splitter, they exhibit a path length difference or optical retardation of 2·x. The beam leaving the interferometer is passed through the sample compartment and is finally focused on the detector D. The quantity actually measured by the detector is thus the intensity I(x) of the combined IR beams as a function of the moving mirror displacement x, the so called interferogram (Figure 2.4**B**).

The interferometer produces and recombines two wave trains with a relative phase

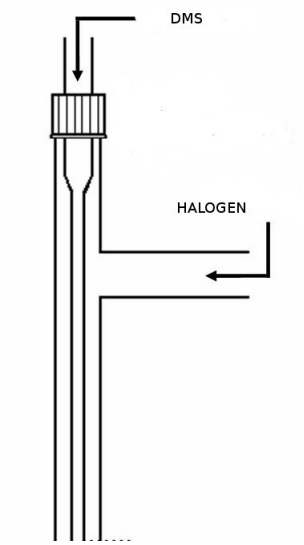

Figure 2.3: *Mixing system used during the infrared matrix isolation experiments*

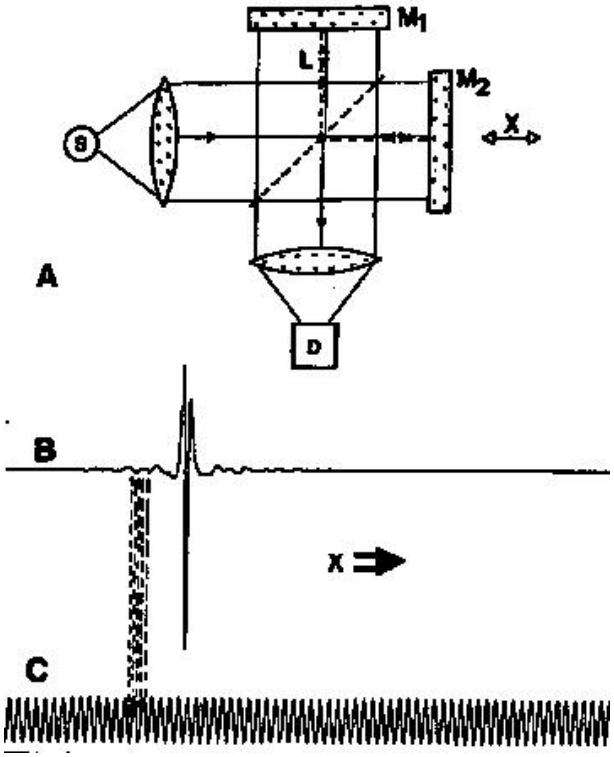

Figure 2.4: ***A)*** *Schematic of a Michelson interferometer.* ***S****; source.* ***D****: detector.* ***M1****: fixed mirror.* ***M2****: movable mirror.* ***X****: mirror displacement.* ***B)*** *signal measured by detector* ***D.*** *This is the interferogram.* ***C)*** *interference pattern of a laser source. Its zero crossings define the positions where the interferogram is sampled (dashed lines).*

difference, depending on the mirror displacement. These partial waves interfere constructively, yielding maximum detector signal, if their optical retardation is an exact multiple of the wavelength λ, i.e. if:

$$2 \cdot x = n \cdot \lambda (n = 0, 1, 2, ...) \tag{2.1}$$

Minimum detector signal and destructive interference occur if 2·x is an odd multiple of $\lambda/2$. The complete dependence of I(x) on x is given by a cosine function:

$$I(x) = S(\omega) cos(2\pi * \omega * x) \tag{2.2}$$

where the wavenumber $\omega = 1/\lambda$ has been introduced and S(ω) is the intensity of the monochromatic line located at wavenumber ν. Equation 2.2 is very useful for practical measurements, because it allows very precise tracking of the movable mirror. Inclusion of the interference pattern of the laser source in Figure 2.4C demonstrates how the IR interferogram is digitized precisely at the zero crossings of the laser interferogram. The accuracy of the sample spacing Δx between two zero crossings is determined by the precision of the laser wavelength itself. As the sample spacing $\Delta\omega$ in the spectrum is inversely proportional to Δx, the error in $\Delta\omega$ is of the same order as the error in $(\Delta x)^{-1}$. Thus, FT-IR spectrometers have a built-in wavenumber calibration of high precision (about 0.001 cm^{-1}).

Besides its high wavenumber accuracy, FT-IR spectroscopy has other features which make it superior to conventional IR spectroscopy. The throughput advantage (or so called Jacquinot advantage) arises from the fact that the circular apertures used in FT-IR spectrometers have a larger area than the linear slits used in grating spectrometers, thus enabling higher throughput of radiation. In conventional spectrometers, the spectrum S(ω) is measured directly by recording the intensity at different monochromator settings ω, one ω after the other. In a FT-IR spectrometer, all frequencies emanating from the IR source impinge simultaneously on the detector. This advantage is called the multiplex or Fellget advantage.

The measuring time in FT-IR spectroscopy is the time needed to move mirror M2 over a distance inversely proportional to the desired resolution. As the mirror can be moved very fast, complete spectra can be measured in fractions of a second.

Finally, the Fellget and Jacquinot advantages permit construction of interferometers having much higher resolving power than dispersive instruments.

2.2 Photoelectron spectroscopy

2.2.1 Basic principles of photoelectron spectroscopy

Photoelectron spectroscopy (PES) is based on Einstein's photoelectric effect [46]. A photon can remove an electron from a molecule if the photon has an energy greater than the energy holding the electron in the molecule. For an atom for a given photon energy, the energy in excess of that needed for ionisation is carried by the outgoing electron in the form of kinetic energy. The kinetic energy of the ejected electron is measured by a photoelectron spectrometer. As shown in equation (2.3), the difference between the photon energy (hν), which is known, and the electron kinetic energy (K.E.), which is measured, is the ionisation energy (I.E.).

$$I.E. = E(h\nu) - K.E.(e^-) \tag{2.3}$$

For a neutral molecule in the gas phase, the photon ionises the molecule (M) and leaves the molecule in a positively charged ion state (M^+) according to equation (2.4).

$$M + photon(h\nu) \rightarrow M^+ + e^- \tag{2.4}$$

Invoking the conservation of energy principle, an expression can be derived for the kinetic energy, K.E., of the electron (Eq. 2.5), where I_i is the ith ionization energy of the molecule and ΔE_{vib} and ΔE_{rot} represent the changes in vibrational and rotational energy

between the molecule and ion that occur on ionisation.

$$K.E. = h\nu - I_i - \Delta E_{vib} - \Delta E_{rot} \tag{2.5}$$

Experimentally, rotational structure is not normally resolved in a u.v.-photoelectron spectrum, so the ΔE_{rot} term can be added to the I_i term to give K.E. = hν - I'$_i$ - ΔE_{vib}. However, vibrational structure may be resolved and a photoelectron band may exhibit vibrational structure corresponding to the vibrational mode or modes that are excited in the ion.

In general, a photoeletron spectrum can provide three types of information [47] related to the molecule and/or ion involved in the ionisation process:

1. The adiabatic ionisation energy, which corresponds to an ionisation from the electronic and vibrational ground state of the neutral molecule, to the vibrational ground state of a particular ionic state, and the vertical ionisation energy which is the ionization energy corresponding to the most intense component in a photoelectron band.

2. The separation of the vibrational components observed in a photoelectron band envelope. These can be used to calculate vibrational constants for the vibrational mode excited in the cation.

3. The relative photoelectron band intensities which can be used to calculate relative photoionisation cross-sections.

4. The relative intensities of vibrational components in a band. These can be used to determine the geometry change between the molecule and the ion.

2.2.2 Vibrational structure in a photoelectron band

Each photoelectron band is associated with the energy necessary to produce an ion in a particular electronic state: the first band is associated with the ionisation to the ground

ionic level, the second band to the first excited ionic state, and so on. PES is not usually able to resolve rotational structure in a band, but it is often possible to resolve vibrational structure associated with the ionisation process associated with the PE band (see Figure 2.5). In this case, the band is resolved into different vibrational components. As mentioned in the previous section, the lowest in energy of these components is defined as the *adiabatic ionisation energy* (AIE) while the most intense component is called the *vertical ionisation energy* (VIE).

The AIE of a band is the energy necessary to ionise a molecule in its ground electronic and vibrational state to the lowest vibrational state of the ionic electronic state related to that particular PE band. In other words, both the molecule and the ion are in their v=0 vibrational level; the adiabatic transition is also referred as the 0-0 transition. The VIE is the transition for which the overlap of the vibrational wavefunctions of the molecule and the ion is a maximum. The relative intensities of the vibrational components in a photoelectron band is expressed by the *Franck-Condon factor* (FCF). The most probable vibrational transition in an ionisation process has the strongest component in a PE band; this is the vertical transition, the component for which the FCF is maximum. The VIE and the AIE coincide only if the most intense component of the band is the lowest in energy, or in other words if the ionic vibrational wavefunction that produces the highest overlap with the v"= 0 vibrational wavefunction of the neutral molecule is v'= 0. This would occur if the electron removed on ionisation is initially in a non-bonding type of orbital. In general, however, v"= 0 and v'$\neq$ 0 for the most intense component; i.e. for removal of an electron from a bonding orbital a broad band is obtained with the AIE$\neq$VIE and the vibrational constant (ω'_e) in the ion less than that in the neutral molecule (ω''_e). In Figure 2.5, the $AB^+(X) \leftarrow AB(X)$ ionisation is a non-bonding atom type ionisation, and gives a PE band where the AIE=VIE, and $AB^+(A) \leftarrow AB(X)$ ionisation is a bonding type ionisation and gives a PE band where AIE$\neq$VIE.

Considering that at room temperature the neutral molecule would be in its ground vibrational level, the spacings observable in a PE band are associated with the vibrational

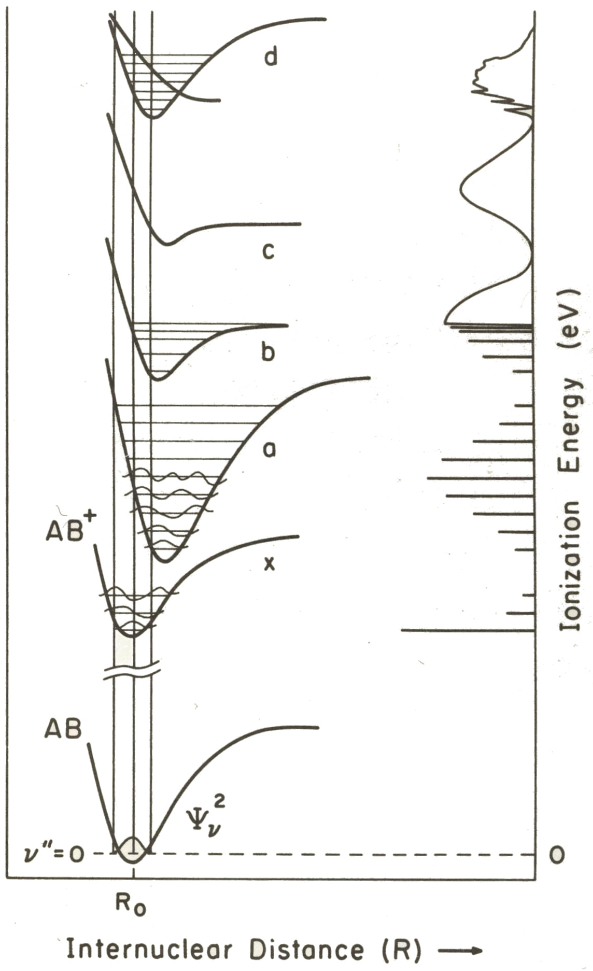

Figure 2.5: *Potential energy curves for the molecule AB in its ground state and the corresponding molecular ion AB^+ in several different ionic states [48]. The Franck-Condon region is between the vertical lines. Photoelectron bands resulting from the various ionisations are shown schematically on the right ordinate*

spacings of the ionic electronic state reached with the ionisation associated with that particular PE band.

2.2.3 The vacuum ultraviolet photon source

The essential components of a gas-phase photoelectron spectrometer [47] are a highly monochromatic source of photons, a region for photoionisation, an electron energy analyzer designed to separate photoelectrons according to their kinetic energies, an electron detector, and some suitable detection and counting electronics. A schematic diagram of

the photoelectron spectrometer [49, 50] used in this work is shown in Figure 2.6.

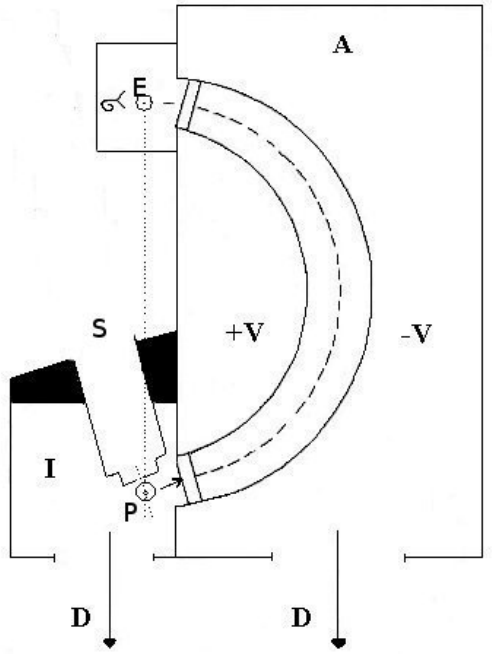

Figure 2.6: *Schematic diagram of a photoelectron spectrometer:* ***A*** *Analyser Chamber,* ***I*** *Ionization Chamber,* ***D*** *diffusion pump,* $\pm$ ***V*** *Hemisphere Voltages,* ***S*** *Sample beam,* ***P*** *Photon beam and* ***E*** *Electron detector.*

The basic requirement of any photon source used in u.v.-PES is that it should provide a high intensity, highly monochromatic source of radiation capable of ionising the valence electrons in most molecules. The most common source of radiation that satisfies these conditions is the HeI resonance line at 584 $\mathring{A}$ (21.22 eV). This can be generated in a dc capillary discharge in helium and such a lamp has been used in this work. The main resonance line arises from the transition ^{1}P(1s2p) $\rightarrow$ ^{1}S(1s^2) in neutral helium and it is termed HeIα (21.22 eV). There are also other higher members of the transition series ^{1}P(1snp) $\rightarrow$ ^{1}S(1s^2) present in the output discharge (termed HeIβ, HeIγ etc...), but their intensity is a small fractions of that of the main HeIα line [47].

2.2.4 The ionisation region

In general the partial pressure of the target gas in the ionisation chamber needs to be between 10^{-5} - 10^{-4} torr to obtain an adequate signal. The background pressure in the ionisation chamber with no sample gas admitted must be 10^{-5} torr or lower to allow electrons to be transmitted without undergoing inelastic collisions with background gas, which means that in the case of gas samples, adequate pumping arrangements have to be made to prevent the sample gas diffusing into the electron analyser. In the instrument used in this work, the gaseous sample is introduced into the ionisation region at 90° to the photon beam and the product photoelectrons are sampled and the energy analysed by a 150° hemisperical analyser.

2.2.5 The electron energy analyser

The method of energy analysis in the spectrometer used in this work, is based on the use of an electrostatic field to deflect the electrons [47, 51]. In the spectrometer, the analyser consists of a 10 cm mean radius hemispherical analyser created by two concentric hemispherical sectors charged to the same voltage but of opposite sign (inner '+ V', outer '- V'). This arrangement permits negatively charged particles of defined energy to be transmitted, the energy of transmission (E) being related to the applied voltage (V) by:

$$V = \frac{E}{2}(\frac{R_2}{R_1} - \frac{R_1}{R_2}) \tag{2.6}$$

where R_1 and R_2 are the radii of the inner and the outer hemispheres, respectively. Variation of the potential between the two concentric hemispheres allows the passage of photoelectrons having different kinetic energies to the electron detector. The photoelectron spectrum is then obtained by sweeping the voltages (+V,-V) on the hemispheres and recording the number of electrons of each kinetic energy reaching the electron detector per second.

This type of analyser has the property that the source, the centre of the spheres and

the focus are all on the same line, which is a useful aid in construction. The electrons can travel in any orbit, starting at S and terminating at E but in different planes (see Figure 2.6). This is called the "double focussing" property of this type of analyser and results in high transmission.

A consequence of the fact that electrons are charged particles is that their path through the analyser may be pertubed by the presence of any stray electric or magnetic fields, and this results in a degradation in signal intensity and resolution. The origin of these fields arises from two main sources: the Earth's magnetic field and any other local fields, as well as patches of surface charge in the critical regions in the path taken by the electrons. The Earth's magnetic field and any local fields can be eliminated by employing three sets of mutually orthogonal Helmholtz coils through which current is passed. The effect of the field produced by these coils is optimised by monitoring the photoelectron signal intensity and resolution of the $Ar^+(^2P_{3/2,1/2}) \leftarrow Ar\ (^1S_0)\ (3p)^{-1}$ bands as a function of the current flowing through each pair of Helmholtz coils. The fields arising from the contact potentials and local areas of surface charge inside the spectrometer are minimised by coating all of the surfaces between the ionisation region and the detector with colloidal graphite to provide a homogeneous surface potential.

The resolution of a photoelectron spectrometer is a measure of the energy spread associated with a particular feature in a photoelectron spectrum and is usually quantified in terms of the full width at half maximum (F.W.H.M.) of the $Ar^+(^2P_{3/2,1/2}) \leftarrow Ar\ (^1S_0)$ photoelectron band for the argon $(3p)^{-1}$ ionisation. A typical value for the resolution of the spectrometer used in this work under operating condition is 25 - 30 meV using HeI radiation.

Two significant contributors to the resolution of the spectrometer are the linewidth of the ionising radiation, which will contribute 3 - 4 meV to the band width and Doppler broadening due to the thermal motion of the molecules being ionised, which can contribute up to 10 meV depending on the mass of the sample and its temperature. However, the largest contribution to the resolution of the spectrometer is that imposed by the

spectrometer's slit widths and radius of the electrostatic analyser. For a stable electron orbit around the hemispheres the centripetal force is balanced by the electrical force on the electron:

$$\frac{mv^2}{R} = eF \tag{2.7}$$

Hence, the energy of the detected electrons, E, is related to the mean radius of the electron orbit, R, by the expression:

$$E = \frac{1}{2}mv^2 = \frac{1}{2}eFR \tag{2.8}$$

where F is the electric field between the two hemispheres, m is the mass of the electron and v is its velocity. However, as the entrance and exit slits have finite width, they allow a range of electron energies (ΔE) to be trasmitted for a given voltage setting on the hemispheres. This energy range, known as analyser bandpass, is then defined as:

$$\Delta E = \frac{1}{2}eF\Delta R \tag{2.9}$$

For an analyser with an entrance slit width dR_1 and an exit slit width dR_2 [52], the variation in R (ΔR) can be approximated as $\Delta R = \frac{1}{2}\ (dR_1 + dR_2) = \frac{S}{2}$, where S is the total slit width. Combining equations (2.7) and (2.8), the resolution of the analyser can be defined by the following equation:

$$\frac{\Delta E}{E} = \frac{S}{2R} \tag{2.10}$$

It can be seen that, for a given electron energy, ΔE decreases as the total slit width is reduced. It is also clear that for a hemispherical analyser, where S and R are fixed, the resolution improves as the kinetic energy of the electrons is decreased.

In equation 2.9 ΔE is the base-width of a band. For typical band shapes obtained with a hemispherical analyser it has been shown that the half-width and the base width are

related via $\Delta E_B = 2.3\ \Delta E_{\frac{1}{2}}$ [53], i.e. :

$$\frac{\Delta E_{\frac{1}{2}}}{E} = \frac{S}{2R} \cdot \frac{1}{2.3} \tag{2.11}$$

This equation therefore gives the instrumental contribution to the experimental resolution arising from the geometric parameters of the analyser and the slits. Typically if E = 5 eV, R = 10 cm, S = 2 mm, $\Delta E_{\frac{1}{2}}$ = 22 meV which is the dominant contribution to the experimental resolution.

2.2.6 Detection of electrons and spectrum recording

With the type of analyser described above, electrons are usually detected with an electron multiplier placed at the focus (E in Figure 2.6).

The detector used is a spirally shaped channel electron multiplier. The front cone is earthed and the far end has a voltage of 2.5 kV applied to it. This causes the electrons which impact on the cone to be amplified by a series of cascade processes in the detector. The signal then passes to a pre-amplifier and then to an amplifier. It is then transmitted to a ratemeter connected either to a PC or a chart recorder.

2.2.7 The vacuum system

In order to allow the passage of the photoelectrons from the ionisation chamber to the electron detector, the pressures within the spectrometer must be low enough such that the mean free path of the electrons exceeds the distance they have to travel. The distance from the generation region to the detection region is approximately 30 cm in the spectrometer used in this work, and this requires that the pressure must be maintained below 10^{-5} torr. This requirement is achieved by pumping the analyser chamber with a diffusion pump which is backed by a direct drive rotary pump. Similarly, the ionisation chamber is pumped by an identical diffusion pump fitted with liquid nitrogen trap to improve the pumping efficiency, and backed by a rotary pump. The task of this second pump is to pump the sample vapour as quickly as possible into the photon beam.

2.2.8 Inlet systems used during PES experiments

The DMS+XY reactions (where XY=Br_2, I_2, ICl and BrCl), the reaction between ozone and tetramethylethylene, and ozone and 2-methylpropene were performed by using the same inlet systems used in previous work on DMS+Cl_2 [12, 13] (Figure 2.7).

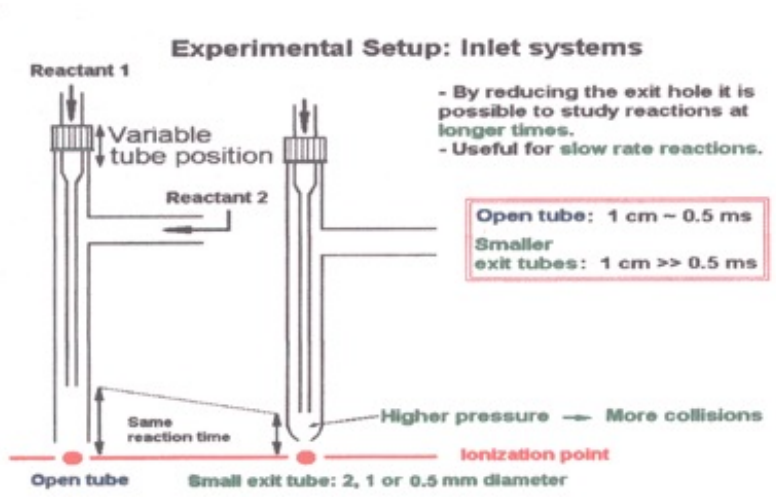

Figure 2.7: *Schematic diagram of the inlet systems used in the PES experiments.*

This consists of a glass tube inlet system, with a lateral outlet (in a T shape), with an inner glass tube which can be moved with respect to the ionization point. With this tube, one of the reactants is admitted into the system through the lateral outlet and the other one is admitted through the inner tube. Either a fully open tube or an open tube with a reduced exit hole (2 mm) was used (see Figure 2.7).

The reaction of ozone with ethylene is very slow and a recommended value for the rate coefficient for the reaction of ozone with ethylene has been given by Calvert et al. [26] as $k = 1.59 \cdot 10^{-18}$ cm^3 molecule^{-1} s^{-1} at 298 K, with an estimated overall uncertainty of 30%. Due to the explosive nature of the mixture of ethylene and ozone at high pressure, a reduction of the exit hole of the inlet tube to increase the reaction time was considered dangerous. An alternative way to extend the reaction time was to increase the mixing distance using an open ended tube (which was increased to 10.5 meters length). In order

to build a system which is easy to use, and taking into account the dimensions of the working space, plastic tubing reinforced internally with short sections of glass tube were chosen as a suitable material for the new inlet tube. The tube was wound as a helix with four reagent mixing points, as shown in Figure 2.8. This system allows changing the total mixing distance by changing the distance between the mixing points over the range of 0.0-10.5 meters. Because the reaction is slow and large mixing distances have to be used with this inlet, it was not possible to detect short lived intermediates (e.g. OH) but this inlet system is useful for studying longer-lived intermediates or stable products of slow reactions.

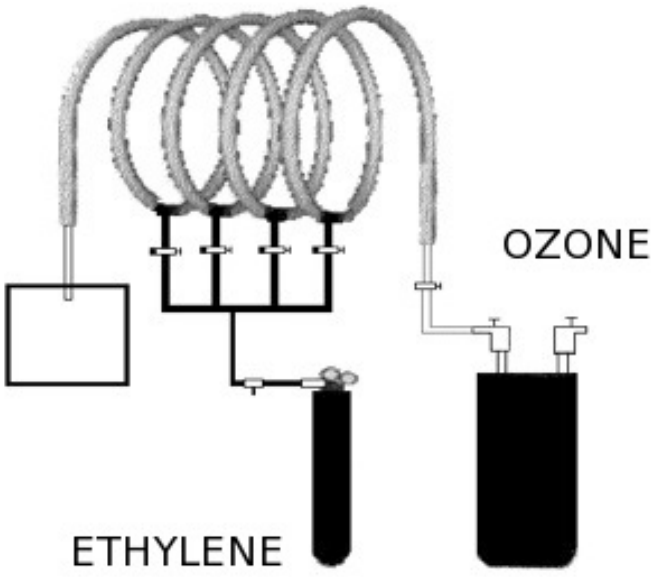

Figure 2.8: *Diagram of the inlet system used to study the $O_3+C_2H_4$ reaction by PES*

2.2.9 Production of short-lived species

A species whose lifetime (τ) is less than a few of seconds at low pressure in the gas-phase is considered a reactive intermediate or a short-lived species. The essential requirements for any investigation of short-lived species are [54]:

1. The production of the species should be as near as possible to the photoionisation

region but the method used must be not generate spurious fields which may interfere with spectral detection.

2. The transportation of the species to the photoionisation region should be in the time $\ll \tau$, where τ is the lifetime of the species under the conditions used.

3. Notwithstanding the requirements in (2), a sufficiently high partial pressure of the short-lived species is needed in the photoionisation region so as to make photoelectron detection a feasible proposition, i.e. to give ultimately a favorable signal-to-noise ratio in the photoelectron spectrum.

4. One should aim to reduce the complexity in the photoelectron spectrum by a suitable choise of reaction conditions. It is often the case that if due consideration is given to such factors as choise of reactants, generation conditions of the molecule of interest, carrier gas pressure etc.., one can optimise favorably the final contribution of the short-lived species to the overall spectrum.

The principal methods which have been used in PES for producing short-lived species in the vapour phase are microwave or d.c. discharges in gases, the pyrolysis of solid and vapours, and rapid gas-phase reactions [54]. Only gas-phase reactions have been used in the work reported in this thesis.

When studying the photoelectron spectrum of a short-lived species, it is often very helpful to have some knowledge of its spectroscopic properties in its ground state, an understanding of the gas-phase kinetics under the conditions in which it is produced, and, if possible, an experimental estimate of its first ionisation energy. Ionisation energies and neutral and ionic state spectroscopic constants obtained from molecular orbital calculations are also useful, and this has been used in this work. A summary of the theoretical methods, used in this work, and their underlying principles, are given in Chapter 3.

2.3 Conclusion

The matrix isolation infrared spectrometer, the u.v.-photoelectron spectrometer and the different inlet systems described in this Chapter have been used to study reactions of atmospheric importance, i.e. DMS with halogens and selected alkenes with ozone, and the results obtained are described in Chapters 4 and 5.

3. Theoretical methods

This chapter describes the theoretical basis on which the electronic strauctures calculations performed in this work are based.

3.1 The Schrödinger equation

Proposed by Schrödinger, this equation defines the wave-like characteristics of particles [55]. The earlier relation derived de Broglie [56] proposed that all matter has wave properties and that the wavelength of the associated wave, is related to the momentum of the particle (Eq. 3.1).

$$\lambda = \frac{h}{p} \tag{3.1}$$

The time-independent Schrödinger equation can be written as:

$$\hat{H}\Psi = E\Psi \tag{3.2}$$

where $\hat{H}$ is the Hamiltonian Operator, E is the total energy of the system and Ψ is the molecular wavefunction. Any function which satisfies this equation is known as an eigenfunction of the operator $\hat{H}$, and the constant E is known as an eigenvalue of the operator $\hat{\mathrm{H}}$.

It is impossible to solve the Schrödinger equation exactly for atoms and molecules containing more than one electron. However, various approximations are introduced to allow approximate solutions to be obtained.

Within the Born - Oppenheimer Approximation [57], the total wavefunction is written as a product of electronic and nuclear parts (Eq. 3.3), where Ψ_e refers to the electronic

wavefunction and Ψ_n refers to the nuclear function.

$$\Psi = \Psi_e \cdot \Psi_n \tag{3.3}$$

On an electronic timescale, nuclei can be considered as fixed, as nuclei are much heavier than electrons. It is therefore reasonable to separate the electronic and nuclear wavefunctions in this way. The wavefunction of the electrons depends on the positions, but not the momenta of the nuclei. It is therefore possible to solve the electronic Schrödinger equation at fixed nuclear positions. The Schrödinger equation for electronic motion can be written as:

$$\hat{H}\Psi_e = E_e\Psi_e \tag{3.4}$$

For many electron systems, approximations must be made to allow approximate solutions to this electronic Schrödinger equation to be obtained.

In order to obtain approximate solutions to the Schrödinger equation for many-electron systems, use must be made of the Variation Theorem [58]. This states that the energy evaluated from an approximate wavefunction will always be greater than or equal to the exact ground state energy for the Hamiltonian. The expectation value of the energy is given by:

$$E = \int \Psi^* H \Psi dv \tag{3.5}$$

The Variation Theorem can therefore be expressed by the relationship (for normalised wavefunctions):

$$E = \int \Psi^* H \Psi dv > E_0 \tag{3.6}$$

where E_0 is the exact ground state energy.

3.2 The Hartree - Fock SCF method

The Hartree - Fock (HF) method [59–62] is an approximate method for the determination of the ground-state wavefunction and ground-state energy of a quantum many-body system.

The Hartree-Fock method assumes that the exact N-body wavefunction of the system can be approximated by a single Slater determinant [63] (in the case where the particles, the electrons, are fermions) of N spin-orbitals[1]. Invoking the variational principle, a set of N coupled equations for the N spin-orbitals can be derived. Solution of these equations yields the Hartree-Fock wavefunction and total energy of the system, which are approximations of the exact ground state wavefunction and total energy.

In the Hartree-Fock method each electron interacts with the mean field created by all other particles rather than the instantaneous field. The equations are solved by means of an iterative, fixed-point type algorithm. For molecules, the Hartree-Fock method is the central method for all *ab initio* quantum chemistry methods.

The Hartree-Fock method is used to solve the time-independent Schrödinger equation for a multi-electron atom or molecule, within the Born-Oppenheimer approximation. Due to the non-linearities introduced by the Hartree-Fock approximation, the equations are solved using an iterative method, which gives rise to the name "self-consistent field method". The Hartree-Fock method is also called the self-consistent field (SCF) method.

The Hartree-Fock method involves five major approximations:

- The Born-Oppenheimer approximation is assumed. The full molecular wavefunction is actually a function of the coordinates of each of the nuclei, in addition to those of the electrons.

- Typically, relativistic effects are completely neglected. The momentum operator is assumed to be completely non-relativistic.

[1] A **Slater determinant** is an expression which describes the wavefunction of a multi-fermionic system that satisfies anti-symmetry requirements; it satisfies the Pauli exclusion principle by changing sign upon exchange of fermions.

- The variational solution is assumed to be a linear combination of a finite number of basis functions, which are usually (but not always) chosen to be orthogonal.
- Each energy eigenfunction is assumed to be describable by a single Slater determinant, an antisymmetrised product of one-electron wavefunctions (i.e. orbitals).
- The mean field approximation is implied. Effects arising from deviations from this assumption, known as electron correlation, are completely neglected.

The greatest limitation of the SCF method is that with the SCF method electron interaction is treated as an average Coulomb potential felt by an electron as well as an exchange term between electrons of parallel spin; this is different from the instantaneous spatial interaction experienced by electrons in a real system. As electrons are not properly correlated in the SCF method, this problem is called *electron correlation*, as mentioned before.

Two types of electron correlation can be distinguished: *dynamic electron correlation* [64] which is a short range effect depending on the instantaneous motions of the single electrons, and *non-dynamic electron correlation* [65] which arises from the fact that a wavefunction based on a single configuration is inadequate to describe particular systems where near-degeneracies in the electronic configuration are possible. Non-dynamic electron correlation varies with the internuclear distance, and its effect is particularly relevant at the dissociation limit. These two factors constitute the general electron correlation effect.

To reach a high chemical accuracy, effective ways to take into account of electron correlation have to be used. Different methods have been developed to tackle the electron correlation problem, and they find extensive application for *ab initio* calculations. Methods that do not include any empirical or semi-empirical parameters in their equations - being derived directly from theoretical principles, with no inclusion of experimental data - are called *ab initio* methods.

Ab initio SCF methods have the great advantage of being universal. They can be used for both open and closed-shell molecules, and fast methods to optimise the molecular ge-

ometries and harmonic vibrational frequencies are available. Modern computation power rapidly increases the feasibility of *ab initio* calculations for large systems: the *ab initio* method is therefore the most important class of theoretical calculations.

The choice of method depends on the particular class of molecule to be studied, as well as the degree of accuracy of the results required and on the computational time needed to perform the calculation.

3.3 Koopmans' theorem

Ionisation energies are the most important pieces of information obtainable in a photoelectron spectrum. It is therefore very useful to calculate them, as these values can assist photoelectron band assignment. The most useful ionisation energy to calculate to assist band assignement is the vertical ionisation energy (VIE). This can calculated via Koopmans' theorem [66] which states that the energy necessary to ionise a closed - shell molecule by extracting an electron from the spin-orbital is equal and opposite to the energy of a spin orbital (ϵ_k) itself calculated at the Hartree - Fock limit, which will be introduced in the next section, i.e.:

$$IE = E_N - E_{N-1} = -\epsilon_k \tag{3.7}$$

where IE is the vertical ionisation energy (see Figure 2.5).

In this way, VIEs can be calculated from a calculation on a closed-shell molecule simply by using the negative of the orbital energies.

Koopmans' theorem is based on a number of approximations: the use of a single determinant in the Hartree - Fock equations, the neglect of electron correlation change between the molecule and the ion, and the neglect of orbital relaxation (the change of spin orbitals when passing from the neutral to the cation). Because of these approximations, it sometimes fails to correctly reproduce the correct order of the ionic states. In fact, the "true" VIE is related to the VIE predicted by Koopmans' theorem (VIE_{KT}) by the

relation:

$$VIE = VIE_{KT} - R + C \tag{3.8}$$

where R is the orbital relaxation term and C is the term for correlation energy change between the molecule and the ion. As defined in this equation, R and C are usually positive. The electron correlation change on ionisation and the orbital reorganisation often tend to compesate each other so Koopmans' theorem sometimes obtains fortuitously the experimental VIEs with a good approximation [67]. The fact that very often Koopmans' theorem overstimates the true VIE implies that R > C.

An alternative approach to calculate VIEs is to calculate the energy of the cation at the neutral equilibrium geometry and to substract from this energy the energy of the neutral molecule at the same geometry. This is called the ΔSCF method [68] and it takes into account the effect of orbital relaxation. As the cation has one electron less than the neutral, the ΔSCF method often leads to calculated vertical ionisation energies which are too low as no allowance has been made for electron correlation in each state. Normally ΔSCF VIEs are lower than the experimental VIEs, while Koopmans' values are higher.

3.4 Basis sets

A basis set is a set of functions used to represent the molecular orbitals, which are expanded as a linear combination of these functions with the weights or coefficients to be determined. Usually the basis functions are atomic basis functions.

In the choice of the basis set, two important factors must be considered. A large basis set usually give rises to a decreased total energy of the system. There is an energy limit called the *Hartree-Fock limit*, beyond which an increase of basis functions does not cause any lowering of the total energy.

The Hartree-Fock limit is defined as the "true" total SCF energy of the system. Therefore, the results given by the basis set must be as close as possible to those obtained at

the Hartree-Fock limit. To reach this degree of accuracy, a large basis set must be used. Unfortunately, the computational time needed for the calculation with a very large basis set can be prohibitive: the number of the two-electron integrals, the most demanding calculational effort rises as n^4 where n is the number of basis functions. Hence a compromise must be made in the choice of the basis functions.

There are two main types of atomic basis functions normally used in the Hartree Fock method:

- Slater-type orbitals (STOs)
- Gaussian-type orbitals (GTOs)

3.4.1 Slater-type orbitals

These orbitals are of the form $\chi_{nml} = N_{nml}\ r^{n-1}\ \exp(-\zeta\ r)\ Y_{lm}\ (\Theta,\Phi)$ [63] where N is a normalisation constant, n is the principal quantum number, l is the azimuthal quantum number, m is the magnetic quantum number and $Y_{lm}\ (\Theta, \Phi)$ is a spherical harmonic. Slater-type orbitals are hydrogen-like atomic wavefunctions. They are physically realistic in that they represent "real" atomic orbitals quite well but the problem with STOs is that two-electron integrals can involve electrons on different nuclei; these integrals, which are, therefore, known as a multicentre integrals cannot be evaluated analytically with STOs, they can only be evaluated numerically. As this is computationally time consuming, this led to the introduction of GTOs.

3.4.2 Gaussian-type orbitals

GTOs, which are used in this work, were first introduced by Boys [69] and are expressed as $\chi_{nlm} = N\ x^l\ y^m\ z^n\ \exp(-\ \zeta\ r^2)\ Y_{lm}\ (\Theta\Phi)$ where n, l and m are now integer values (not quantum numbers).

The advantage of GTOs is that the product of two GTOs is another GTO and, as a result, two-electron integrals can be evaluated analytically.

GTOs have the disadvantage that they are not very good representations of atomic orbitals, as they do not possess a cusp at the nucleus, which atomic orbitals do. They also decrease too rapidly with r. It is therefore necessary to use a linear combination of several GTOs to represent an atomic orbital. This computational effort can be reduced by fixing certain expansion coefficients in the basis set relative to each other. This is known as contracting the basis set and this allows a large basis set to be broken down into a smaller number of groups. Therefore, only the coefficients multiplying the contracted GTOs, are used as variational parameters in the Self-Consistent Field calculation.

Double-zeta basis sets [70], used in this work, can be expressed as shown in equation (3.9). In this way, one atomic orbital can be represented by two functions.

$$\chi_\mu = D_{\mu a} e^{-\zeta_a r} + D_{\mu b} e^{-\zeta r} \tag{3.9}$$

Triple-zeta basis sets [71], also used in this work, contain yet another basis function, improving the accuracy of the molecular calculation (Eq. (3.10)).

$$\chi_\mu = D_{\mu a} e^{-\zeta_a r} + D_{\mu b} e^{-\zeta_b r} + D_{\mu c} e^{-\zeta_c r} \tag{3.10}$$

These basis sets may be augmented with diffuse functions and this is denoted by adding the aug-prefix to the basis set keyword. These are very shallow Gaussian basis functions, which more accurately represent the "tail" portion of the atomic orbitals, which are distant from the atomic nuclei.

Basis sets for atoms beyond the third row of the Periodic Table, such as iodine in this work, are often dealt with in a different way than lighter elements. For these atoms, electrons close to the nucleus are treated in an approximate way, by using effective core potentials (ECPs) [72]. The core electrons and orbitals are assumed to have minor effects on most chemical properties. In an ECP basis set, the core is represented as a core potential and only valence electrons are treated, and so the computational effort is highly reduced.

In this work, cc-pVDZ [73] basis sets were used, except for the chlorine, bromine and

iodine atoms for which aug-cc-pVDZ [74] basis sets were utilised. Besides, for the iodine atom a ECP [72] basis set was applied. The cc prefix stands for "correlation-consistent". Correlation consistent basis sets are built up by adding shells of functions to a core set of atomic Hartree-Fock functions. Each function in a shell contributes very similar amounts of correlation energy in an atomic calculation.

The "correlation consistent" part of the name implies that in these basis sets the exponents and contraction coefficient have been variationally optimised not only for Hartree-Fock calculations, but also for calculations which include allowance of electron correlation.

Various augmentations to these base sets have also been developed. These include the addition of diffuse functions, as described above, to describe better anions and weakly interacting molecules (aug-cc-pVnZ), as well as special basis sets designed for describing the effects of correlating the core electrons (cc-pCVnZ and cc-pwCVnZ).

3.5 Density Functional Theory

Density functional theory [75] (DFT) represents an alternative approach to the approximate solution to the Schrödinger equation. In the DFT method, the exact exchange term for a single determinant from Hartree Fock Theory is replaced by a more general expression, the exchange correlation functional, which includes terms accounting for the exchange energy and electron correlation energy - omitted from Hartree-Fock Theory.

One widely used functional is known as BLYP (from the name Becke for the exchange part [76] and Lee, Yang and Parr for the correlation part [77]). Even more widely used is the B3LYP functional, which is used in this work. This is a hybrid functional in which the exchange energy is combined with the exchange energy from Hartree-Fock theory. Along with the component exchange and correlation functionals, three parameters define the hybrid functional, specifying how much of the exact exchange is mixed in.

The exchange-correlation hybrid functional is usually a linear combination of the Hartree-Fock exchange and some other exchange functional or a combination of exchange and correlation functionals. The parameters controlling the amount of each functional

can be arbitrarily selected and are usually fitted to reproduce well some set of observables (bond lengths, vibrational frequencies, etc.).

3.6 Perturbative methods

Möller-Plesset perturbation theory (MP) [78] is one of several quantum chemistry post-Hartree-Fock *ab initio* methods. It improves the Hartree-Fock method by adding some electron correlation by means of Rayleigh-Schrödinger perturbation theory (RS-PT) [79, 80], usually to second (MP2), third (MP3) or fourth (MP4) order.

It starts by assuming the sum of all the Fock operators for every electron within the molecule as the unperturbed Hamiltonian $\hat{H}_0$. A perturbation treatment is then applied by expressing the exact Hamiltonian $\hat{H}$ as:

$$\hat{H} = \hat{H}_0 + \lambda \hat{V} \tag{3.11}$$

where λ is an arbitrary real parameter and V is the perturbative operator. In MPn-theory the zeroth-order wave function is an exact eigenfunction of the Fock operator, which thus serves as the unperturbed operator. The perturbation is the correlation potential. In a MP-n calculation, λ is set equal to 1 and the perturbation expansion of the energy and wavefunction is truncated at the n-th term.

The main level of theory used is MP2. It includes significant dynamic correlation and a small amount of non-dynamic correlation.

3.7 Conclusion

In this work, calculations were used to facilitate the assignments of the infrared spectra recorded for the study on the reactions of DMS with halogen molecules. Also, they were used to estabilish the mechanism for these reactions, by calculating relevant parts of the potential energy surfaces.

Calculations at the B3LYP and MP2 levels of theory were used in all the geometrical optimisations and the calculations of vibrational frequencies.

The comparison between the experimental and the computed spectra will be described in detail in Chapter 4.

4. Reactions of DMS with molecular halogens

4.1 Introduction

The reaction between DMS and Cl_2 has been investigated in previous work by u.v.-photoelectron spectroscopy [12–14] and by infrared matrix isolation spectroscopy [81, 82], and electronic structure calculations have been carried out in order to investigate the potential energy surface and identify possible reaction intermediates [13, 14].

In the infrared work by Orville-Thomas *et al.* [82], in a nitrogen matrix, an absorption was found at 525 cm^{-1} which was assigned to the Cl-Cl stretching mode of a reaction intermediate. In the later work by Machara and Ault [81], in an argon matrix, a very intense product band at 360 cm^{-1} was observed and it was assigned to the Cl-Cl stretching mode of the Cl_2 complex with $(CH_3)_2S$, along with two other bands at 1035 and 1331 cm^{-1}, although the structure of the complex was not established.

In the work at the University of Southampton [13, 14], infrared matrix isolation experiments on the DMS+Cl_2 reaction have been also made which have confirmed the results found by by Machara and Ault [81]. U.v.-photoelectron spectroscopy experiments were then performed by using the inlet systems mentioned and described in Chapter 2. The PE spectra recorded at short reaction times showed unknown features that have been assigned to a reaction intermediate. The computed structure of a reaction intermediate which gave VIEs which fitted the experimental VIEs, is a *covalent* structure and a diagram of this species is shown in Figure 4.1.

However, a different minimum energy structure was initially computed. This structure can be defined as a van der Waals structure and it is shown in Figure 4.2.

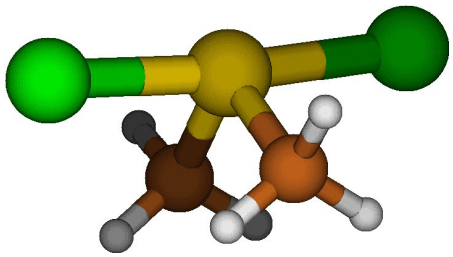

Figure 4.1: *Structure computed by Dyke et al. [12–14] for the DMS(Cl_2) reaction intermediate observed in gas-phase PES studies*

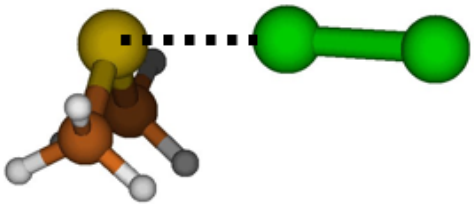

Figure 4.2: *Van der Waals structure for the DMS:Cl_2 reaction intermediate*

Despite a possible reasonable agreement for the IR spectrum recorded in a matrix for the reaction intermediate (shown in Figure 4.2), such a complex did not have computed VIEs which fitted the experimental PE spectrum.

The final products of the reaction have been found to be monochlorodimethyl sulfide ($ClCH_2SCH_3$) and hydrogen chloride by using both the techniques.

A computed relative energy diagram obtained from results at the MP2 level of theory [13] is presented in Figure 4.3 and shows the key parts of the reaction surface.

Given the importance that this reaction might have in climate studies (see Chapter 1), the aim of this work was to investigate the reactions of DMS with other halogen and interhalogen molecules that might be present in the atmosphere, that is Br_2, I_2, ICl and BrCl. It should be noted that no experimental evidence exists in the literature on these reactions in the gas-phase.

In this chapter, results obtained by using i.r. matrix isolation spectroscopy and u.v.-photoelectron spectroscopy will be presented and discussed, along with results of electronic

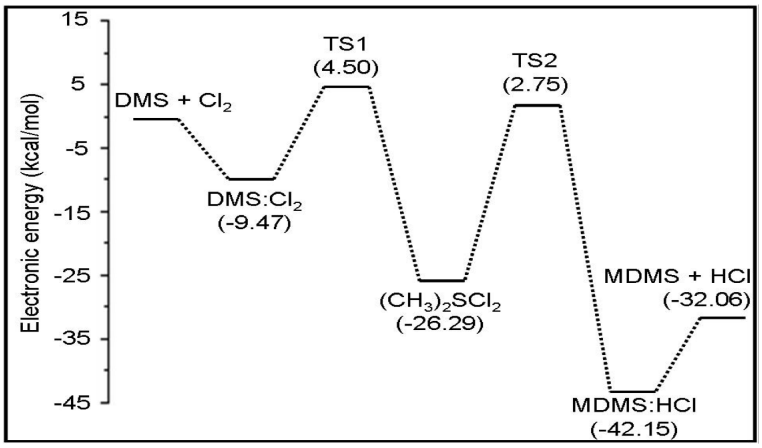

Figure 4.3: *Energy diagram for the DMS+Cl_2 reaction obtained from electronic structure calculations at the MP2 level of theory [13]*

structure calculations.

4.2 Infrared matrix isolation results

Matrix isolation experiments were carried out using both argon and molecular nitrogen as matrix gases (purities 99.99%) and the spectra were recorded at 3.0 cm^{-1} resolution. For small selected ranges of the spectra, the resolution was increased to 1.0 cm^{-1}.

The experiments were performed using a flow tube inlet system described in Chapter 2. In this inlet system, the inner tube is movable with respect to the outer tube; in this way DMS and halogens (the latter diluted with the matrix gas by a factor of 10) were introduced into the inlet system and the inner tube was moved, in order to change the reaction distance (reaction time) from the cold deposition window.

Spectra of DMS alone in nitrogen and in argon were first recorded (Figure 4.4), and the results are in good agreement with the experimental values found in the literature by Nxumalo *et al.* [83] (Table 4.1). Wavenumbers lower than 1000 cm^{-1} are associated to CH_3 wagging vibrations; wavenumbers between 1000 and 2000 cm^{-1} are due to CH_3 scissoring while the highest wavenumbers arise from C-H_3 stretching.

In general, the spectra of the reaction intermediates were obtained by using the mixing

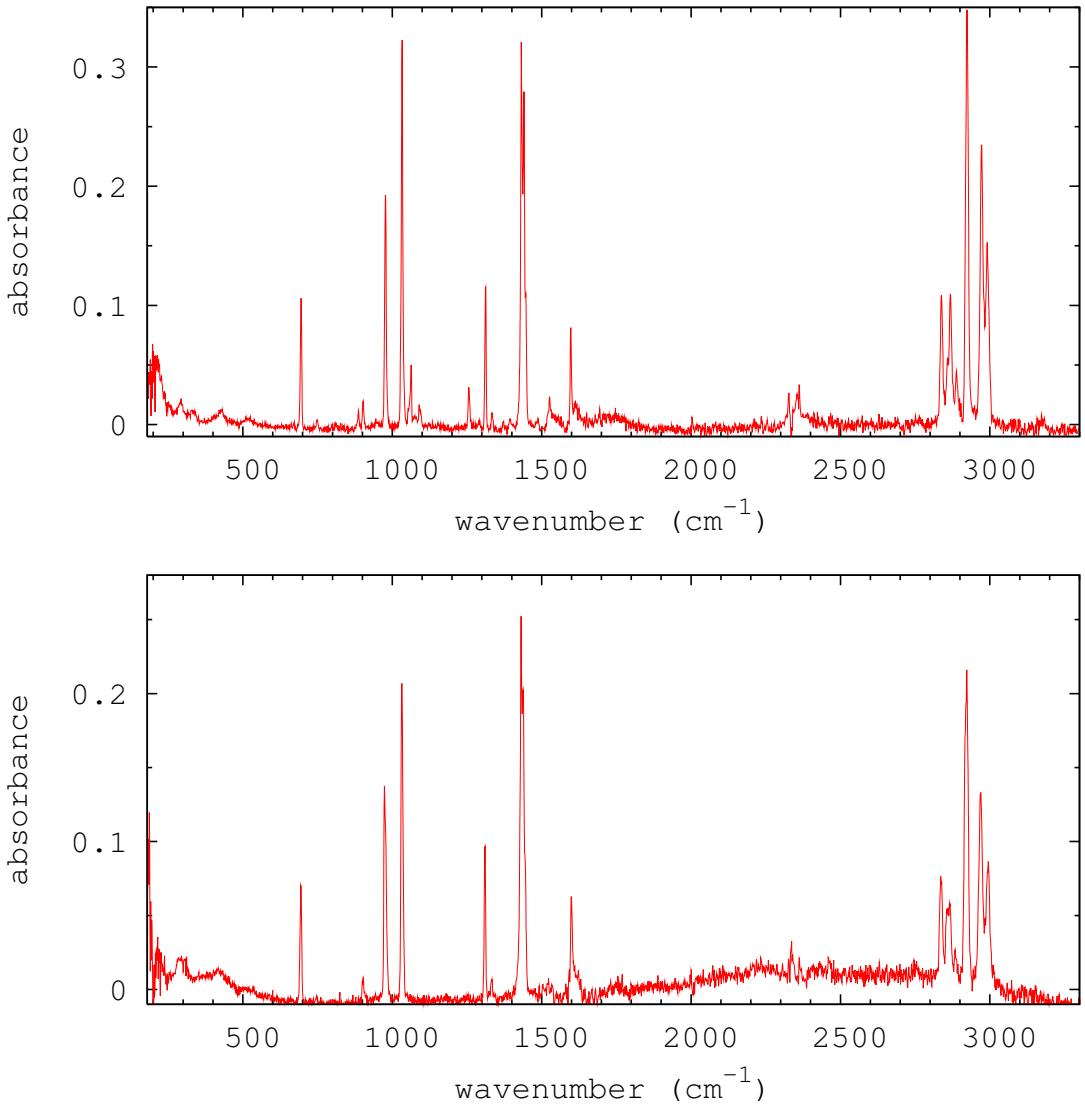

Figure 4.4: ***Top****: infrared spectrum of DMS in a nitrogen matrix;* ***bottom****: infrared spectrum of DMS in an argon matrix*

system described in Chapter 2, mixing the reagents at about 2 cm above the CsI window on which they are frozen.

DMS+Cl_2

The Cl_2+DMS reaction was initially studied in this work using the spectrometer and the mixing system described in Chapter 2, and the results were compared with the earlier work. When Cl_2 and $(CH_3)_2S$ were codeposited into a nitrogen matrix, many of the bands found are coincident with those in the parent DMS, but characteristic bands associated

DMS in N_2		*DMS in Ar*	
This work	Nxumalo's work [83]	This work	Nxumalo's work [83]
694.3	695.6	694.1	694.5
902.5	925.4	904.55	926.8
978.3	978.3	977.7	972.3
1033	1033.2	1033.2	1030.3
1313.1	1313.6	1311.3	1310.9
1432.2	1432.7	1431.7	1432.2
1441.2	1442.1	1437.9	1439.8
1446.5	1448.7	1445.3	1447.1
2868.3	2862.5	2857.7	2858.5
2889.9	2887.9	2865.4	2886.9
2924.2	2926.6	2924	2928.2
2972.6	2975.4	2967.8	2973.7
2991.4	2994.6	2995.4	2997.7

Table 4.1: *Comparison between this work and Nxumalo's work (wavenumbers in cm^{-1})*

with the reaction intermediate were observed at about 1331, 1040, 285, 306 and 326 cm^{-1} (see Figure 4.5), and in an argon matrix, the same band at 1331 cm^{-1} appears and also bands at about 1035, 287, 313 and 354 cm^{-1} were observed (see Figure 4.6). No band at 525 cm^{-1} was found. The shift between 1035 and 1040 cm^{-1} is due to the two different gases used as matrix-gas.

Unfortunately, in Ault's paper [81] no table showing experimental absorptions and relative intensities is available and a full infrared spectrum is not presented but only a section of the spectrum in the region 1340-600 cm^{-1} is shown.

Under particular conditions of the DMS+Cl_2 reaction, spectra with *virtually* no unreacted DMS were observed. In this way it was possible to identify more clearly the infrared bands associated with reaction intermediates (Figure 4.7 and Figure 4.8).

The final products of the reaction between DMS and Cl_2 were studied and their infrared spectra obtained. Bands were observed at 657, 702, 754, 984, 1234, 1427, 1438, 2850 and 2933 cm^{-1}, which belong to monochlorodimethylsulfide, and at 2848 cm^{-1} which can be assigned to HCl (see Figure 4.9). These results are in agreement with spectra found in the literature [84, 85].

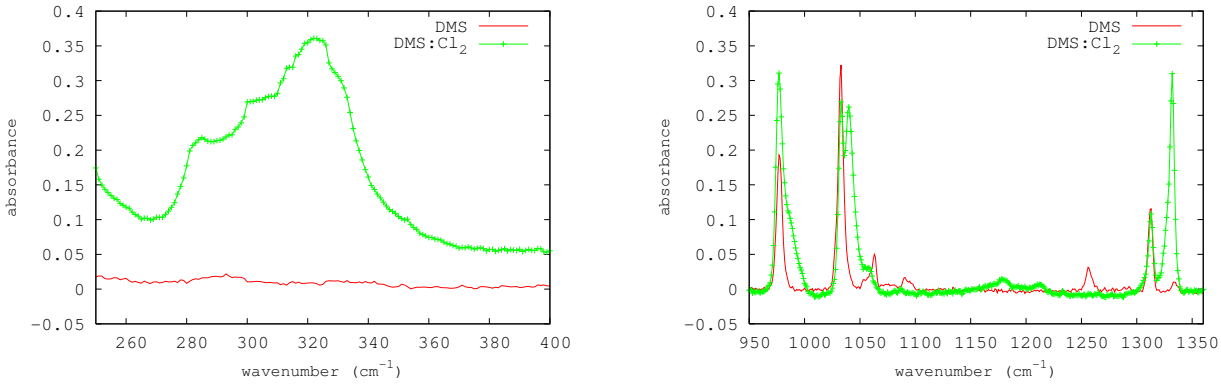

Figure 4.5: *Comparison between $(CH_3)_2S$ spectrum and $(CH_3)_2SCl_2$ spectrum in a nitrogen matrix*

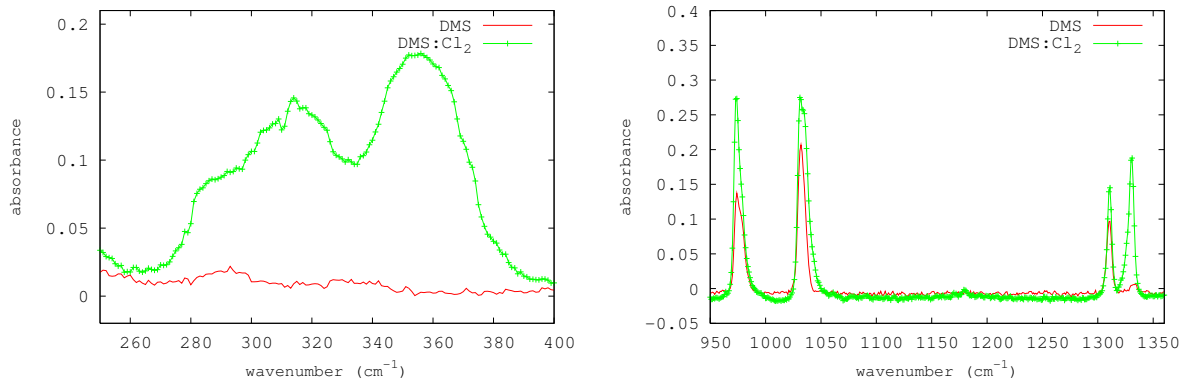

Figure 4.6: Comparison between $(CH_3)_2S$ spectrum and $(CH_3)_2SCl_2$ spectrum in an argon matrix.

DMS+Br_2

The reaction intermediate in the Br_2+DMS reaction was also studied by the infrared matrix isolation technique. Experiments were performed in an argon matrix first and bands at 1035, 1330 and 204 cm^{-1} were found (Figure 4.10). Further experiments followed, in nitrogen as the matrix gas, giving the same results.

In an experiment designed to study the final products of the DMS+Br_2 reaction, no final products were observed (i.e. monobromodimethylsulfide and HBr) and only bands associated with the reaction intermediate were observed. The bands at 1035 and 1331 cm^{-1} were observed as well as a band at 204 cm^{-1}. The compound obtained as a product of the DMS+Br_2 reaction is an orange-yellow volatile solid product. The compound was

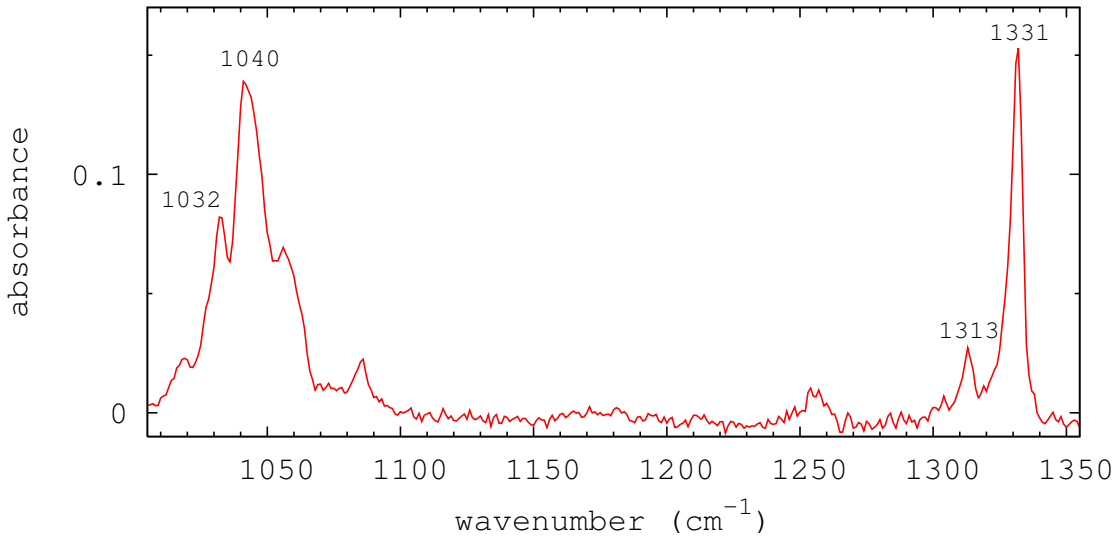

Figure 4.7: *DMS : Cl_2 infrared spectrum with no unreacted DMS in a nitrogen matrix: the characteristic 1040 and 1331 cm^{-1} bands associated with the intermediate can be clearly seen (impurities are denoted by *)*

obtained by mixing DMS and Br_2 on a vacuum line, with DMS slightly in excess which was pumped away after the reaction occured.

The dimethyl sulphide-bromine complex has been previously studied by Raman spectroscopy [86, 87] and X-ray diffraction [88] in the solid phase. The structure proposed in these previous works for the compound in the solid phase, is a Me_2S-Br_2 charge-transfer structure, not a covalent complex.

To make sure that the compound studied in this work is the same as studied previously, Raman spectra were run on the sample obtained in the solid phase. The results are in good agreement with the work by Askew *et al.* [87] (see Figure 4.11).

The bands positions are shown in Table 4.2. The instrument used for these measurements was a Perkin Elmer 2000 Series FT-Raman Spectroscopy equipped with 1064 nm excitation from a Nd:YAG laser. The power used for the laser was 110 mW with a 2 cm^{-1} resolution and 40 scans were performed. The sample was a solid in an evacuated tube which was placed in the sample cell and held in place with a sticky adhesive (BluTack) as a support.

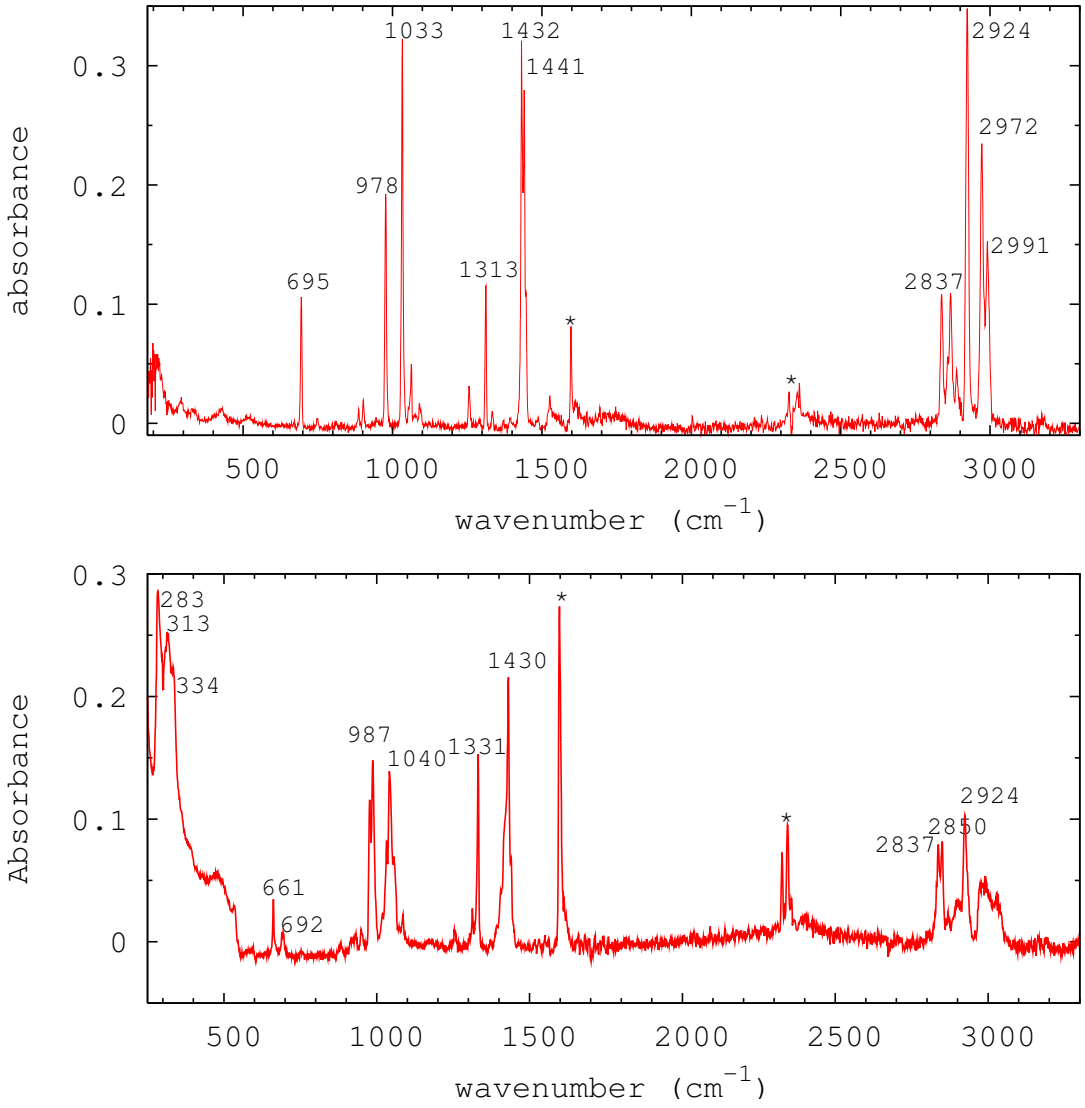

Figure 4.8: ***Top:*** *infrared spectrum of DMS in a N_2 matrix;* ***bottom*** *$DMS : Cl_2$ infrared spectrum with no unreacted DMS in a N_2 matrix; it appears that this is all due to to the complex $DMS : Cl_2$ apart from the bands denoted by * which are due to impurities*

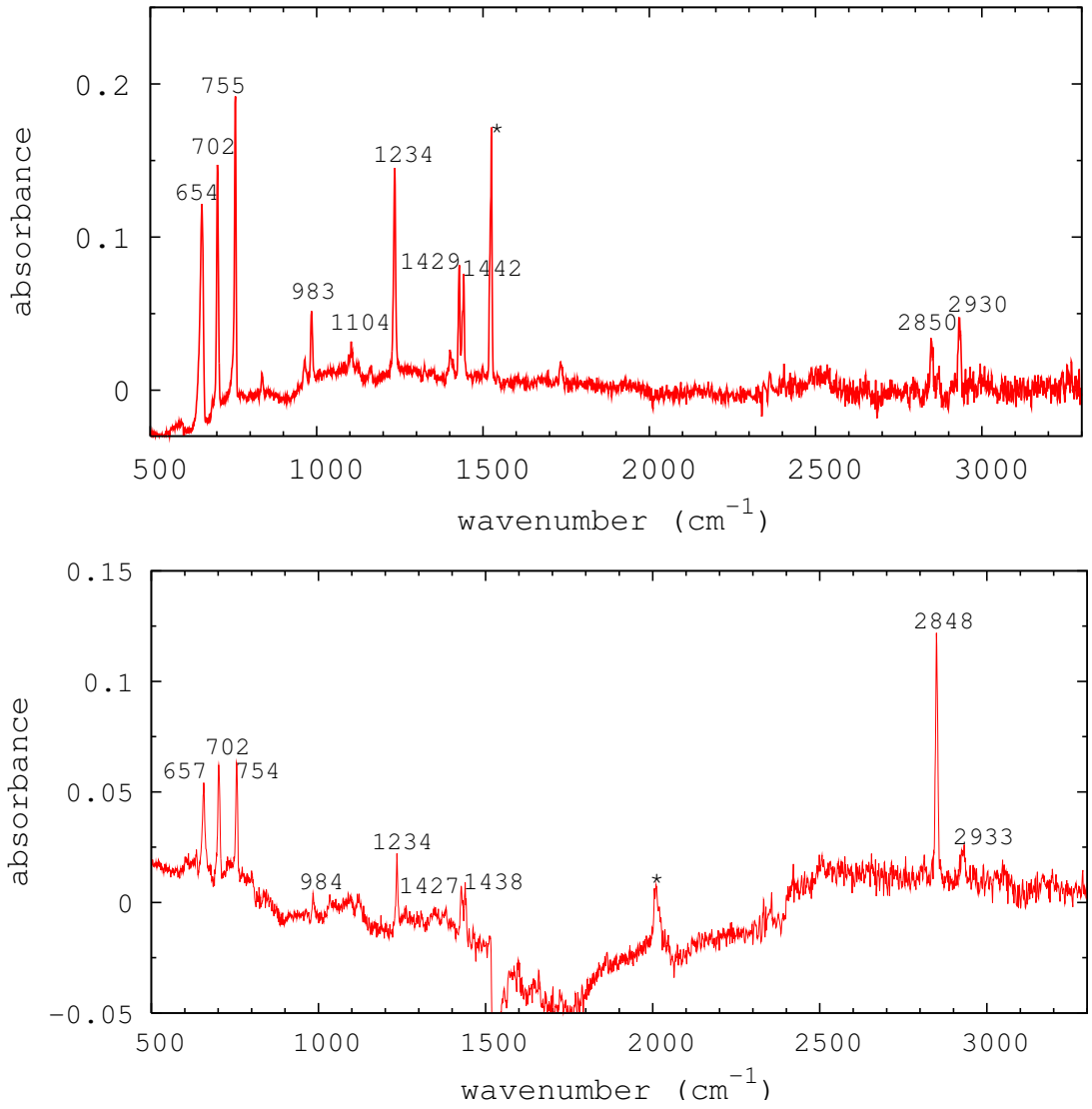

Figure 4.9: ***Top:*** *infrared spectrum of monochlorodimethylsulfide in a N_2 matrix;* ***bottom****: infrared spectrum of the final products from the reaction $DMS + Cl_2$ in a N_2 matrix (impurities are denoted by *)*

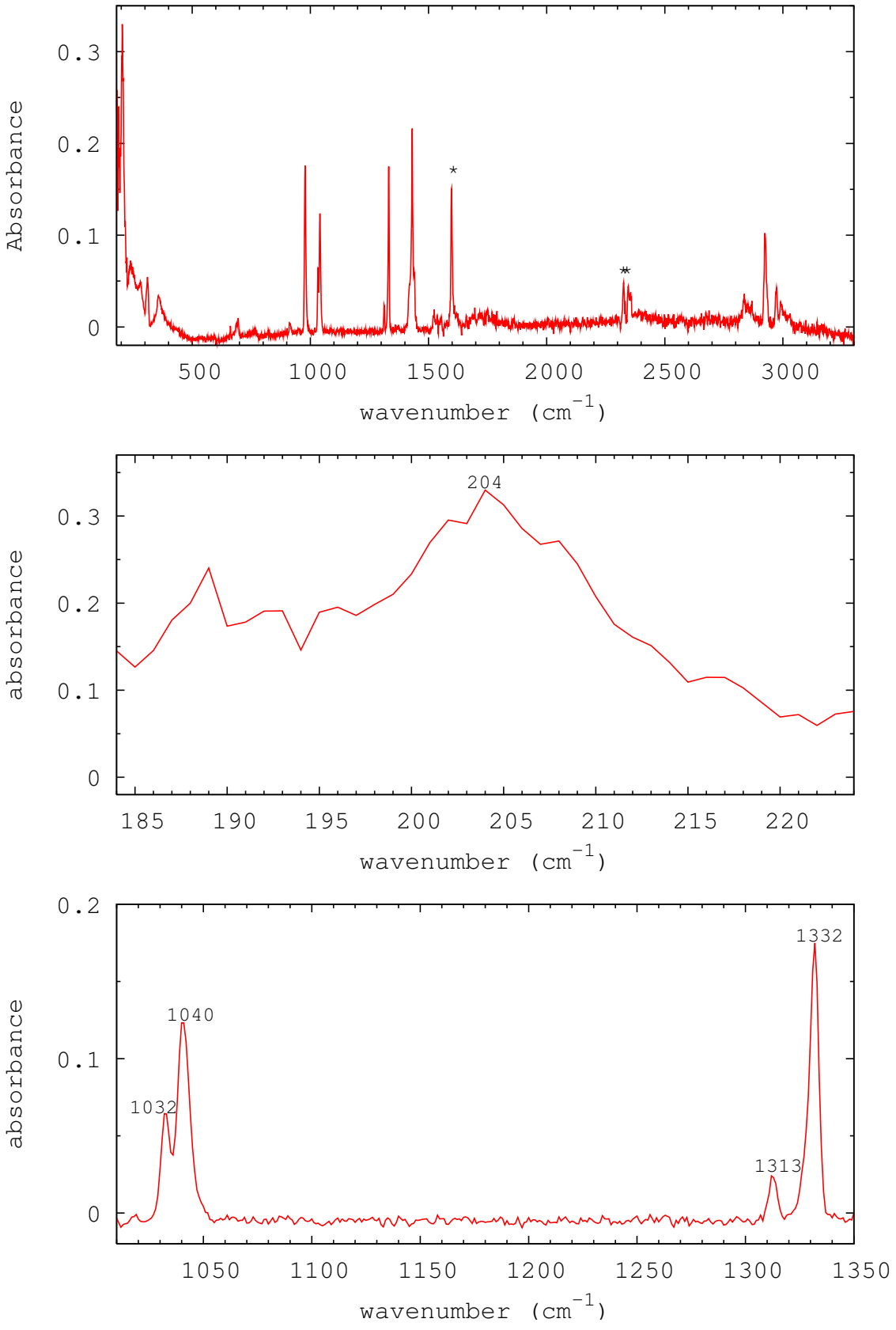

Figure 4.10: *DMS : Br_2 infrared spectrum in a nitrogen matrix with virtually no unreacted DMS(impurities are denoted by *)*

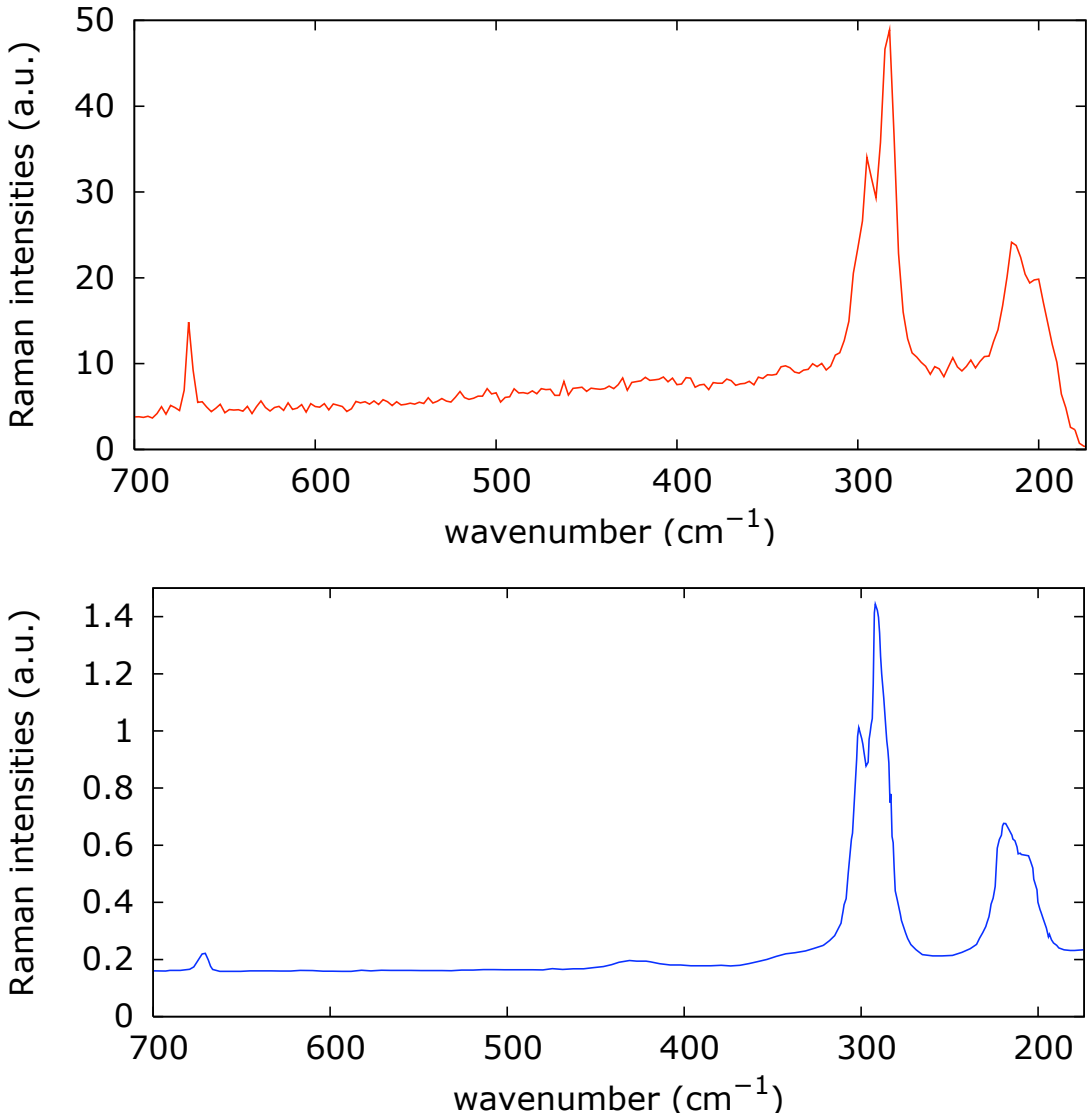

Figure 4.11: ***Top**: $DMS : Br_2$ Raman spectrum obtained in this work; **bottom**: $DMS : Br_2$ Raman spectrum by Askew et al. [87]*

This work	Work of Askew *et al.*[87]
202	204
215	215
283	285
294	295
303	304
669	672
717	720

Table 4.2: *Raman bands (cm^{-1}) observed for the $DMS : Br_2$ complex*

DMS+I_2

The reaction intermediate was studied also for the DMS+I_2 reaction; iodine in the gas-phase was obtained by heating some solid iodine, and a very weak reaction intermediate band was found at 1330 cm^{-1}, due to the low iodine vapour pressure. Then, an attempt was made to study the final products by mixing solid iodine and liquid DMS on a vacuum line. Again, spectra of the DMS:I_2 reaction intermediate were obtained, showing, this time, a clear band at 1331 cm^{-1} with a small amount of DMS present in the infrared spectra recorded (Figure 4.12). No clear band is present in the lower wavenumber part of the spectrum, as it appears to be very noisy. The compound, a liquid at room temperature, is very volatile and dark red coloured.

DMS+BrCl

An attempt to study the reaction intermediate of the DMS+BrCl reaction was also made.

The BrCl sample was obtained by mixing bromine and chlorine together, with initially an excess of chlorine. Then, the mixture was diluted with the matrix gas (nitrogen) and reacted with DMS just above the cold window at a distance of 2 cm. Since there was an excess of chlorine, a small amount of monochlorodimethylsulfide was found, with bands at 660, 701, 753, 1235 and 1427 cm^{-1}, together with the band due to HCl at 2849 cm^{-1} (see Figure 4.13). Also, bands at 283, 311, 337, 1045 and 1331 cm^{-1}, associated with the reaction intermediate, were observed. The bands are clearly different from those observed for $(CH_3)_2SCl_2$ in a nitrogen matrix (Figure 4.7).

However, the spectra recorded were not clear enough due to excess Cl_2 present in the BrCl sample. New experiments were then performed.

The spectrum in Figure 4.14 shows clearly the bands at 1043 and 1332 cm^{-1} which are characteristic of an intermediate (DMS:BrCl). Excess Br_2 was present in the BrCl sample, and that explains the band 204 cm^{-1} which is due to the DMS:Br_2 complex.

Experiments in order to observe the final products from this reaction, were also performed by i.r. matrix isolation. Two experiments were carried out: one with the BrCl

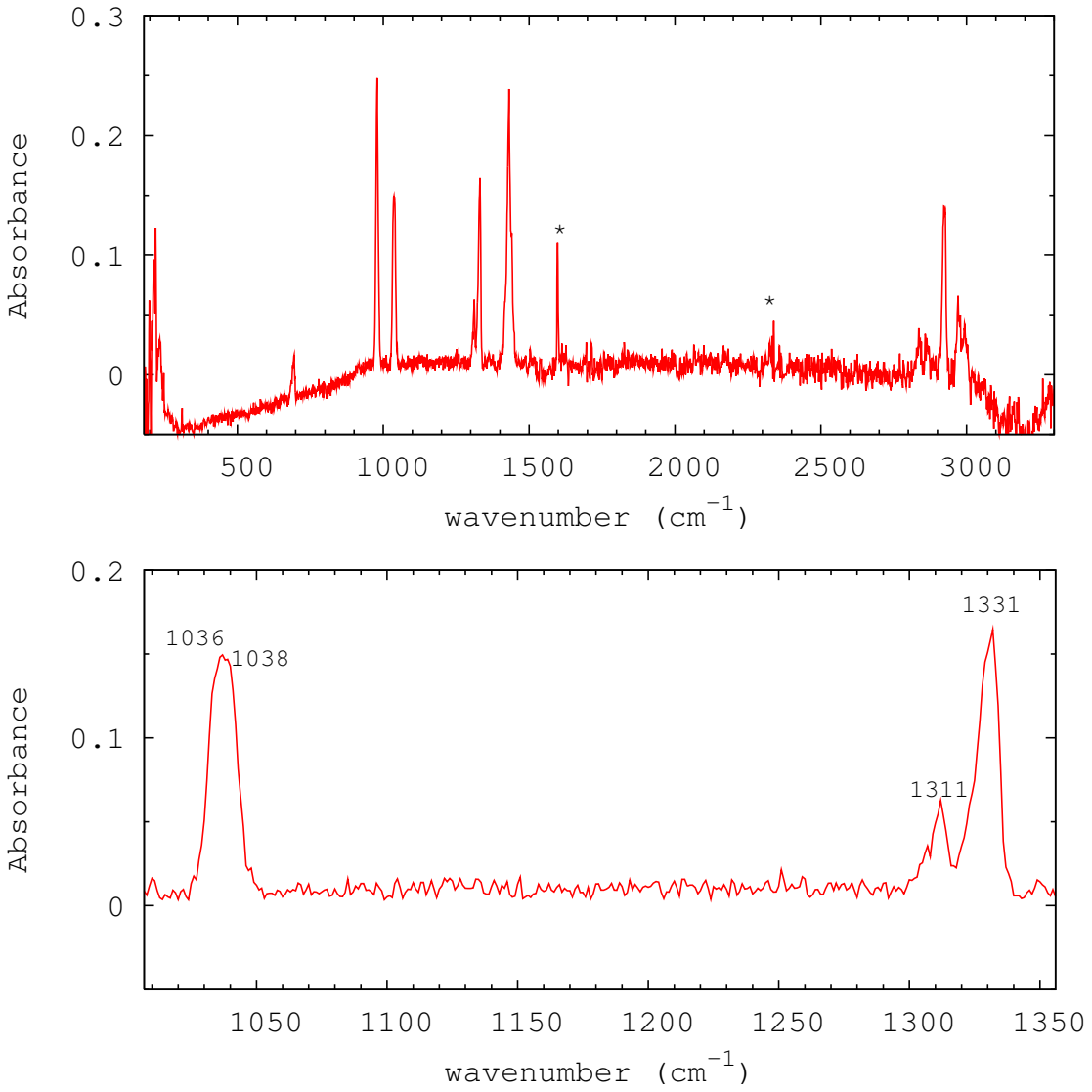

Figure 4.12: *DMS : I_2 infrared spectrum in a nitrogen matrix with virtually no unreacted DMS (impurities are denoted by *)*

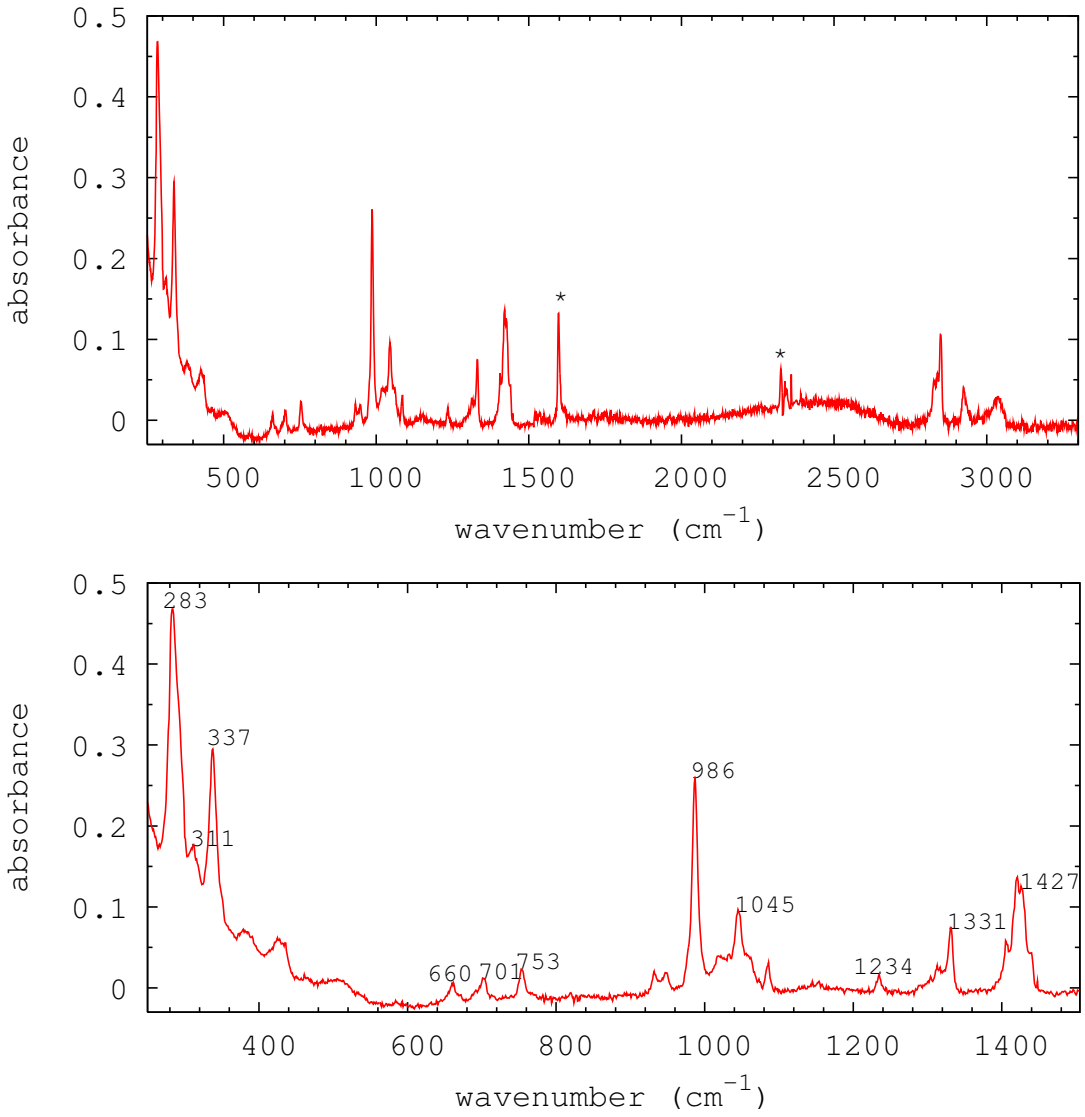

Figure 4.13: *DMS : BrCl infrared spectrum in a nitrogen matrix recorded with an excess of Cl_2 (impurities are denoted by *)*

sample prepared with excess Cl_2 and one with excess Br_2 (see Figure 4.15). Spectra obtained from both experiments do not show the characteristic bands associated with the van der Waals complexes observed in the other systems (i.e. DMS+Cl_2 and DMS+Br_2). Monochlorodimethylsulfide bands were observed as well as bands not yet identified, like a band at 593 cm^{-1}, a broad band at 960 cm^{-1} and a band at 1304 cm^{-1}. HCl is present and this fact might mean that the unidentified bands might belong to monobromodimethylsulfide. Unfortunately an infrared spectrum of monobromodimethylsulfide is not available from the literature.

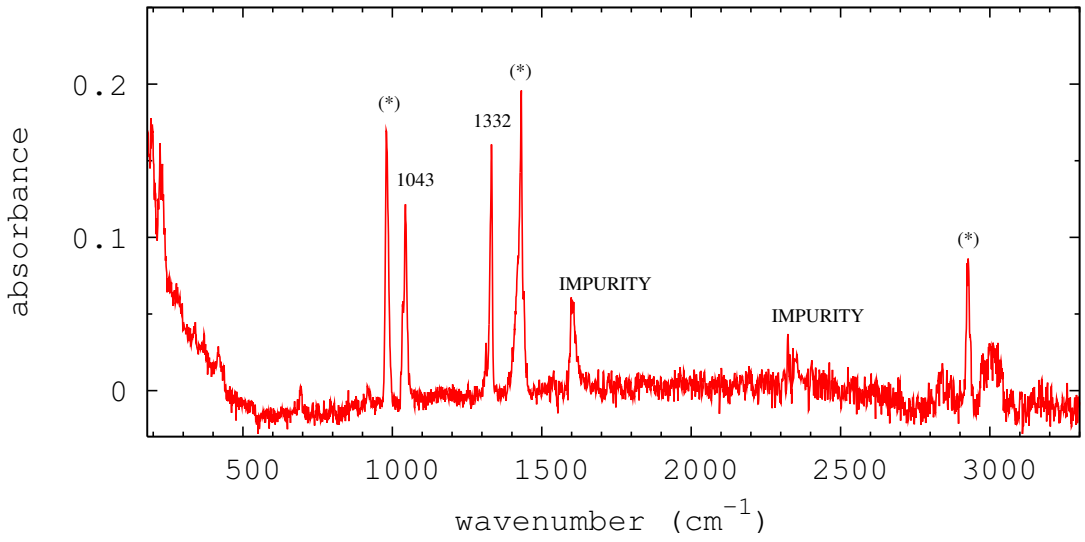

Figure 4.14: *Infrared spectrum of the DMS:BrCl reaction intermediate in a nitrogen matrix with excess Br_2 (bands marked with a '*' are overlapping of DMS, DMS:Br_2 and DMS:BrCl bands; bands marked with wavenumber values are thought to arise from DMS:BrCl complex)*

DMS+ICl reaction

Finally, the DMS+ICl reaction was studied by making reacting the sublimed ICl sampled and DMS in the flow tube inlet system. As expected, bands associated with a reaction intermediate were found, with bands at 1040 and 1333 cm^{-1}, with two broad bands at 297 and 335 cm^{-1}, as shown in Figure 4.16; this Figure shows clearly the two stretching vibration modes due to $I^{35}Cl$ and $I^{37}Cl$ at 368 and 375 cm^{-1}. In the spectra shown in

Figure 4.16, unreacted DMS is also present.

The final products of the DMS+ICl reaction were then studied by infrared matrix isolation. The compound obtained is a brown-orange coloured solid at room temperature.

In theory, two product channels are possible: CH_3SCH_2Cl+HI and CH_3SCH_2I+HCl. The experimental infrared spectra, showed some not very strong bands associated with monochlorodimethylsulfide; bands at 657, 702, 755 and 1234 cm^{-1} were observed (the other monochloro DMS bands were too weak in intensity to be observed), a band at 2850 cm^{-1}, that might be HCl, and the DMS:ICl complex characteristic bands, that is 297, 1040 and 1333 cm^{-1} were also observed (see Figure 4.16). No HI was present in the spectra (expected at 2237 cm^{-1} [89]). These results lead to the conclusion that the small amount of monochlorodimethylsulfide in the spectra might come from the dissociation of a part of the ICl sample in to I_2 and Cl_2, suggesting that monochlorodimethylsulfide and HCl are not final products of the reaction (but arise from the DMS+Cl_2 reaction) and that the DMS+ICl reaction does not go further the formation of the DMS:ICl complex. The DMS+I_2 complex formation is also possible but the reaction intermediate characteristic bands cannot be distinguished from those of the other complexes and the band in the lower part of the spectrum cannot be seen clearly, as explained before.

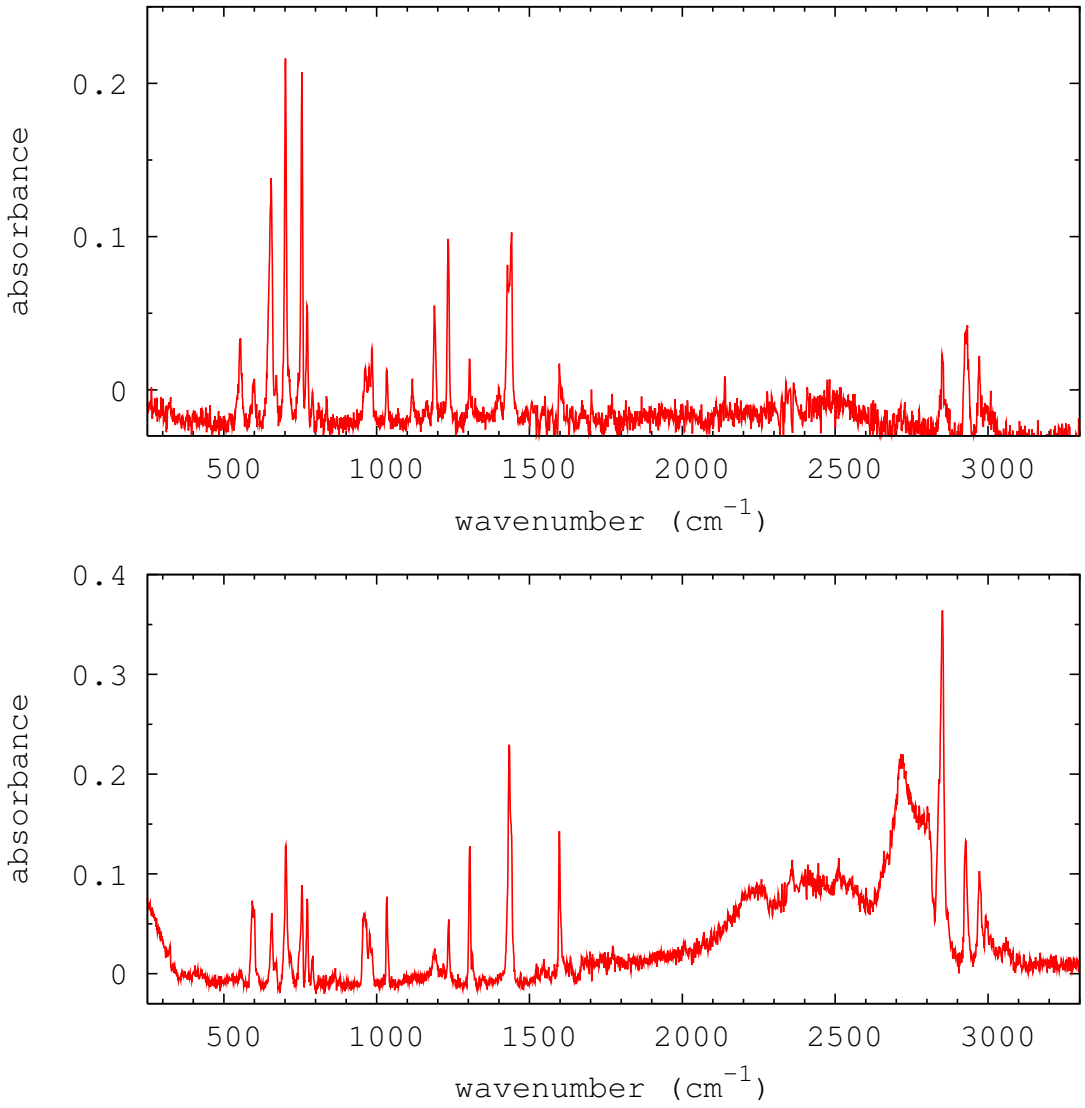

Figure 4.15: ***Top****:Infrared spectrum of the $DMS + BrCl$ final products with excess Cl_2 in a nitrogen matrix;* ***bottom****: infrared spectrum of the DMS+BrCl final products with excess Br_2 in a nitrogen matrix (the very broad band is solid HCl)*

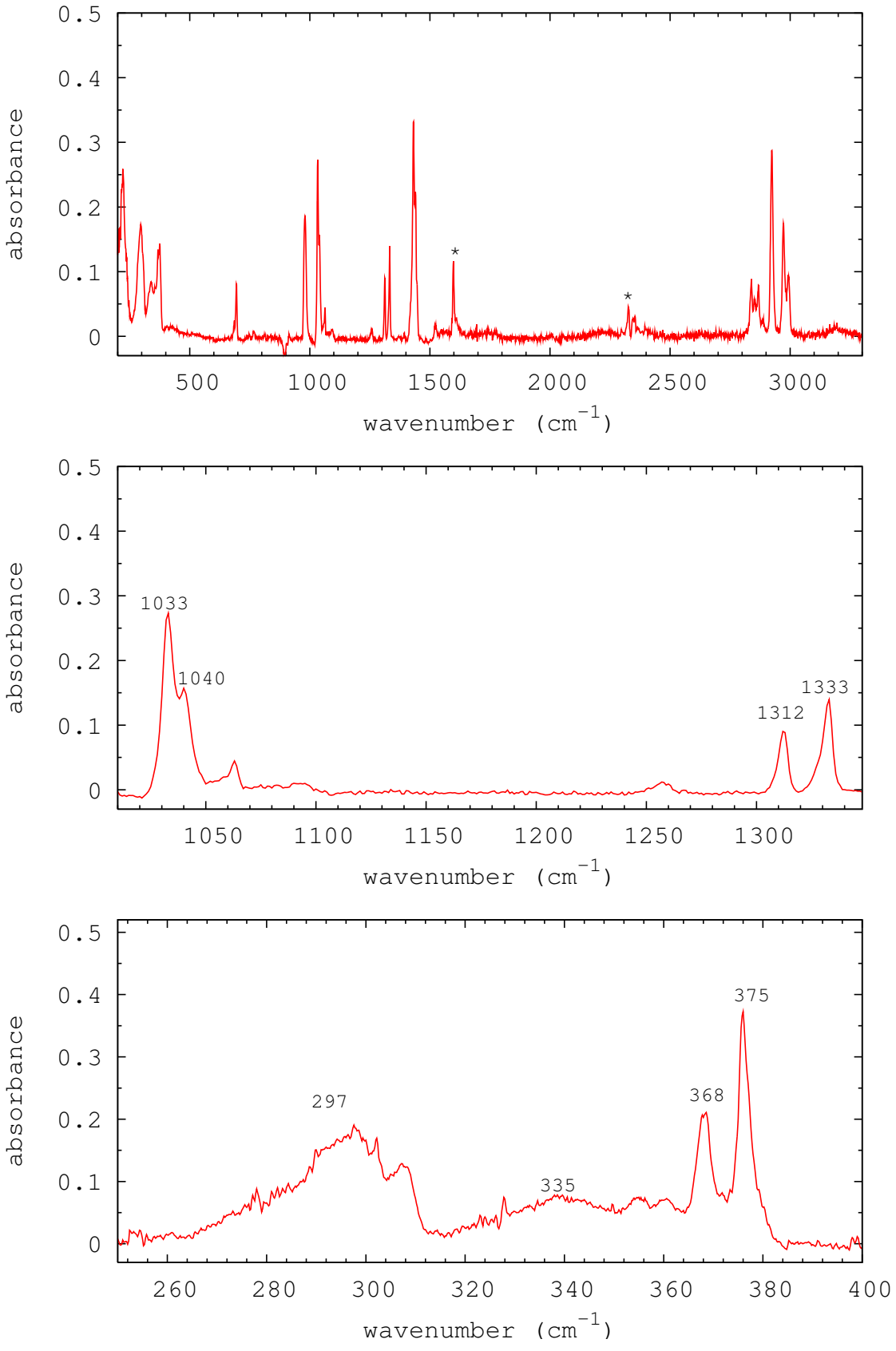

Figure 4.16: *DMS : ICl infrared spectrum recorded in a nitrogen matrix with excess DMS*

4.3 Molecular orbital calculations

Molecular orbital calculations were then performed using the Gaussian programme [90] for the each reaction, to compute the minimum energies geometries and infrared spectra of the reactants, reactive intermediates and reaction products. These calculations were carried out at both the B3LYP [76, 77] and MP2 [78] levels of theory. For the DMS+Cl_2 and DMS+Br_2 reactions, cc-pVTZ basis sets [74] were used at the B3LYP level and cc-pVDZ basis sets [73] were used at the MP2 level, except for the bromine atom for which the aug-cc-pVTZ basis set, at the B3LYP level of theory, and the aug-cc-pVDZ basis, at the MP2 level of theory, basis sets were utilized [73, 74]. Also, in the study of the DMS+BrCl, DMS+I_2 and DMS+ICl reactions, an ECP basis set was chosen for the bromine atom and the iodine atom.

The structure of each reaction intermediate was initially thought to be as the same proposed by Dyke *et al.* [13] for the $(CH_3)_2SCl_2$ covalent complex, in which the sulphur atom is four-coordinate.

The geometry optimization for the DMS:I_2 and DMS:ICl complexes was not successful at the B3LYP level of theory, but a minimum energy geometry was obtained at the MP2 level in both cases.

The agreement with the experimental infrared band positions is reasonably good. Although a shift is present in the band positions, the computed spectra reproduce quite well the experimental spectra. Despite that, the computed relative bands intensities show only modest agreement with the experimental relative band intensities.

With the support of the Molden programme, the normal modes associated with the vibrations at about 1331 cm^{-1} and 1040 cm^{-1} were found to be C-H bends in all cases while the lower frequency vibrations can be assigned to stretching and bending vibrations between the sulfur atom and the halogen atoms.

As mentioned before, the dimethyl sulfide-bromine complex has been previously studied by Raman spectroscopy [86, 87] and X-ray diffraction [88] in the solid phase and the structure proposed in these previous works for the compound in the solid phase, is a

Me_2S-Br_2 charge-transfer structure. In the study of the DMS+Cl_2 reaction intermediate at the University of Southampton by PES [14], a minimum energy structure was optimized for the dimethyl sulfide-chlorine complex.

Given the very poor agreement between the computed intensities and the experimental intensities in the case of the covalent structure, a van der Waals structure for the reaction intermediates was then considered.

DMS+Cl_2 reaction

The computed infrared spectrum obtained for the van der Waals minimum energy structure, is in better agreement with the experimental i.r. matrix isolation spectrum than the computed spectrum for the covalent structure (Figure 4.17).

An energy diagram was also plotted in order to understand better the relative positions of energy minima in the DMS+Cl_2 reaction, and transition states were also computed and included in the diagram (see Figure 4.18).

When DMS and Cl_2 are brought together, the DMS:Cl_2 complex is formed. From this structure the reaction proceeds through the formation of another structure which has all real frequencies and can be described as $(CH_3)_2$SCl:Cl complex. A transition state is found (TS1) to connect this structure with the DMS(Cl_2) covalent structure. If one of the S-Cl bonds is broken in this covalent structure and the "liberated" chlorine atom moves towards one of the methyl groups, and a second transition state is formed (TS2). The imaginary frequency of this transition state corresponds to a movement bringing the Cl atom very close to one of the hydrogens, which is detached from the methyl group to form HCl. HCl remains attached to the rest of the molecule forming an intermediate $CH_3SCl{=}CH_2$:HCl. From $CH_3SCl{=}CH_2$:HCl, if the chlorine attached to the sulphur atom moves towards the terminal methylene group in a concerted movement with the HCl molecule, MClDMS:HCl is obtained. The final products are MClDMS and HCl. These results confirm the previous work on the DMS+Cl_2 reaction [14].

It might be possible that, when the reaction occurs in a matrix, that it does not go

further the van der Waals complex; this structure is therefore a good candidate for study obtained by infrared matrix isolation but not for study obtained in the gas-phase by PES [13, 14]. Attempts were then made in order to detect the covalent complex by infrared matrix isolation spectroscopy.

The inlet system used in these experiments (see Figure 4.20) was different from the one used in the previous experiments, in that a twin-jet mixing was used rather than a coaxial system. Also, the reaction path before the frozen window was slightly shorter. The spectrum in Figure 4.21 shows the characteristic reaction intermediate bands plus a band at 480 cm^{-1} that was not observed either in previous work [81] or in other Cl_2+DMS experiments in this work in which the 1332, 1040 and 338 cm^{-1} bands were observed. The 480 cm^{-1} band could arise from the DMS+Cl_2 covalent structure. Blank spectra were run on the Cl_2 sample to check that no impurity was present.

Similar experiments were also performed using Ar as the matrix gas and a band has been observed at around 500 cm^{-1}. In previous work [82] on the DMS+Cl_2 reaction, by using infrared matrix isolation spectroscopy and Ar as matrix gas, a band has been detected at 525 cm^{-1}. The difference in wavenumbers between these two values is too high to think that these two values might come from the same vibrational mode of a reaction intermediate, although the observed band at 480 cm^{-1} in nitrogen (500 cm^{-1} in argon) is broad.

DMS+Br_2 reaction

A van der Waals structure has also been computed for the reaction intermediate from the DMS+Br_2 reaction and the correspective i.r. spectrum is shown in Figure 4.22.

An energy diagram was also computed for the DMS/Br_2 system at the MP2 level of theory (see Figure 4.23). However, in this case the difference in energy between the van der Waals and the covalent structure is small (0.56 $kcalmol^{-1}$) but the energy barrier, indicated by the transition state TS1, is much higher (15 $kcalmol^{-1}$). This explains why the DMS + Br_2 reaction under ambient conditions, unlike DMS + Cl_2 reaction, proceeds

no further than the 1:1 van der Waals adduct.

The steps of this reaction are similar to the ones of the DMS+Cl_2 reaction and they are summarised in Figure 4.23.

DMS+I_2 reaction

In the iodine case, the agreement between the experimental spectrum and the computed infrared spectrum for the van der Waals structure is really good (see Figure 4.25). The position and the intensity of the bands for the van der Waals structure are much more in agreement with respect to the covalent structure bands.

As shown in the energy diagram (see Figure 4.26), the van der Waals structure is the lowest in energy, while the covalent structure and the final products are higher in energy with respect to the reactants, which could explain why the reaction does not go further the formation of the adduct.

A search of transition states for this reaction has not been done, but as in the bromine case, the energy barrier between the two intermediates might be high.

DMS+BrCl reaction

Two van der Waals structures were computed for the DMS/BrCl case and the DMS:BrCl van der Waals structure is lower in energy than the DMS:ClBr van der Waals structure at the MP2 level of theory (see Figure 4.29). In the work of Askew *et al.* [87], in a reaction between aluminium bromide, bromine and dimethyl sulfide in dichloromethane, a complex corresponding to C_2H_6SBrCl has been isolated as an unstable yellow solid. From the Raman spectra obtained in this work [87], a structure of DMS:BrCl seemed more probable from the DMS+BrCl reaction.

Comparing the experimental infrared spectrum with the two infrared computed spectra (one for the DMS:BrCl van der Waals complex and one for DMS:ClBr van der Waals complex), good agreement in wavenumber and in intensity is found with the experimental spectrum in this present work, but no decision could be made as to whether the structure

is Me_2S-BrCl or Me_2S-ClBr (see Figure 4.27 and 4.28). However, the computed relative energies at the MP2 level of theory of Me_2S-BrCl or Me_2S-ClBr show that the Me_2S-BrCl structure is lower in energy with respect to the Me_2S-ClBr complex energy by 6.8 kcal mol^{-1} (see Figure 4.29), showing that the Me_2S-BrCl structure is likely to be the structure for the DMS:BrCl van der Waals complex. Below 500 cm^{-1}, the computed spectra show a strong band in this region which is not observed in the experimental infrared spectrum. This is thought to be due to a reduction in detection efficiency in this region.

DMS+ICl reaction

Also in the case of the DMS/ICl system two structures were considered at the MP2 level of theory. A minimum energy structure was obtained for DMS+ICl but for the DMS:ClI structure it was not possible to obtain a minimum energy geometry. The comparison between the experimental and computed spectrum is then shown in Figure 4.30.

As in the DMS+BrCl case, two channels are possible: CH_3SCH_2Cl+HI and CH_3SCH_2I+HCl. Figure 4.31 shows that at the MP2 level of theory, the second possibility is lower in energy, as expected.

The computed spectrum for the van der Waals structure is more in agreement than the computed spectrum for the covalent structure. However, the agreement is not so good as in the iodine case as the intensity of the bands seems to match less.

Future work is then necessary for a better understanding of the mechanism of this reaction, investigating transition states and energy barriers.

4.4 Photoelectron spectroscopy experiments

In order to obtain an understanding of the structure of the reaction intermediates in the gas-phase, PES experiments were performed. The photoelectron spectrometer used is described in Chapter 2.

Attempts were made to study the DMS:Br_2, DMS:I_2 and DMS:ICl compounds. At first, u.v.-photoelectron spectra of DMS and the halogen molecules only were run separately

and compared with photoelectron spectra in the literature [91].

Then, the compounds were prepared by making them on a vacuum line and pumping on the products through a needle valve attached to the inlet system of the spectrometer. Only bands of DMS and the molecular halogens (Br_2, I_2 and ICl) were observed in these experiments.

The inlet systems described in Chapter 2 were then used to perform the reactions in the gas-phase and the distance between the mixing point and the photon beam was changed, but no new bands in the spectra were observed.

In the case of the DMS/Br_2 system, both open and inlet systems with a reduced exit hole were used. In the latter case, a yellow deposit was observed on the inner wall of the outer tube when DMS and Br_2 were reacted. This suggests that a product is formed in the gas-phase but a third body is needed to stabilise it and this role is fulfilled by the walls of the inlet system.

The reaction between dimethyl sulfide and BrCl was also studied in the gas phase. As bromine does not appear to react with DMS in the gas phase, the BrCl sample was prepared with excess bromine so that new bands in the spectra recorded must be associated with a reaction intermediate or final products from the DMS+BrCl reaction.

The spectrum obtained from the BrCl sample (a Br_2 and Cl_2 mixture with excess Br_2) was compared with the BrCl spectrum in the literature [92] and it showed good agreement. After that, the reaction was carried out by using an inlet system with a constricted exit (2 mm hole). As happened in the case of the DMS:Br_2 reaction, a yellow/orange solid deposit formed on the wall of the inner tube. The spectra recorded, show bands of DMS, BrCl, Br_2 and very weak bands at 9.18 eV and at 12.66 and 12.72 eV. The 9.18 eV band belongs to MClDMS (monochlorodimethylsulfide) [13] while the other two are HCl. The calibration was carried out using the first bands of DMS and Br_2 whose PE spectra are well known [91].

The compound deposited on the wall was heated; this resulted in the previously observed PE bands (e.g. MClDMS and HCl) being observed with increased intensity. From

the spectrum shown in Figure 4.32 the first band of DMS can be seen at 8.72 eV, the first MClDMS band at 9.18 eV can be seen followed by the Br_2 and BrCl bands, and the HCl bands. The remaining bands belong to DMS, MClDMS and Br_2. The presence of the the MClDMS band together with the weak bands associated to HCl might come from the low concentration of Cl_2 in the BrCl sample prepared. In fact, it appeared hard to obtain a sample with *virtually* no Cl_2 present. If the complex is described as in the work by Askew et al. [87], that is as an unstable yellow solid with a $(CH_3)_2$S-BrCl charge transfer structure, when the compound is heated, dissociation of the BrCl molecule will occur giving rise to Cl_2+Br_2, and hence the DMS+Cl_2 reaction will occur.

4.5 Discussion and conclusion

The reactions of DMS with Br_2, I_2, ICl and BrCl were studied by infrared matrix isolation spectroscopy and u.v.-photoelectron spectroscopy with the support of *ab initio* molecular calculations.

It is well estabilished now that the DMS+Cl_2 reaction at room temperature and low pressure leads to the formation of MClDMS and HCl as final products, passing through the covalent reaction intermediate, DMS(Cl_2), that has been detected by u.v.-PES [13]. The present work showed that a van der Waals adduct is also formed just after DMS and Cl_2 are brought together, and it can be easily observed by infrared spectroscopy in a matrix at low temperatures.

The results described above show that under ambient conditions, unlike the DMS+Cl_2 reaction, the DMS+Br_2, DMS+I_2, DMS+ICl reactions proceed no further than the van der Waals adducts, that in each case dissociate at low pressure. In fact, attempts to observe these molecules in the gas-phase by using u.v.-PES proved unsuccessful and this suggests that a third body is necessary to stabilise these van der Waals complexes. The role of the third body in this work was fulfilled by the matrix and by the walls of the inlet system in the case of the tube with the constricted exit hole. In the atmosphere, a similar role can be played by N_2, O_2 or by particles and cloud surfaces.

A different situation appears in the case of the DMS+BrCl reaction. Experiments aimed at identifying a reaction intermediate by infrared matrix isolation spectroscopy, showed bands characteristic of the van der Waals complex, while the experiments performed to observe the final products did not give a clear understanding of the reaction path.

Two channels are possible: MClDMS+HBr and MBrDMS +HCl. Bands belonging to MClDMS and HCl were observed as in the PES experiments, but no HBr band either in a matrix (2546 cm^{-1} [89]) or in the gas phase was observed. A dissociation of the DMS:BrCl complex to give DMS and BrCl, which will dissociate partially to Br_2 and Cl_2, could lead to the reaction of DMS and Cl_2 to give MClDMS and HCl. Unknown bands were observed in the i.r. matrix isolation experiments but only DMS and and Br_2 were seen in the gas-phase PES experiments.

The study of this reaction appeared to be the most difficult, probably due to the complex preparation of the BrCl sample. Future work focused on this reaction by both techniques is then necessary to fully understand the reaction mechanism.

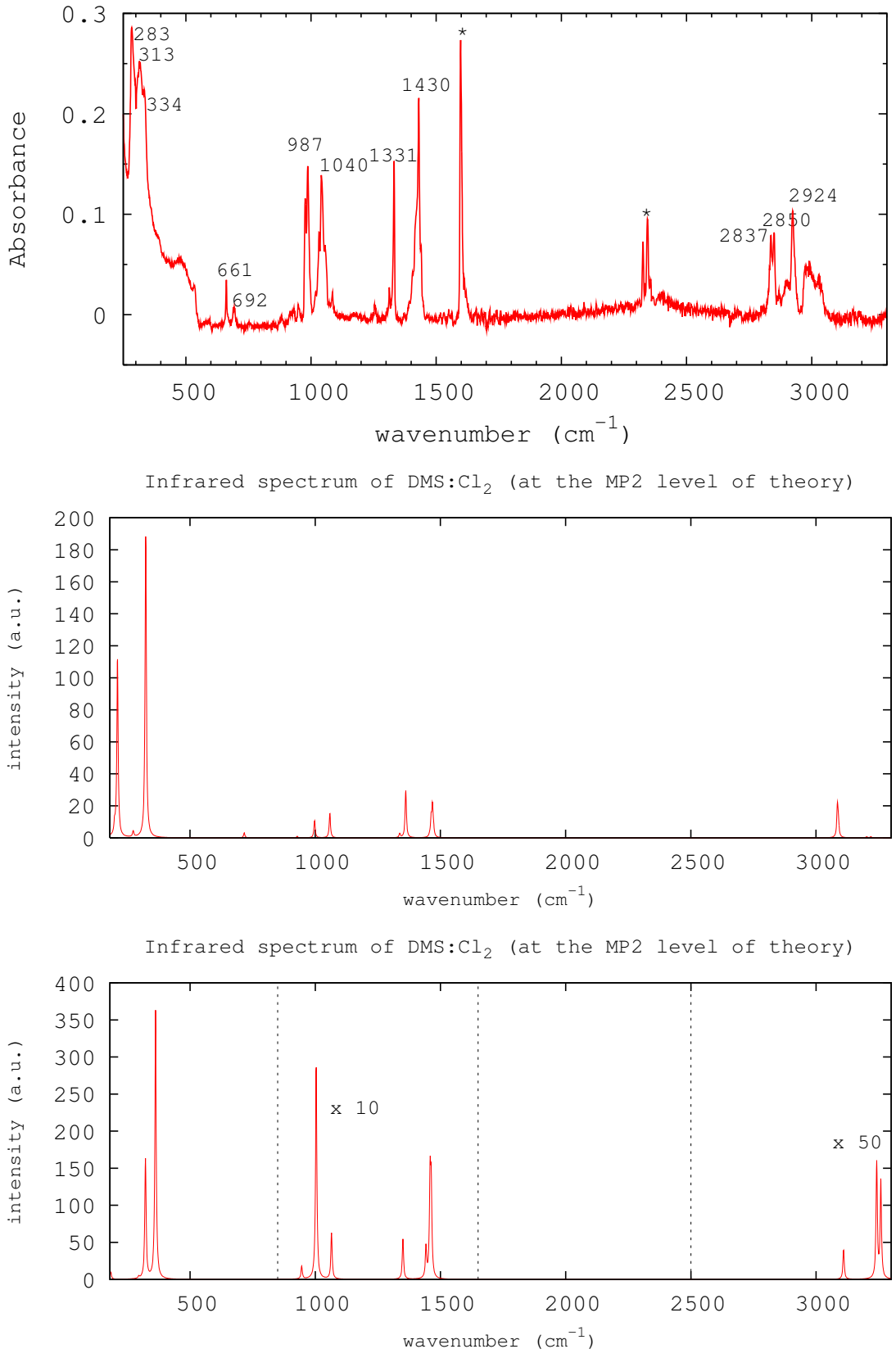

Figure 4.17: ***Top****: $DMS : Cl_2$ experimental ir spectrum (impurities are denoted by *);* ***middle****: $DMS : Cl_2$ charge transfer complex computed spectrum;* ***bottom****: $DMS : Cl_2$ covalent complex computed spectrum*

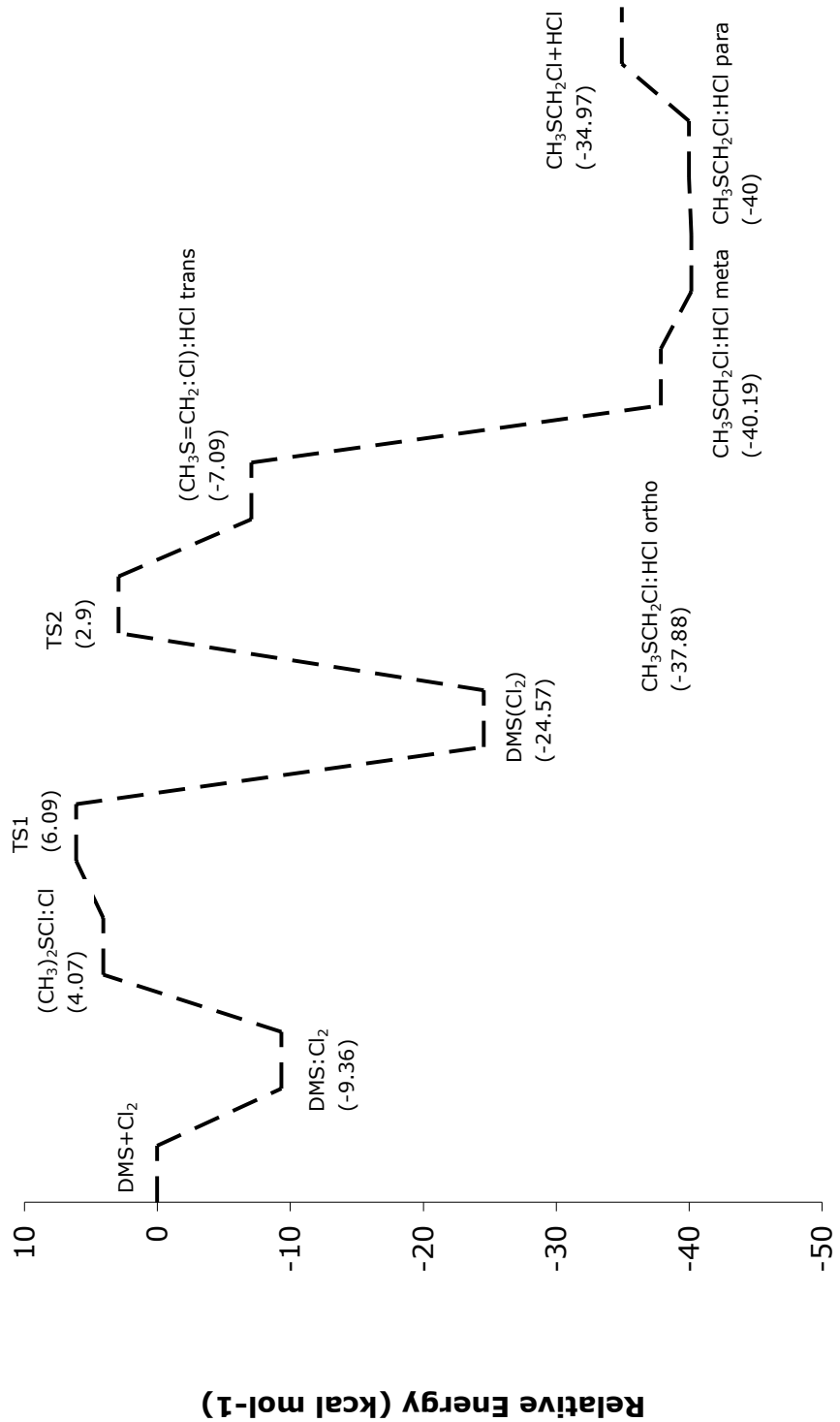

Figure 4.18: *Energy diagram for the DMS+Cl_2 reaction computed at the MP2 level of theory*

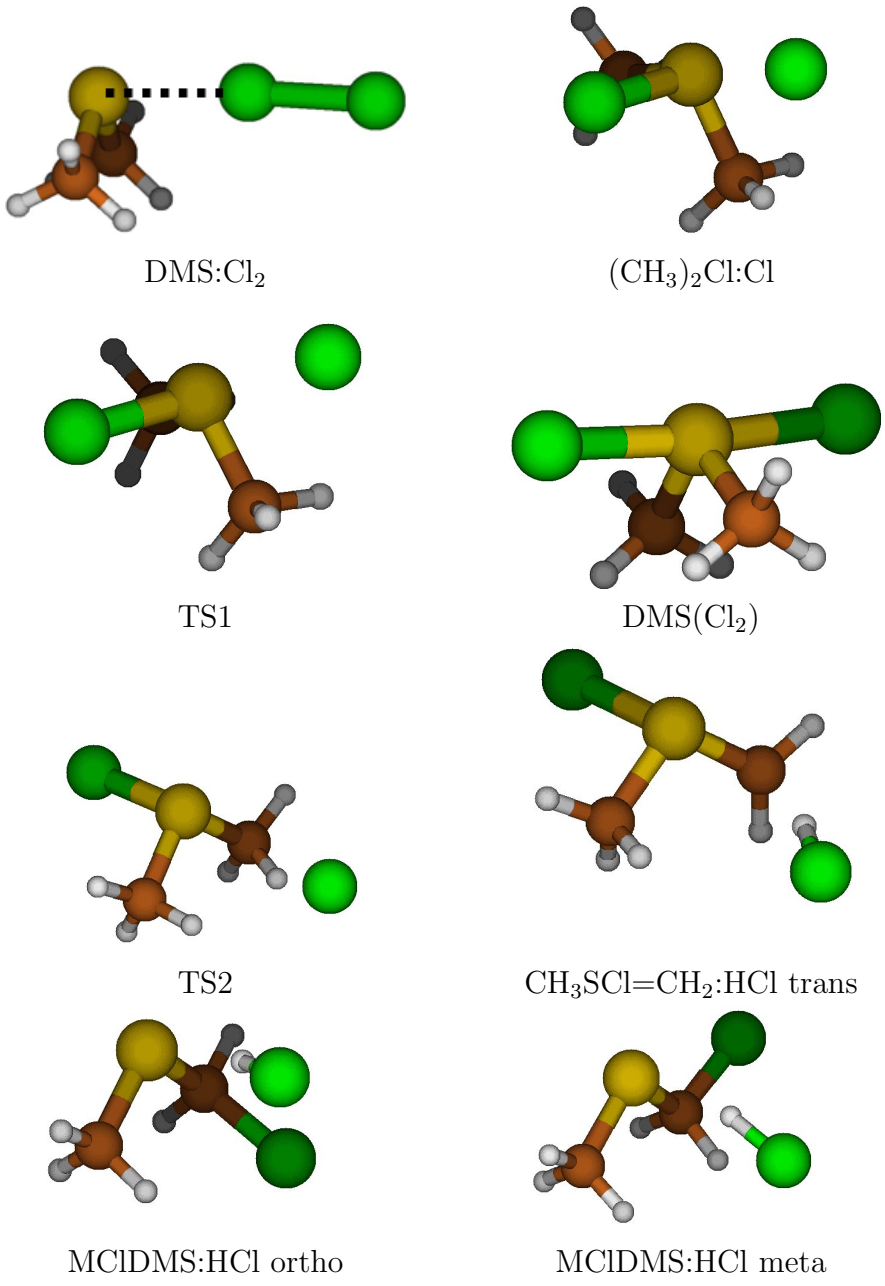

Figure 4.19: *Geometries of intermediates and transition states of the DMS+Cl_2 reaction at the MP2 level of theory computed in this work*

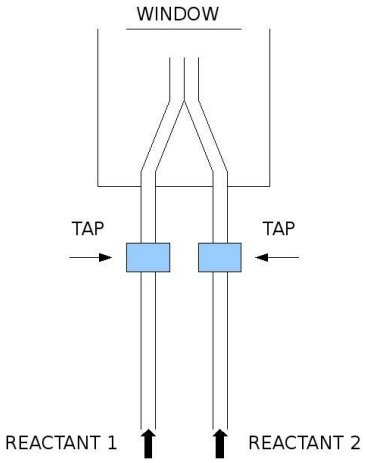

Figure 4.20: *Twin-jet inlet system used during the infrared matrix isolation experiments in attempts to detect the DMS(Cl_2) covalent structure*

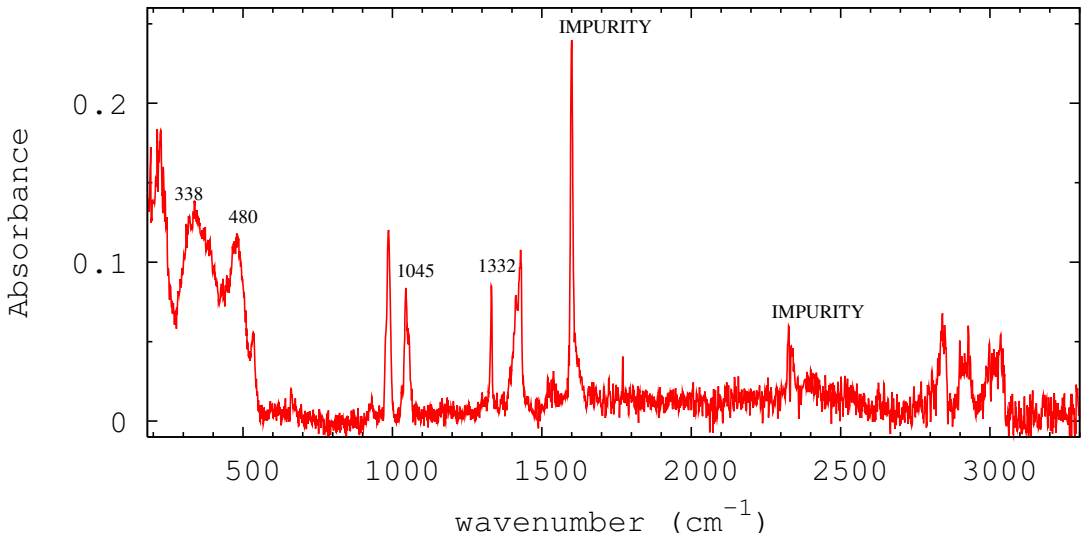

Figure 4.21: *Infrared spectrum DMS:Cl_2 reaction intermediate in a nitrogen matrix. The bands at 338, 1045 and 1332 cm^{-1} are believed to arise from the DMS:Cl_2 van der Waals complex. The band at 480 cm^{-1} is believed to arise from the covalent complex. Other bands arise from overlapped bands of the DMS:Cl_2 complexes and DMS.*

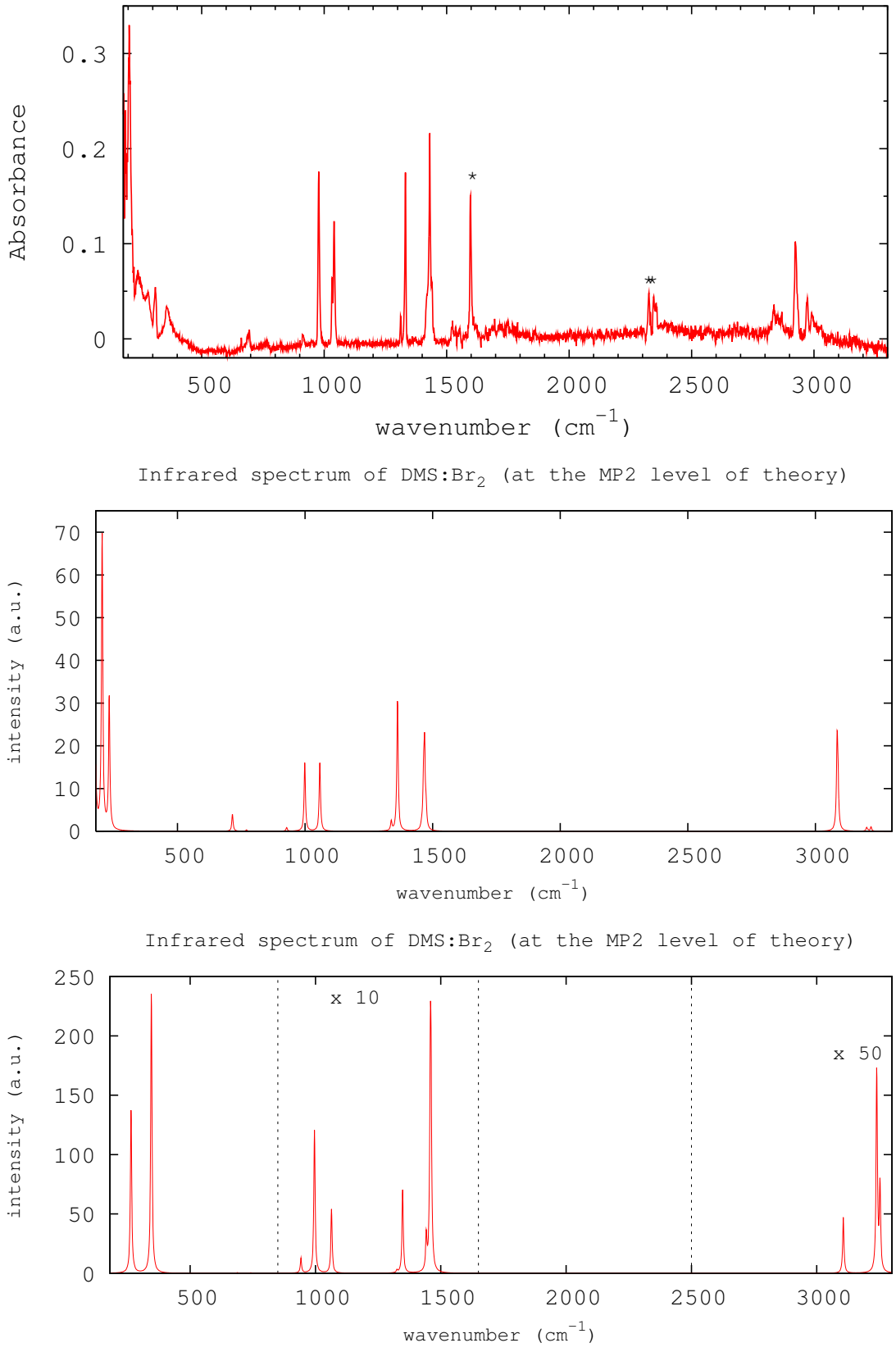

Figure 4.22: ***Top****: $DMS : Br_2$ experimental ir spectrum (impurities are denoted by *);* ***middle****: $DMS : Br2_2$ charge transfer complex computed spectrum;* ***bottom****: $DMS : Br_2$ covalent complex computed spectrum*

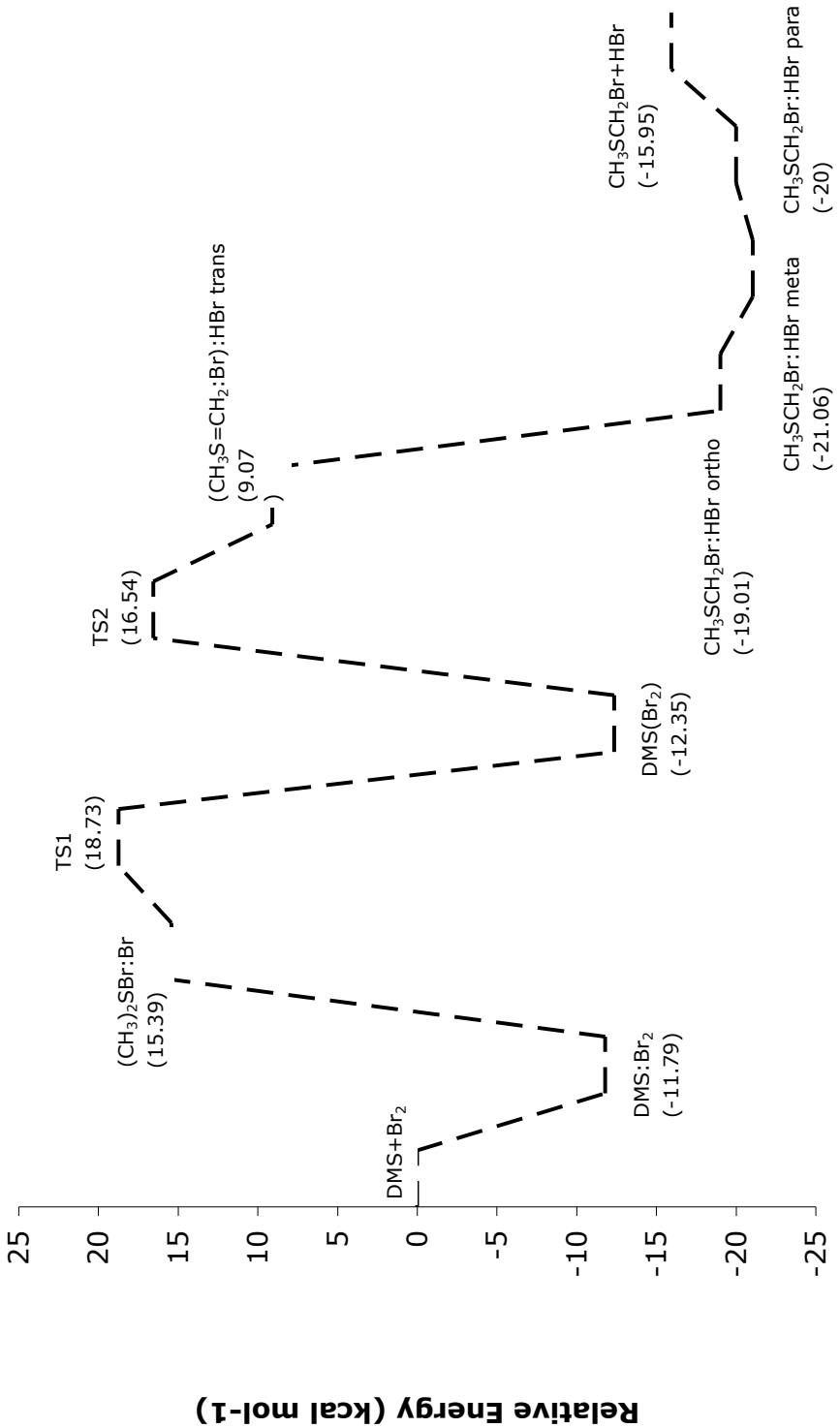

Figure 4.23: *Energy diagram for the DMS+Br_2 reaction computed at the MP2 level of theory*

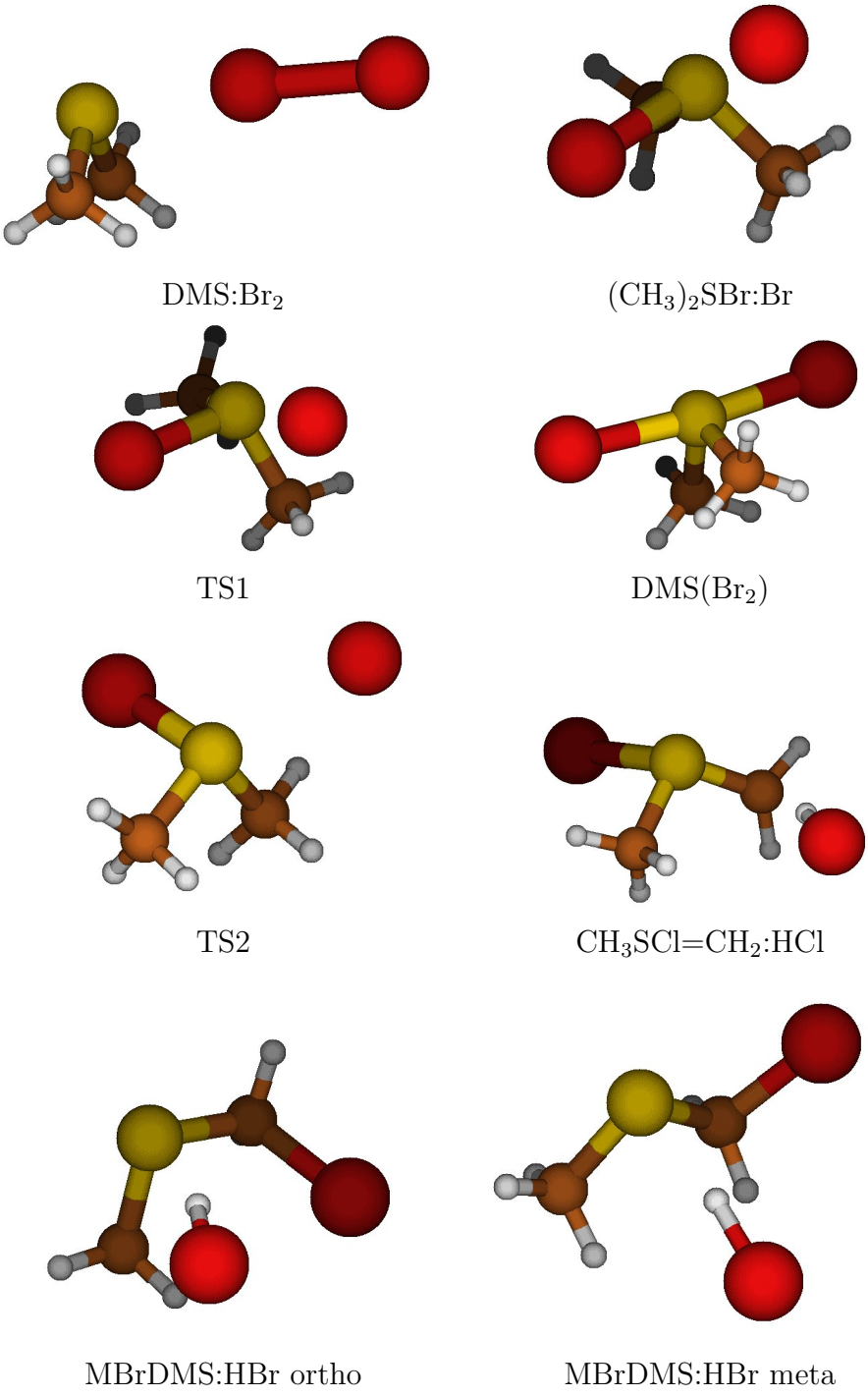

Figure 4.24: *Geometries of intermediates and transition states of the DMS+Br_2 reaction at the MP2 level of theory computed in this work*

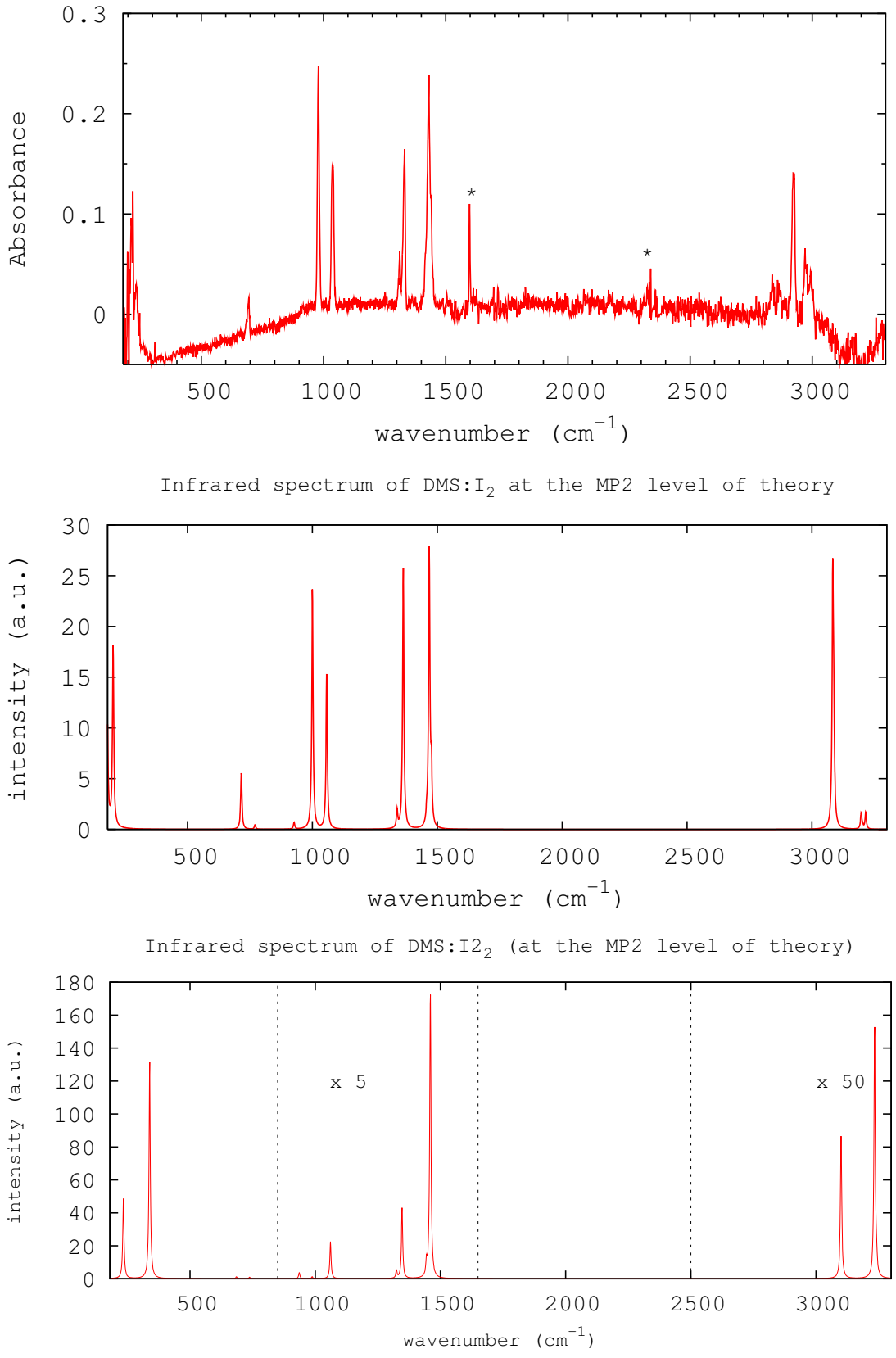

Figure 4.25: ***Top****: $DMS : I_2$ experimental ir spectrum (impurities are denoted by *);* ***middle****: $DMS : I_2$ charge transfer complex computed spectrum;* ***bottom****: $DMS : I_2$ covalent complex computed spectrum*

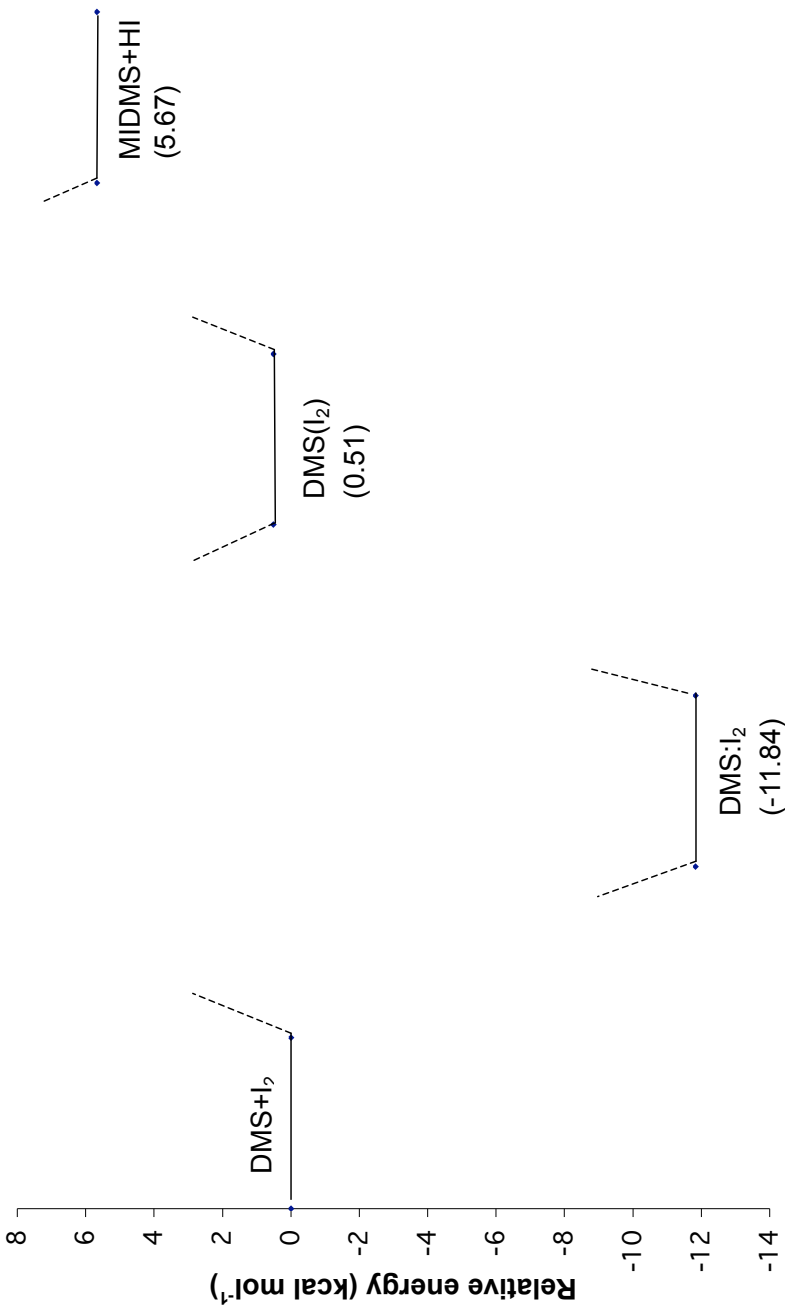

Figure 4.26: *Energy diagram for the DMS+I_2 reaction at the MP2 level of theory*

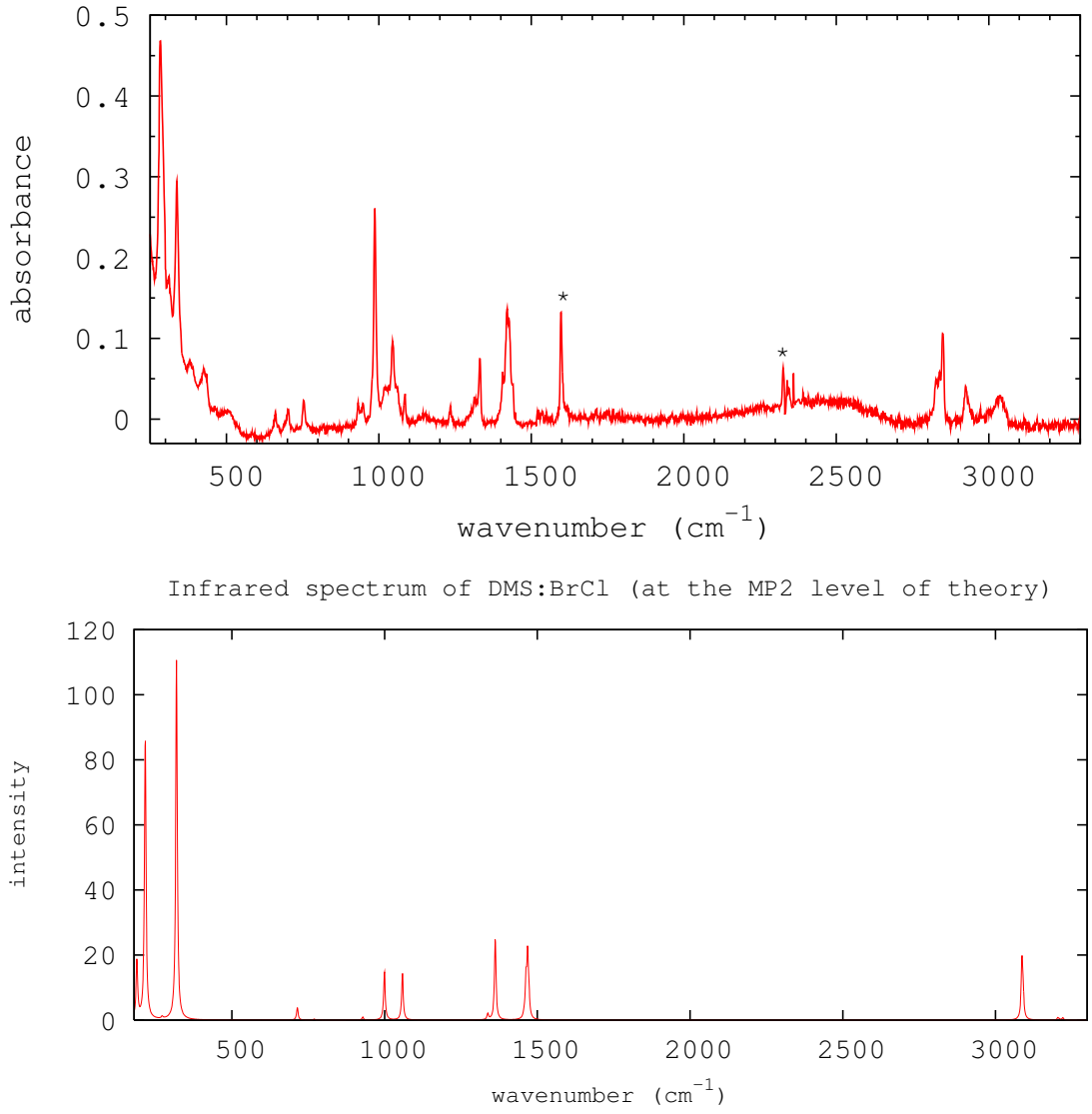

Figure 4.27: ***Top****: $DMS : BrCl$ experimental ir spectrum (impurities are denoted by *);* ***bottom****: $DMS : BrCl$ charge transfer complex computed spectrum*

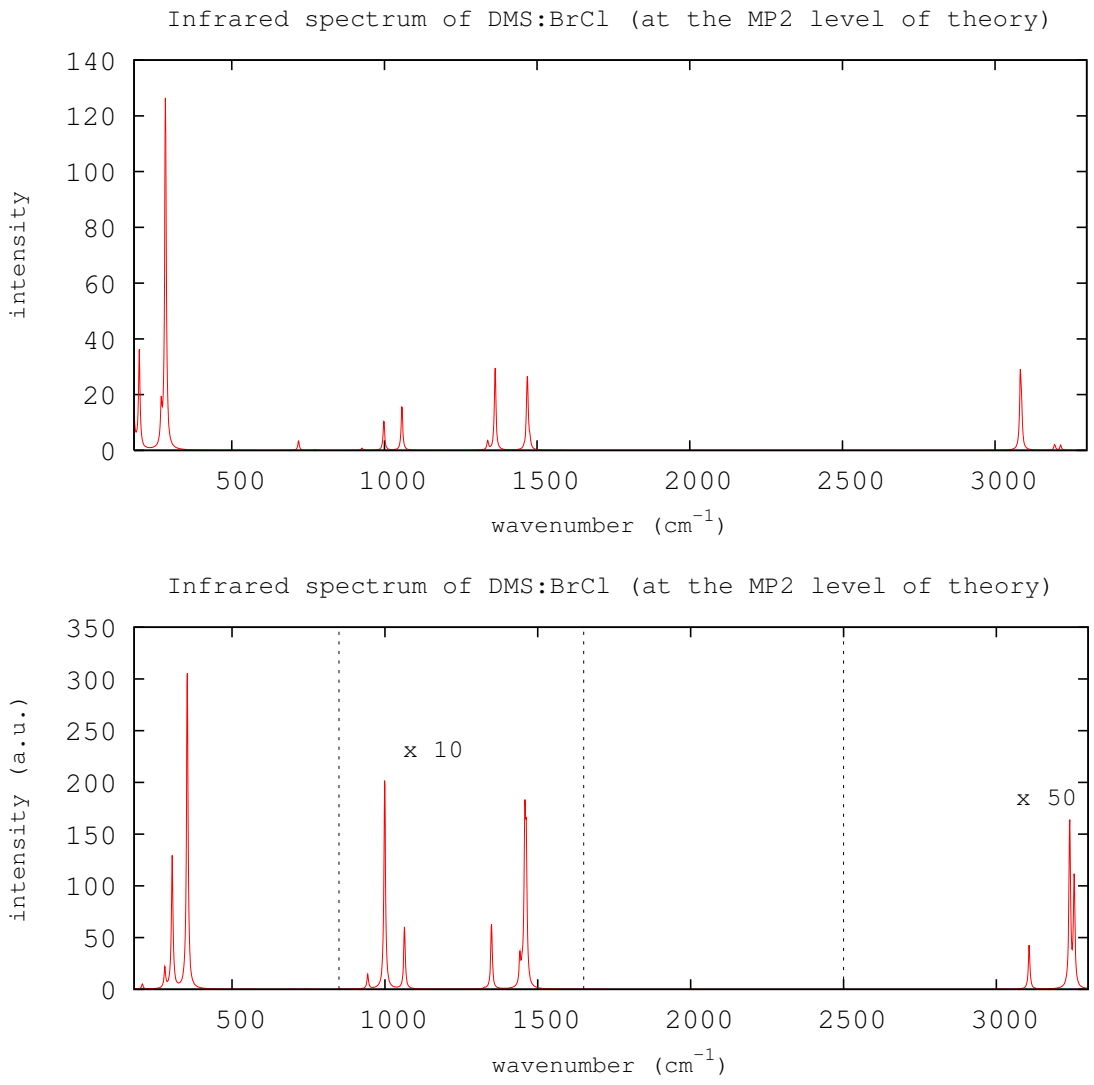

Figure 4.28: ***Top****: $DMS : ClBr$ charge transfer complex computed spectrum;* ***bottom****: $DMS : BrCl$ covalent complex computed spectrum*

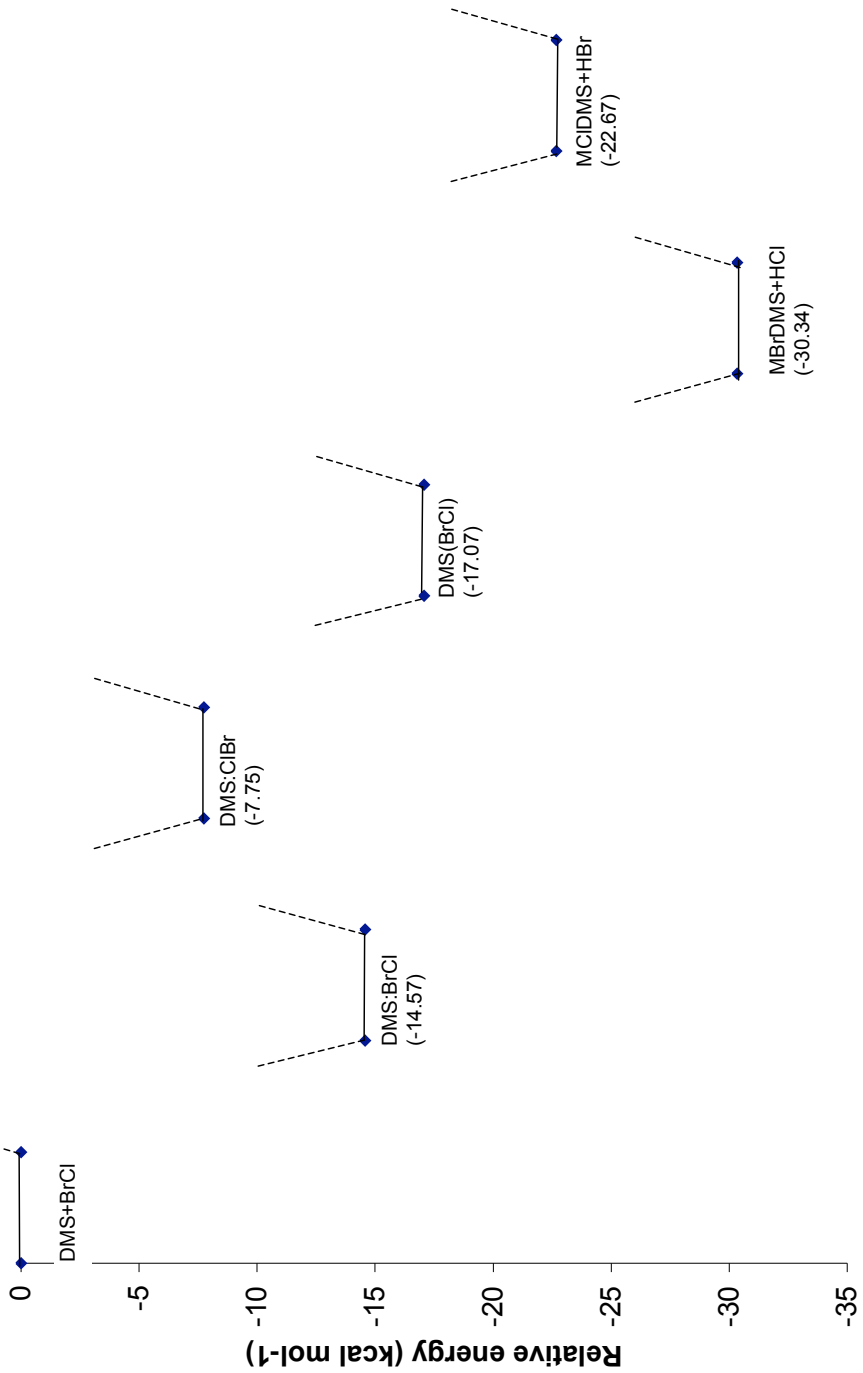

Figure 4.29: *Energy diagram for the DMS+$BrCl_2$ reaction at the MP2 level of theory*

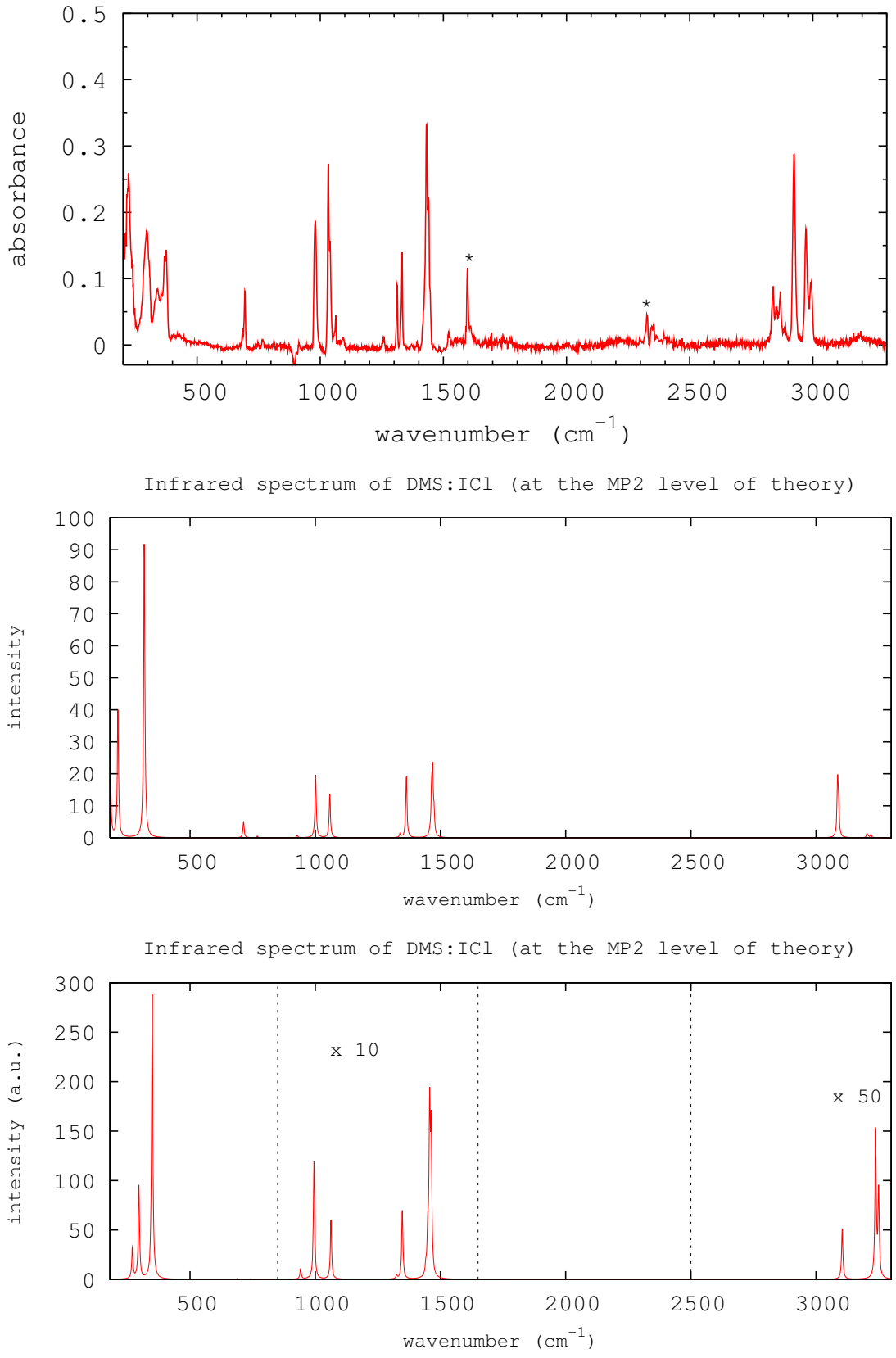

Figure 4.30: ***Top****: DMS : ICl experimental ir spectrum (impurities are denoted by *);* ***middle****: DMS : ICl charge transfer complex computed spectrum;* ***bottom****: DMS : ICl covalent complex computed spectrum*

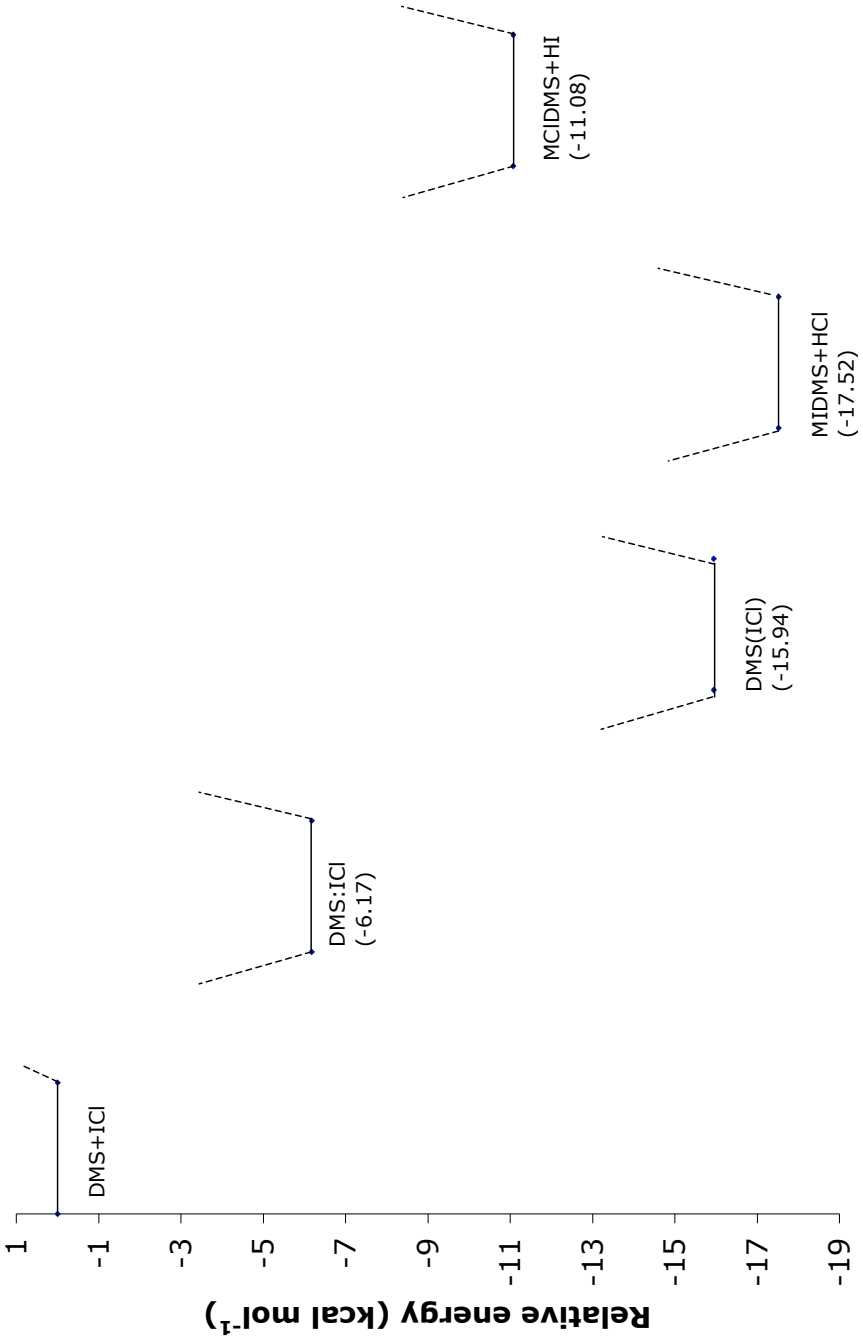

Figure 4.31: *Energy diagram for the DMS+ICl_2 reaction at the MP2 level of theory*

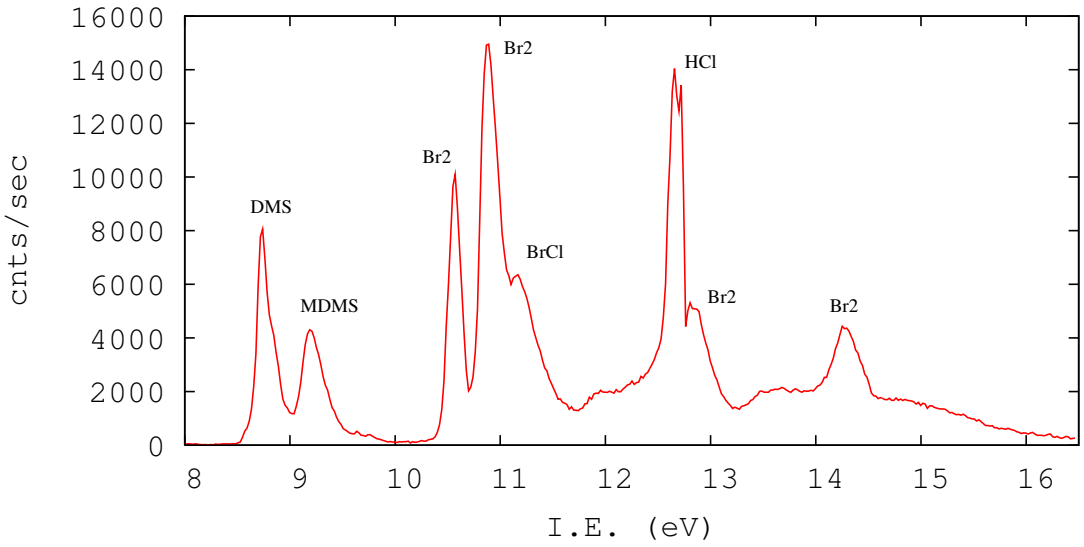

Figure 4.32: *PE spectrum obtained from the DMS+BrCl reaction performed by using the inlet system after heating the sample deposited on the inner wall of the outer tube*

5. Reactions of ozone with alkenes

5.1 Introduction

The gas phase reactions of ozone with alkenes have received a lot of attention in recent years due to their importance in atmospheric chemistry, especially in air pollution processes in urban areas. As discussed in Chapter 1, ozone-alkene reactions can be a source of HO_x (HO_x = OH, HO_2) and RO_2 radicals, which are important oxidants in the atmosphere. The Criegee mechanism [35, 36] is generally accepted as the main mechanism of these reactions (see Chapter 1).

Several studies, both theoretical and experimental, have been undertaken on the reactions of ozone with alkenes. Primary ozonides and secondary ozonides have been observed for a few systems. For example, some more reactive POZ's were first directly observed by NMR [93] and by infrared spectroscopy in low-temperature matrices [94, 95], and the microwave spectrum of the ethylene POZ has been obtained in a seminal paper by Gillies *et al.* [96] while a study of the ethylene SOZ in the gas-phase has been carried out by FTIR spectroscopy [97].

In contrast the Criegee intermediate has generally eluded observation and characterisation. Recently, simultaneous observation of the primary ozonide, Criegee intermediate and secondary ozonide has been found in the study of the ozonolysis of cyclopentene and cyclopentadiene [98]. Evidence of the Criegee intermediate formaldehyde oxide (CH_2OO), is available from photoionisation mass spectroscopic experiments involving chlorine-initiated gas-phase oxidation of dimethyl sulfoxide (DMSO) [37].

Electronic structure calculations have provided insight into the nature of the ozonolysis reactions, as well as to the reasons for the difficulties in observing Criegee intermediate experimentally[99–102].

The aim of this work was to investigate by u.v.-photoelectron spectroscopy the reactions between ozone and tetramethylethylene, ethylene and 2-methylpropene by using the photoelectron spectrometer described in Chapter 2 in order to study the reaction products observed as a function of time and search for any reaction intermediates.

5.2 Experimental and results

5.2.1 Production of ozone

Ozone was obtained by silent electric discharge of oxygen and stored on silica gel held at -78 °C in a dry ice-acetone slush bath. The presence of O_3 on the gel was indicated by a deep blue coloration of the gel. In this way O_3 can be stored safely for as long as the slush bath was maintained. The U-tube containing the silica gel was connected via PVC tubing to a stainless steel needle valve through which the sample of gas could be introduced into the spectrometer. Initially the needle valve was opened slightly to remove residual oxygen from the U-tube. The removal of O_2 was checked by recording spectra at 15 minutes intervals. After about one hour, the needle valve was opened wider and a spectrum recorded. This indicated ozone bands with little oxygen contribution. The gel was maintained at - 78 °C throughout the experiments. Part of the photoelectron spectrum of ozone in the ionisation energy region 12.5 - 13.5 eV, is shown in Figure 5.1.

The spectrum is in good agreement with previous work [103, 104].

5.2.2 Reaction of Alkenes with Ozone

After obtaining a pure spectrum of ozone, the reactions with alkenes were performed. All alkenes were bought commercially from Aldrich (purity 99%).

The first reaction studied was the reaction between tetramethylethylene C_6H_{12} (TME) and ozone. The rate constant of this reaction at room temperature is 1.51 x 10^{-15} cm^3 $molecule^{-1}$ sec^{-1} [26]. The inlet systems used to study this reaction were the same as the ones used to study the reactions between DMS and halogen molecules in the gas phase

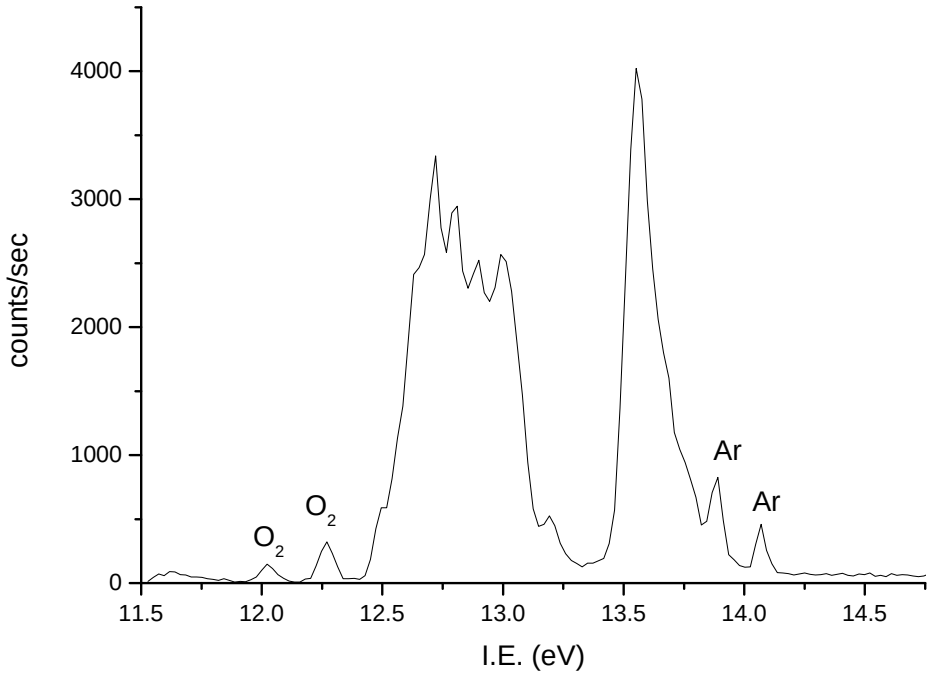

Figure 5.1: *Part of the photoelectron spectrum of O_3. This is in good agreement with previous work [103, 104]*

by u.v.-photoelectron spectroscopy (see Figure 2.7).

The reaction was performed with either the open or the constricted inlet system at different mixing distances. In Figure 5.2 the spectra at 40, 20, 0 cm mixing distance are shown using a constricted inlet system with a 2 mm hole, where the concentration of ozone is in excess with respect to the concentration of TME. Similar results were obtained by using the open inlet system.

TME (labelled as C_6H_{12}) and O_3 bands are present in all spectra and decrease with increasing reaction time. Formaldehyde (first VIE = 10.88 eV) [91], acetone (first VIE = 9.71 eV) [91], CO (first VIE = 14.01 eV) [91], CO_2 (first VIE = 13.78 eV) [91] and O_2 ($^3\Sigma_g^-$) [91] are reaction products and their intensities increase with increasing reaction time.

Figure 5.3 shows a plot of the relative intensities of the reactants and the reaction products against time.

PE spectra of the reaction between ozone and ethylene were then recorded. The inlet system used has been described in Chapter 2 (see Figure 2.8). This reaction is very slow and the rate constant at room temperature is estimated to be 3.3 x 10^{-18} cm^3 $molecule^1$ sec^{-1} [26]. Using the taps at different positions, the reaction was studied at different reaction distances (see Figure 5.4).

Also in this case formaldehyde, CO, CO_2, O_2 ($^3\Sigma_g^-$) were observed as reaction products [91]. Acetaldehyde was also observed. Its first band, vertical ionization energy at 10.26 eV [91], appears very weakly but increases in intensity with mixing distance. However, an important feature detected in these experiments is the presence of the first band of O_2 ($a^1\ \Delta\ _g$) at 11.09 eV (AIE) [105, 106]. The band of O_2 ($a^1\ \Delta\ _g$)) increases with mixing distance showing a maximum in intensity at the largest mixing distance used.

Figure 5.5 shows how the intensity of C_2H_4 and O_3 decrease with increasing reaction time and how the intensity of the reaction products increases with reaction time.

The last reaction studied was the reaction between ozone and 2-methylpropene (C_4H_8, rate constant 1.13 x 10^{-17} cm^3 $molecule^1$ sec^{-1} at room temperature [26]). The inlet systems used were the same as in the study of the O_3+TME reaction.

Acetone, formaldehyde, CO, CO_2, O_2 ($^3\Sigma_g^-$) were again observed as reaction products together with O_2 ($a^1\ \Delta\ _g$). Figure 5.6 shows spectra at three reaction distances and Figure 5.7 shows a relative intensity plot for all the reaction distances studied.

5.3 Discussion

In this work the results obtained are consistent with the overall mechanism proposed by Criegee, but the Criegee intermediates were not observed. For example, the first AIE of CH_2OO is expected at 10 eV [37], but this was not seen.

In the following sections a discussion of the results obtained is presented and a reaction mechanism is proposed for each reaction investigated.

Ethylene

The mechanism proposed for the O_3+C_2H_4 reaction is presented in Figure 5.8. The first step of the reaction is the formation of the POZ which decomposes into H_2CO (formaldehyde) and the Criegee intermediate. The Criegee intermediate in turn can be stabilised by a third body or undergo the production of either CO+H_2O or CO_2+H_2. The presence of CO and CO_2 in the spectra recorded in this work would suggest the formation of also H_2 (first VIE = 15.98 eV [91]) and H_2O (first VIE = 12.61 eV [91]). The H_2 bands are not observed because of the low cross section of the spectrometer [49, 50] while H_2O was observed partially overlapped with the O_2 and the O_3 bands in the 12 eV - 13 eV region.

The alternative reaction path is the formation of the secondary ozonide (SOZ), which can decompose into acetaldehyde and molecular oxygen. Both molecules are observed in this work. In this case, if the spin is conserved, O_2 a^1 Δ_g would be produced and then collisionally deactivated to O_2 $^3\Sigma_g^-$. The deactivation would occur by the reaction of O_2 a^1 Δ_g with ethene (deactivation rate constant=2 x 10^{-18} cm^3 $molecule^{-1}$ sec^{-1} [107]).

Theoretical work by Anglada *et al.* [99], by using the method CASSCF, suggests that the O_3+C_2H_4 reaction gives ethylene oxide (C_2H_4O) and O_2 a^1 Δ_g. The VIE for ethylene oxide is at 10.57 eV [91], but it is not observed in this work.

Another source of O_2 a^1 Δ_g could be the reaction between the Criegee intermediate and ozone. It would produce formaldehyde and two molecules of O_2 a^1 Δ_g, conserving the spin, otherwise formaldehyde and two molecules of O_2 $^3\Sigma_g^-$ (see Eq. 5.1).

$$\begin{cases} CH_2OO + O_3 & \rightarrow CH_2O + 2O_2a^1\Delta_g \\ & \rightarrow CH_2O + 2O_2^3\Sigma_g^- \end{cases} \tag{5.1}$$

The observation of the first excited state of oxygen could be important due to its relevance to the chemistry of the atmosphere. O_2 a^1 Δ_g is present in relatively high partial pressures in the troposphere, being produced with O (^{1}D) from photolysis of ozone, and is one of the strongest contributors of the airglow [108]. Experimental evidence shows that O_2 a^1 Δ_g is present in the lower atmosphere [109], especially in polluted urban

environments.

Several studies [110, 111] have shown how O_2 $a^1\ \Delta_g$ could be involved in the oxidation chemistry of the lower atmosphere, notably that reaction with unsaturated compounds could generate oxygenated organic radicals known to be able to effect the transformation of NO to NO_2.

Tetramethylethylene

In a similar way, the TME+O_3 reaction undergoes the formation of the POZ which decomposes into acetone and the Creigee intermediate Me_2COO (see Figure 5.9). The Creigee intermediate may decompose into either C_2H_6 (ethane) and CO_2 or CO and CH_3OCH_3 (dimethyl ether). The first VIE for ethane and dimethyl ether are respectively 11.99 eV [91] and 10.04 eV [91] but they are not observed in this work. Ethane has a broad first band in the region 11.4-12.8 eV and this might be overlapped with other bands, e.g. O_2 and O_3, and hence not observed. However, the first band of dimethyl ether is sharp and should be observed.

On the formation of the SOZ, the products are O_2 $a^1\ \Delta_g$ (if the spin is conserved) and 3-methyl-butan-2-one or 2,2,3,3-tetramethyl-oxirane (see Figure 5.9). The first VIE of the 3-methyl-butan-2-one is 9.3 eV [112] while it appears that no photoelectron spectrum of 2,2,3,3-tetramethyl-oxirane is the available in the literature. Neither $a^1\ \Delta_g$ nor 3-methyl-butan-2-one were observed in the spectra recorded. The deactivation rate constant of O_2 $a^1\ \Delta_g$ with TME is 4.9 x 10^{-16} cm^3 $molecule^{-1}$ sec^{-1} [113] at 298 K. This reaction is then faster than the deactivation reaction of O_2 $a^1\ \Delta_g$ with ethylene, and this would explain why O_2 $a^1\ \Delta_g$ is not observed in this case.

However, this reaction mechanism does not explain why formaldehyde was observed. In previous work carried out by Grosjean *et al.* [114] by using liquid cromatography, the presence of formaldehyde as a reaction product has been explained by using a reaction

sequence involving the Creigee intermediate $(CH_3)_2COO$ (see eq. 5.2).

$$\begin{cases} (CH_3)_2COO & \rightarrow (CH_2 = C(CH_3)OOH)^* \\ (CH_2 = C(CH_3)OOH)^* & \rightarrow (CH_3COCH_2OH)^* \\ (CH_3COCH_2OH)^* & \rightarrow CH_3CO + CH_2OH \\ CH_2OH + O_2 & \rightarrow HO_2 + HCHO \end{cases} \tag{5.2}$$

This reaction sequence could explain the not negligible amount of formaldehyde seen in the spectra obtained in this work.

2-Methylpropene

The alkene 2-methypropene was chosen as it is an intermediate alkene between ethylene and TME. Given the asymmetry of the molecule, two Creigee intermediates may be formed in the reaction with ozone. The mechanism of the reaction is shown in Figure 5.10.

After the formation of the POZ, two channels are possible: (i) production of formaldehyde and the Criegee intermediate $(CH_3)_2OO$ or (ii) production of acetone and the Creigee intermediate CH_2OO. The decomposition of the two Creigee intermediates is shown in Figure 5.10. The SOZ may undergo the decomposition into oxygen and 2,2-dimethyloxirane or acetone.

Formaldehyde is present in the spectra as well as acetone. Both channels (i) and (ii) give CO and CO_2 as products, which are also observed in the spectra. It is then not clear which channel the reaction is more likely to follow. Again, no evidence of ethane or dimethyl ether was found. However, acetone may come from the decomposition of the SOZ together with O_2 $a^1\ \Delta_g$, observed in the spectra.

No u.v.-photoelectron spectrum for 2,2-dimethyloxirane was found in the literature.

A weak band can be seen in the spectra at about 10.2 eV, which is the first VIE of acetaldehyde. The band intensity seems to increase with the reaction time. Acetaldehyde has been observed also in the work by Grosjean *et al.* [114] as a minor carbonyl and

had been associated to impurity of the alkene in thei work. This molecule could come from a decomposition of the SOZ different from the one proposed above, that is into acetaldehyde, molecular oxygen and ethylene. However, ethylene was not observed and the reaction of ethylene with any excess of ozone should give again acetaldehyde. The acetaldehyde band should then be stronger than the band found in this work.

Further investigation is required on the production of acetaldehyde in this reaction.

No previous work has been carried to measure the deactivation rate constant of O_2 $a^1\ \Delta_g$ with 2-methylpropene. However, given the structure of the molecule, it would be expected to be between the deactivation rate constant for ethylene and that for TME. The general trend observed is that as the number of alkyl groups in a substituted ethylene increases the deactivation rate constant increases [115]. The reaction would then be slower than the O_2 $a^1\ \Delta_g$+TME reaction and this would allow the observation of O_2 $a^1\ \Delta_g$.

5.4 Conclusion

In this chapter the preliminary results of reactions between ozone and selected alkenes in the gas-phase by u.v-photoelectron spectroscopy were presented and discussed.

Possible reaction mechanisms were suggested following the mechanism proposed by Creigee and general good agreement was found with the experimental results, although the Creigee intermediates were not observed.

Noteworthy is the formation of the important atmospherically costituent O_2 $a^1\ \Delta_g$, reported for the first time as a reaction product of the reactions of ozone with etheylene and 2-methypropene.

The next step in this study would be to measure the relative cross-sections of the products in order to place the reaction yields on an absolute basis.

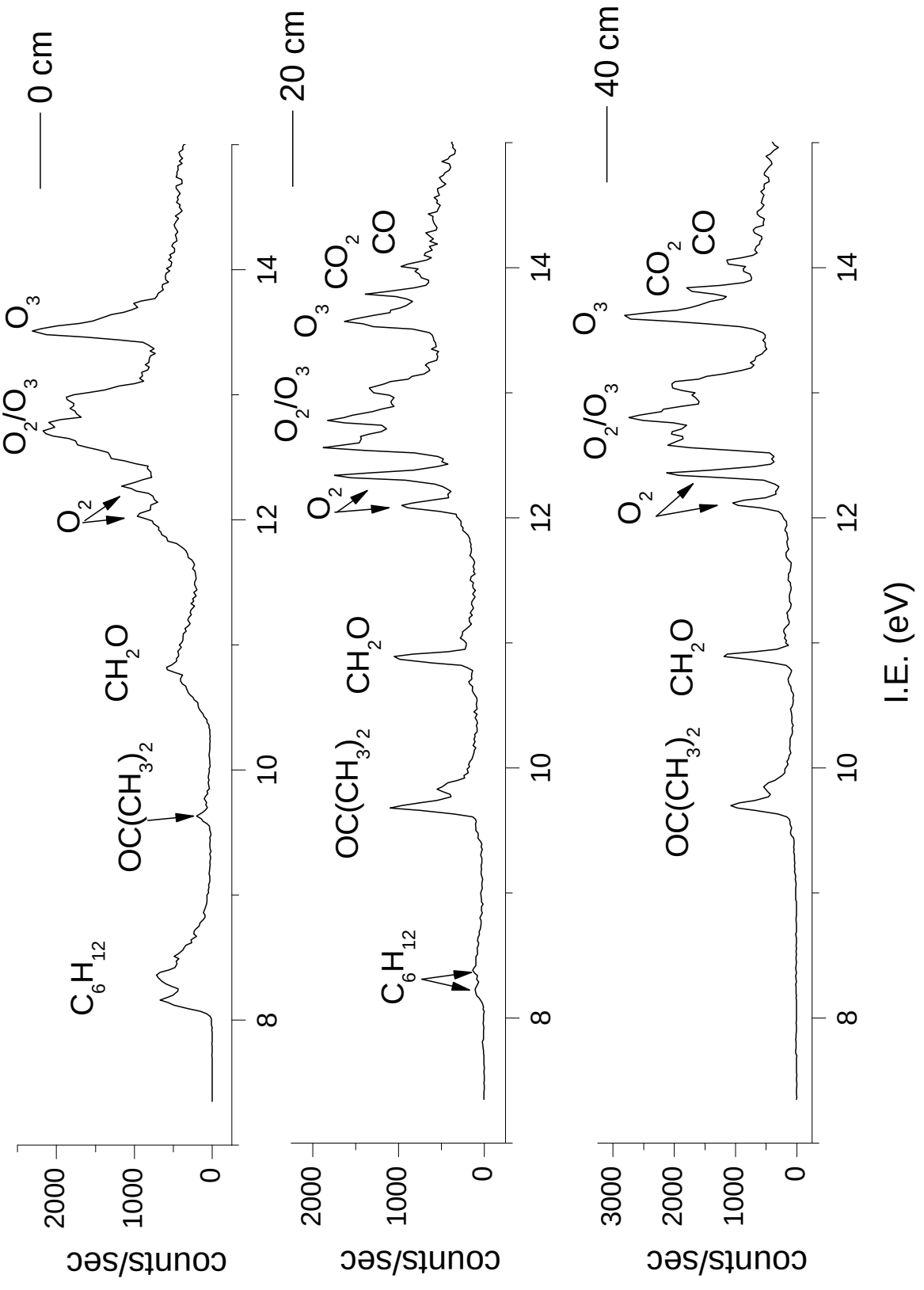

Figure 5.2: *Photoelectron spectra recorded for the TME+O_3 reaction with a 2 mm exit hole tube at three different mixing distances*

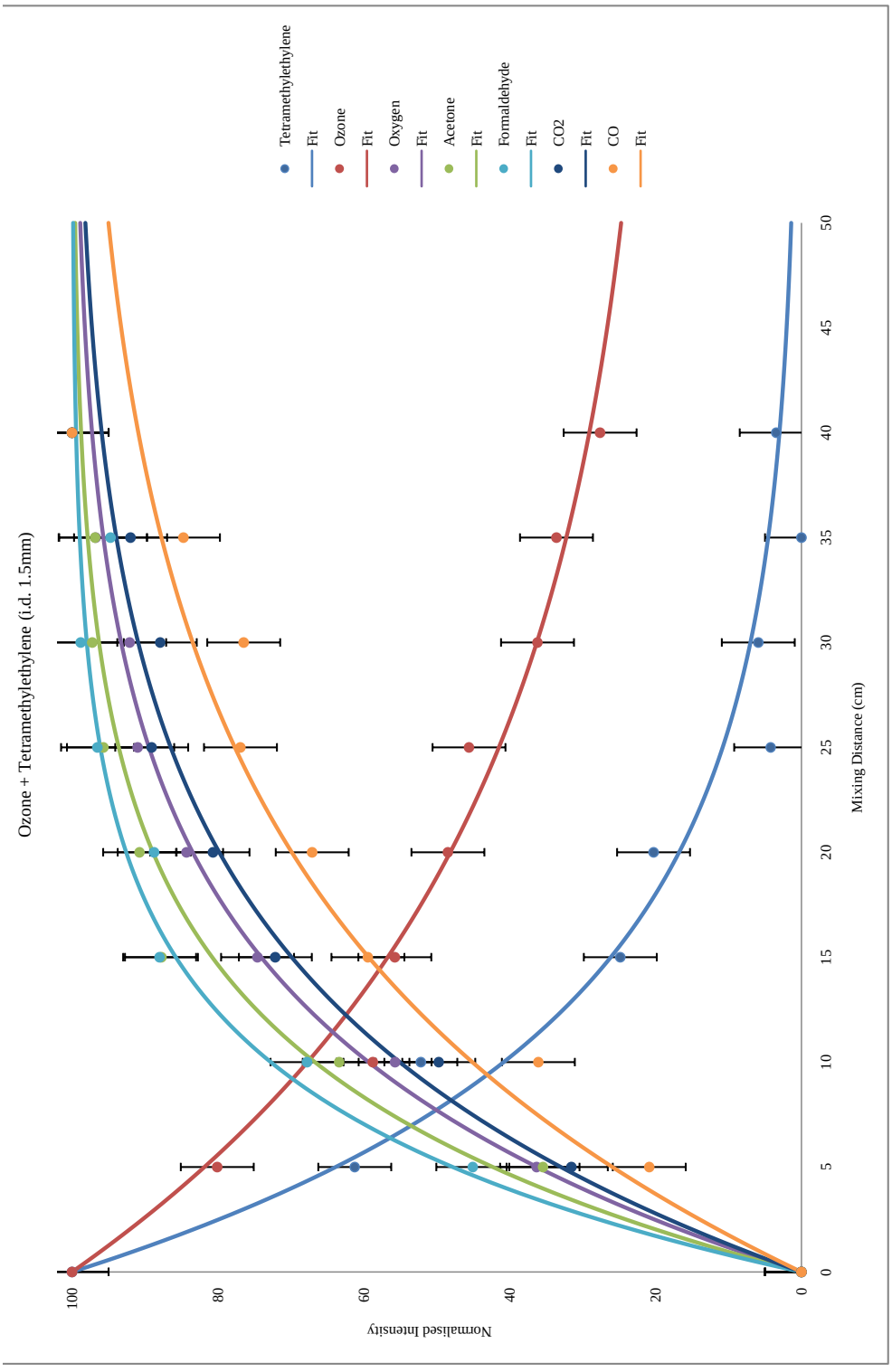

Figure 5.3: *A plot of relative intensities against mixing distance for the TME+O_3 reaction with a 2 mm exit hole tube*

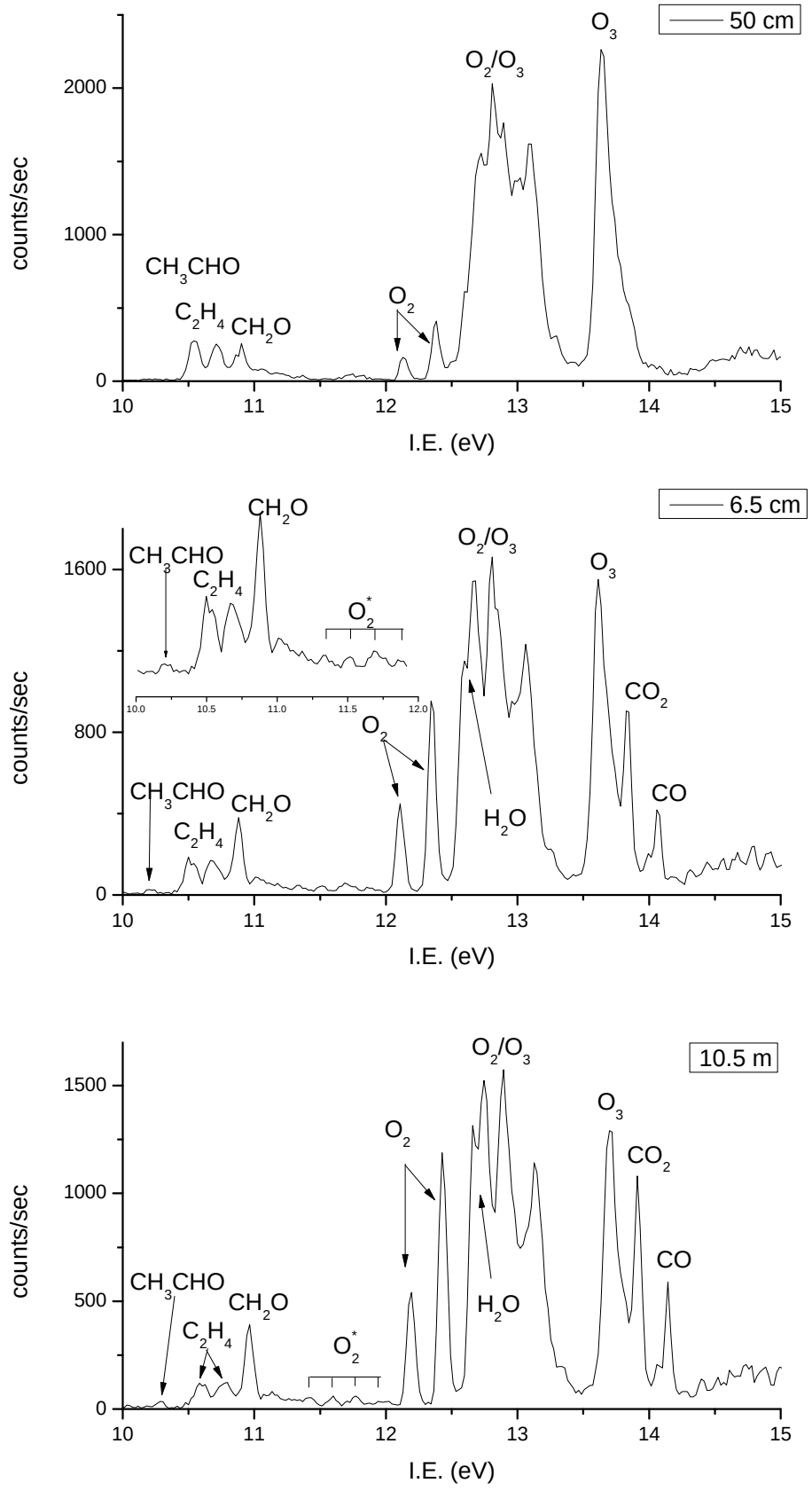

Figure 5.4: *Photoelectron spectra recorded for the $C_2H_4+O_3$ reaction at three different mixing distances*

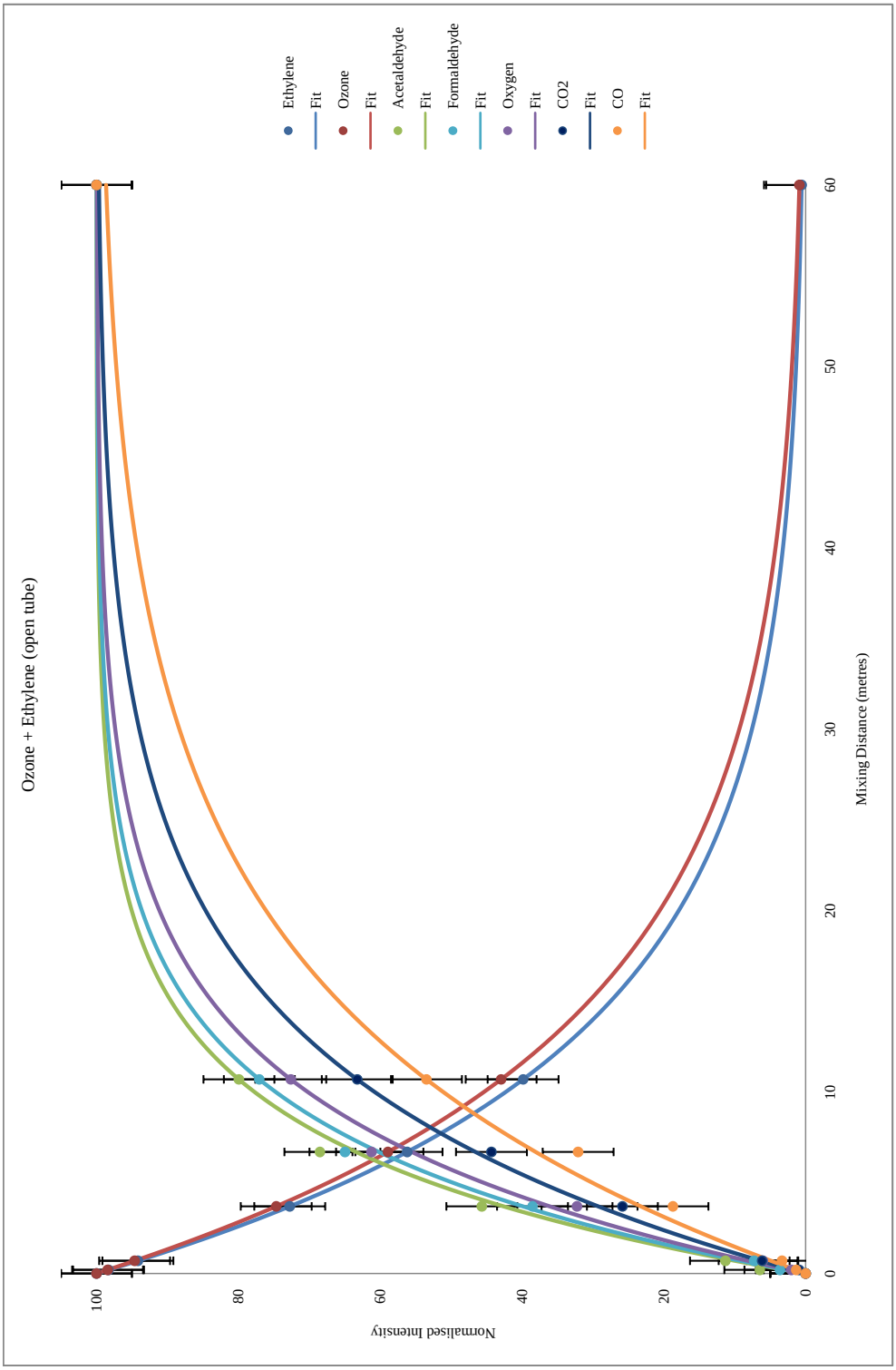

Figure 5.5: *A plot of relative intensities against mixing distance for the $C_2H_4+O_3$ reaction*

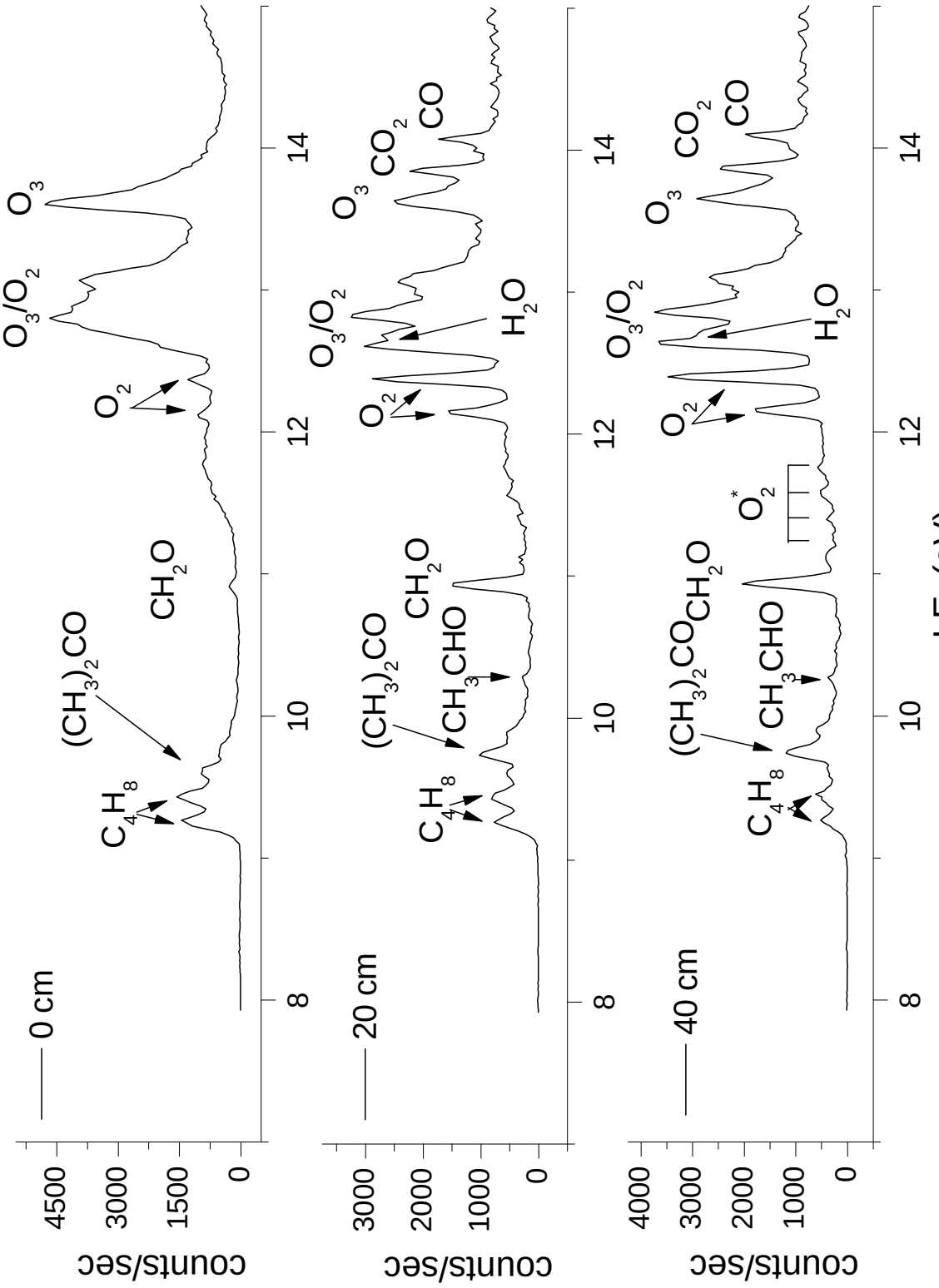

Figure 5.6: *Photoelectron spectra recorded for the $C_4H_8+O_3$ reaction at three different mixing distances*

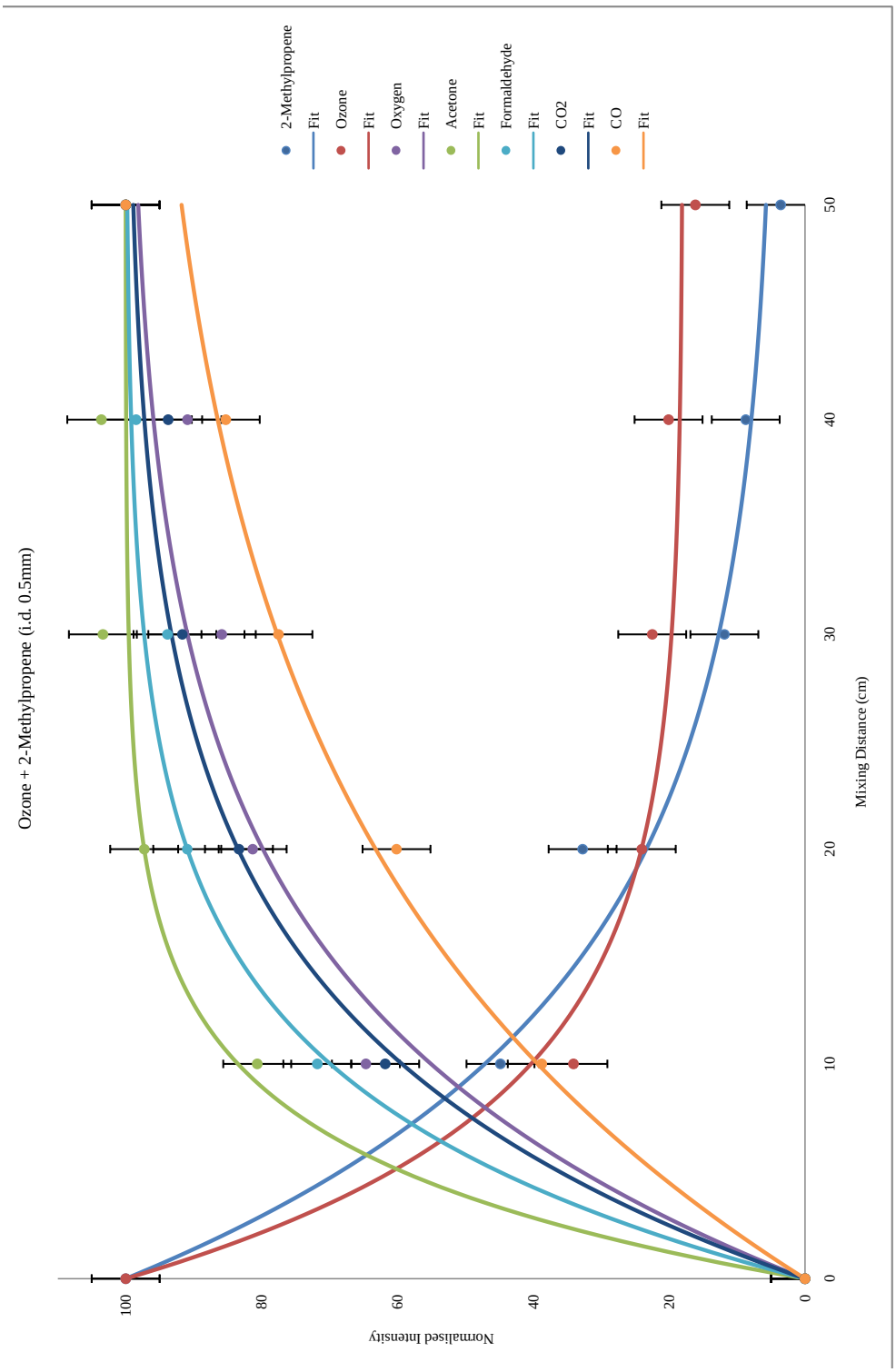

Figure 5.7: *A plot of relative intensities against mixing distance for the $C_4H_8 + O_3$ reaction*

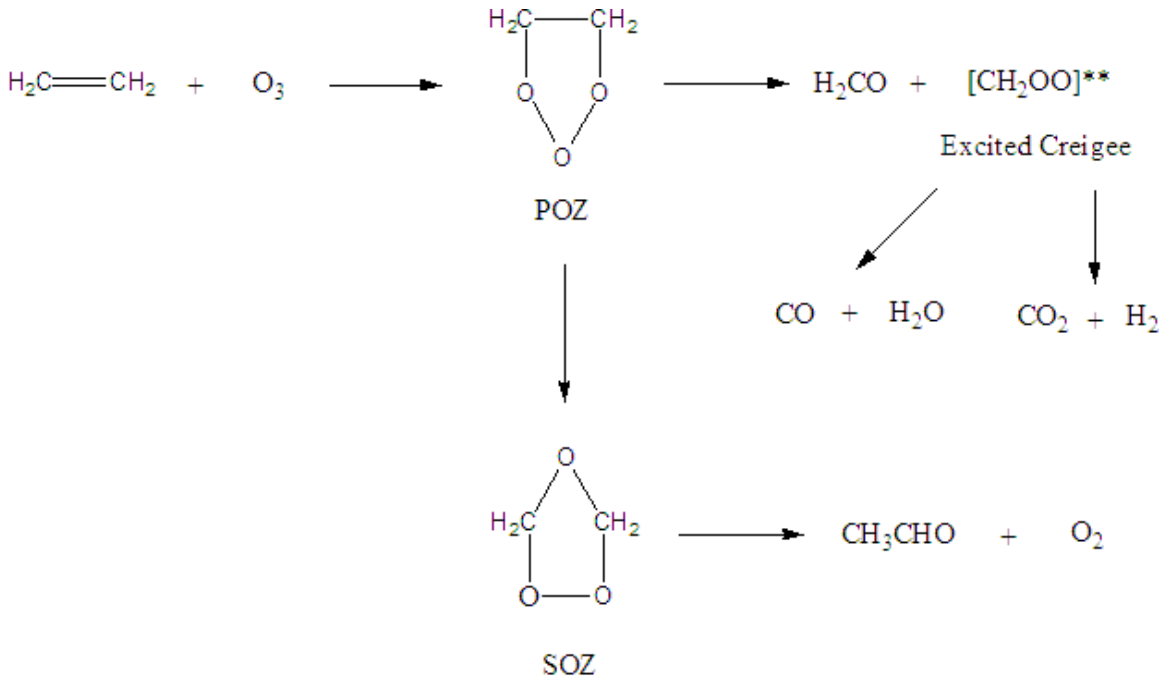

Figure 5.8: *Basic mechanism for the O_3+C_2H_4 reaction*

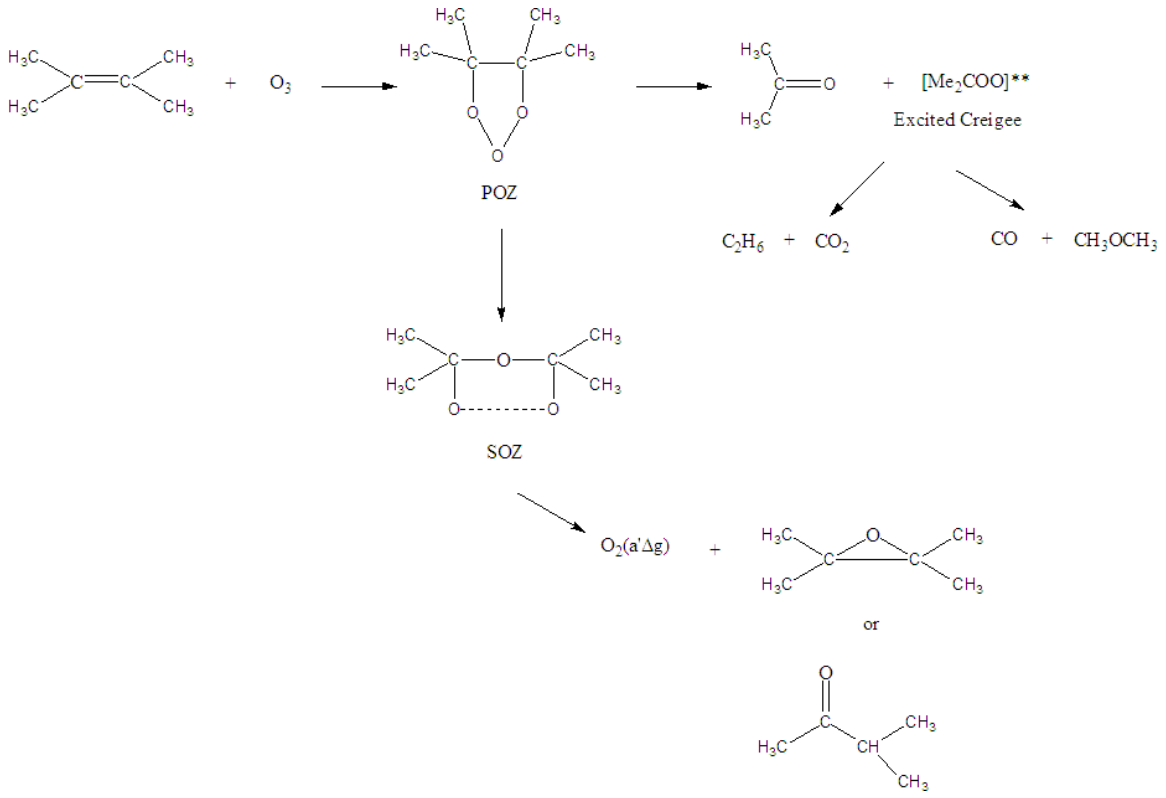

Figure 5.9: *Basic mechanism for the O_3+TME reaction*

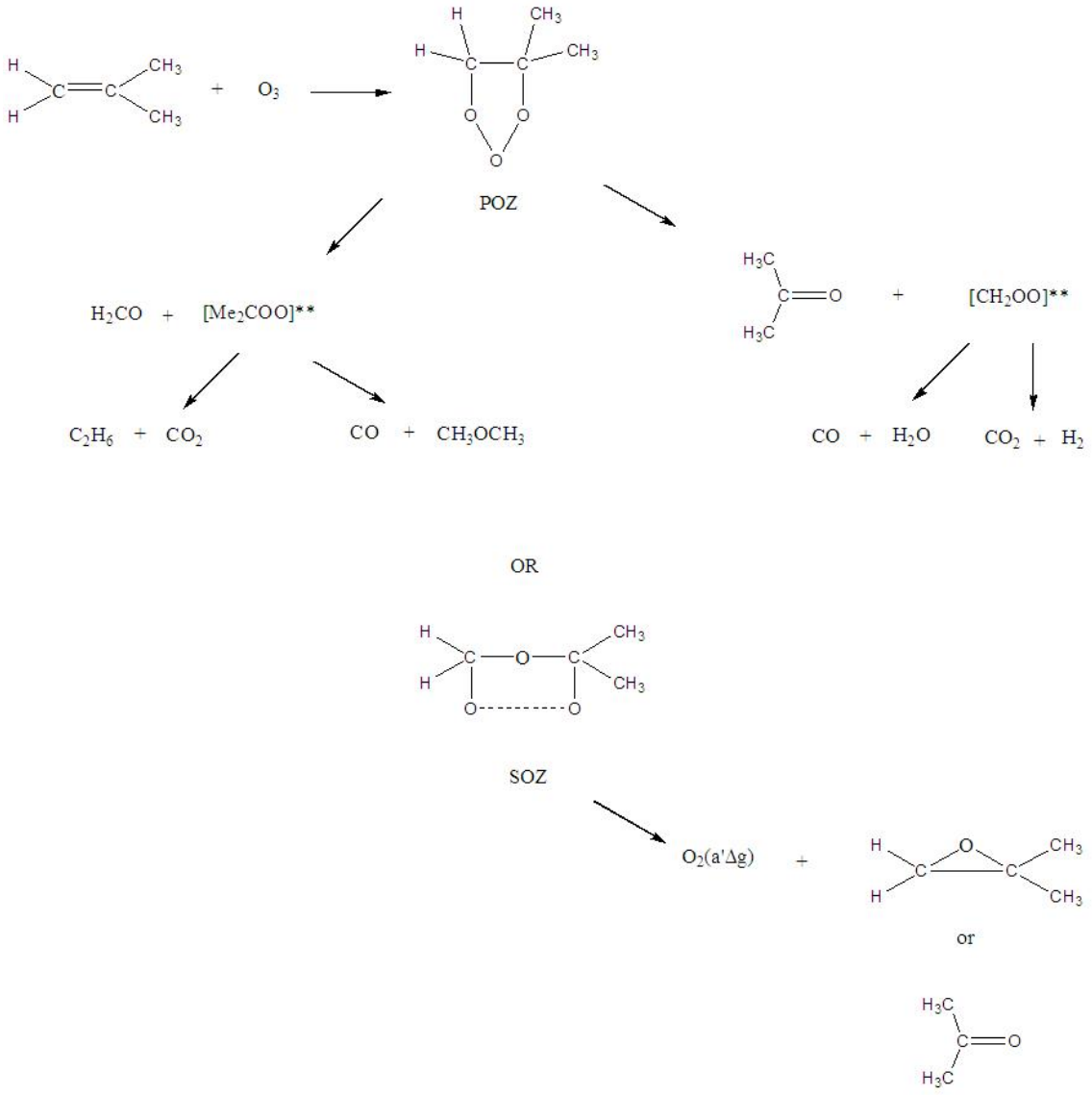

Figure 5.10: *Basic mechanism for the O_3+C_4H_8 reaction*

6. Conclusions

The reactions between dimethyl sulphide and molecular chlorine, molecular bromine, molecular iodine, bromine monochloride and iodine monochloride were studied in this work by matrix isolation infrared spectroscopy in a nitrogen and argon matrix, and in the gas-phase by u.v.-photoelectron spectroscopy.

The reactions were investigated under conditions of slight DMS excess and in all cases characteristic bands associated with reaction intermediates were observed at about 1331 and 1040 cm^{-1} in a nitrogen matrix and at 1331 and 1053 cm^{-1} in an argon matrix plus bands at lower wavenumbers characteristic of each intermediate.

Unlike the DMS+Cl_2 reaction, which gives MClDMS (monochlorodimethylsulphide) and HCl as final products, the other reactions do not go further the formation of the reaction intermediate, except for the DMS+BrCl reaction for which unknown bands were identified in the i.r. spectra when studying the final products.

Molecular orbital calculations, at the MP2 level of theory, of vibrational frequencies and intensities assigned the intermediate bands to a van der Waals structure DMS:XY (XY = Cl_2, Br_2, I_2, BrCl and ICl). The normal modes associated with vibrations at approximately 1331 and 1040 cm^{-1} are C-H bending modes while the lower frequency vibrations can be assigned to stretching modes between the sulphur and the halogen atoms.

The u.v.-PES experiments did not show any products for any DMS+XY reaction, indicating that a third body is necessary for the van der Waals adducts to be stabilised. The role of the third body in the matrix isolation experiments was probably fulfiled by the matrix gas. If these reactions occured in the atmosphere, N_2 and atmospheric particles (i.e. ice) could play the role of the third body.

Future work should focus on the behaviour of the DMS+BrCl reaction in a matrix and in the gas-phase to understand in detail the reaction mechanism for this reaction.

Reactions between ozone and simple alkenes were also studied by u.v.-PES. The alkenes chosen for this work were ethylene, tetramethylethylene and 2-methylpropene.

The results obtained in this work are in good agreement with the reaction mechanism proposed by Creigee and previous work carried out on these reactions. However, the Creigee intermediates and some of the expected products were not observed. The experimental observation for the first time of the O_2 $a^1\ \Delta_g$ bands in the reaction of ozone with ethylene and 2-methylpropene is of great importance, given the impact that this species might have on the chemistry of the troposphere.

The information presented in this work contributes to a better understanding of the mechanism of the reaction of ozone with alkenes. Nevertheless, future work must be carried out in order to determine better the major reaction pathways for each reaction studied in this work.

Bibliography

[1] J. E. Lovelock, R. J. Maggs and R. A. Rasmussen. *Nature* **237**, 452 (1972)

[2] R. J. Charlson, J. E. Lovelock, M. O. Andreae and S. G. Warren. *Nature* **326**, 655 (1987)

[3] S. F. Watts. *Atmospheric Environment* **34**, 761 (2000)

[4] R. P. Wayne. Chemistry of Atmospheres (USA, Oxford University Press, 2000)

[5] A. R. Ravinshankara, Y. Rudich, R. Talukdar and S. B. Barone. *Phil. Trans. R. Soc. Lond. B* **352**, 171 (1997)

[6] J. B. Nowak, D. D. Davis, G. Chen, F. L. Eisele, R. L. Mauldin, D. J. Tanner, C. Cantrall, E. Kosciuch, A. Bandy, D. Thornton and A. Clarke. *Geophys. Res. Letters* **28**, 2201 (2001)

[7] N. I. Butokovskaia, G. Poulet and G. L. Bras. *J. Phys. Chem.* **99**, 4536 (1995)

[8] M. O. Andreae and P. J. Cutzen. *Science* **276**, 1052 (1997)

[9] R. Vogt, P. J. Crutzen and R. Sander. *Nature* **383**, 327 (1996)

[10] C. W. Spicer, E. G. Chapman, B. J. Finlaytson-Pitts, R. A. Plastridge, J. M. Hubbe, J. D. Fast and C. M. Berkowitz. *Nature* **394**, 353 (1998)

[11] Y. Sadanaga, J. Hirokawa and A. Akimoto. *Geophysical Research Letters* **28**, 4433 (2001)

[12] J. M. Dyke, M. V. Ghosh, D. J. Kinnison, G. Levita, A. Morris and D. E. Shallcross. *Phys. Chem. Chem. Phys.* **7**, 866 (2005)

[13] J. M. Dyke, M. V. Ghosh, M. Goubet, E. P. F. Lee, and G. Levita. *Chemical Physics* **324**, 85 (2006)

[14] G. Levita. Some spectroscopic studies related to atmospheric chemistry and the thermal decomposition of organic azides. Ph.D. thesis, University of Southampton (2005)

[15] R. Sander, W. C. Keene, A. A. P. Pszenny, R. Arimoto, G. P. Ayers, E. Baboukas, J. M. Cainey, P. J. Crutzen, R. A. Duce, G. Hönninger, B. J. Huebert, W. Maenhaut, N. Mihalopoulos, V. C. Turekian and R. Van Dingenen. *Atmospheric Chemistry and Physics* **3(5)**, 1301 (2003)

[16] J. Hirokawa, K. Onaka, Y. Kajii and H. Akimoto. *Geophysical Research Letters* **25**, 2449 (1998)

[17] W. C. Keene, J. Stutz, A. A. P. Pszenny, J. R. Maben, E. V. Fischer, A. M. Smith, R. von Glasow, S. Pechtl, B. C. Sive and R. K. Varner. *J. Geophys. Res.* **112**, D10S12 (2007)

[18] P. O'Driscoll, K. Lang, N. Minogue and J. Sodeau. *The Journal of Physical Chemistry A* **110(14)**, 4615–4618 (2006)

[19] P. Shepson, P. Matrai, L. Barrie and J. Bottenheim. *Eos Trans. AGU* **84(36)**, 349 (2003)

[20] C. W. Spicer, R. A. Plastridge, K. L. Foster, B. J. F. Pitts and J. W. Bottenheim. *Atmos. Environ.* **36**, 2721 (2002)

[21] K. L. Foster, R. A. Plastridge, J. W. Bottenheim, P. B. Shepson, B. J. F. Pitts and C. W. Spicer. *Science* **291**, 471 (2001)

[22] G. A. Impey, C. M. Mihele, K. G. Anlauf, L. A. Barrie, D. R. Hastie and P. B. Shepson. *J. Atmos. Chem* **34**, 21 (1999)

[23] G. A. Impey, P. B. Shepson, D. R. Hastie, L. A. Barrie and K. G. Anlauf. *J. Geophys. Res.* **102**, 16005 (1997)

[24] A. S. Lopez and J. M. C. Plane. *Geophys. Res. Lett.* **31**, L04112 (2004)

[25] NASA. Earth Observing System (EOS) Science Plan. Chapter 7. Ozone and Stratospheric Chemistry (1999)

[26] J. C. Calvert, R. Atkinson, J. A. Kerr, S. Madronich, G. K. Moortgat, T. J. Wallington and G. Yarwood. The mechanisms of Atmospheric Oxidation of the Alkenes (Oxford University Press, USA, 2000)

[27] P. Neeb and G. K. Moortgat. *J. Phys. Chem. A* **103**, 9004 (1999)

[28] T. Pfeiffer, O. Forberich and F. J. Comes. *Chemical Physics Letters* **298**, 351 (1998)

[29] R. Atkinson and W. P. L. Carter. *Chemical Reviews* **84**, 437 (1984)

[30] V. A. Isidorov, I. G. Zenkevich and B. V. Ioffe. *Atmos. Environ.* **19**, 1 (1985)

[31] A. M. Winer, J. Arey, R. Atkinson, S. M. Ashmann, W. D. Long, C. L. Morrison and D. M. Olszyk. *Atmos. Environ.* **26A**, 2647 (1992)

[32] B. Lamb, D. Gay, H. Westberg and T. Pierce. *Atmos. Environ.* **27A**, 1673 (1993)

[33] R. C. McDonald and R. Fall. *Atmos. Environ.* **27A**, 1709 (1993)

[34] C. N. Hewitt and A. V. Jackson. Handbook of Atmospheric Science (Blackwell Publishing, 2003)

[35] R. Criegee. *Record Chem. Prog.* **18**, 111 (1957)

[36] R. Criegee. *Angew. Chem.* **14**, 745 (1975)

[37] C. A. Taatjes, G. Meloni, T. M. Selby, A. J. Trevitt, D. L. Osborn, C. J. Percival and D. E. Shallcross. *Journal of the American Chemical Society* **130(36)**, 11883 (2008)

[38] E. Whittle, D. A. Dows and G. C. Pimentel. *J. Chem. Phys.* **22**, 1943 (1954)

[39] A. Barnes, W. J. Orville-Thomas, R. Gaufrs and A. Müller. Matrix Isolation Spectroscopy (Springer, 1981)

[40] I. R. Dunkin. Matrix-Isolation Techniques - A Practical Approach (Oxford: Oxford University Press, 1998)

[41] W. B. David. A Bibliography of Matrix Isolation Spectroscopy 1954-1985 (Rice Univ Studies, 1988)

[42] B. Nelander. *Kem. Tidskr.* **92**, 48 (1980)

[43] M. E. Jacox. *Chem. Soc. Rev.* **31**, 108 (2002)

[44] J. S. Ogden and R. S. Wyatt. *J. Chem. Soc. Dalton Trans* **4**, 859 (1987)

[45] J. Chalmers and P. R. Griffiths. (Eds.) Handbook of Vibrational Spectroscopy (Chichester: John Wiley Sons Ltd., 2002)

[46] A. Einstein. *Ann. Phys.* **17**, 549 (1905)

[47] J. H. D. Eland. Photoelectron Spectroscopy (London, Butterworths, 1984)

[48] J. W. Rabalais. Principles of Ultraviolect Photoelectron Spectroscopy (JOHN WILEY SONS, 1977)

[49] D. Bulgin, J. M. Dyke, F. Goodfellow, N. Jonathan, E. Lee and A. Morris. *A. J. Electron Spectrosc. Relat. Phenom.* **12**, 67 (1977)

[50] J. M. Dyke, N. Jonathan and A. Morris. *Int. Rev. Phys. Chem.* **2**, 3 (1982)

[51] K. Siegbahn. ESCA: atomic, molecular and solid state structure studied by means of electron spectroscopy (Almqvist and Wiksells, Uppsala, 1967)

[52] A. Morris. Lectures on experimental photoelectron spectroscopy (University of Southampton, 1980)

[53] A. Pauline and D. Roy. *J. Phys. E. Sci. Instrum.* **11**, 35 (1978)

[54] J. M. Dyke, N. Jonathan and A. Morris. Electron spectroscopy Theory, Techniques and Applications Vol. 3 (Accademic Press London, 1979)

[55] E. Schrödinger. *Ann. Phys.* **79**, 361 (1926)

[56] L. de Broglie. *Ann. Phys.* **3**, 22 (1925)

[57] M. Born and J. R. Oppenheimer. *Ann. Phys.* **84**, 457 (1927)

[58] H. Eyring, J. Walter and G. E. Kimball. Quantum Chemistry (John Wiley Sons Inc, 1944)

[59] D. R. Hartree. *Proc. Camb. Phil. Soc.* **24**, 89 (1928)

[60] D. R. Hartree, W. Hartree and B. Swirles. *Phil. Trans. Roy. Soc. A* **238**, 229 (1939)

[61] V. Fock. *Z. Physik* **61**, 161 (1930)

[62] C. C. J. Roothaan. *Rev. Mod. Phys.* **23**, 69 (1951)

[63] J. C. Slater. *Phys. Rev.* **36**, 57 (1930)

[64] O. Sinanoglu. *Adv. Chem. Phys.* **98**, 315 (1964)

[65] O. Sinanoglu and D. F.-T. Tuan. *J. Chem. Phys.* **38**, 1740 (1963)

[66] T. Koopmans. *Physica* **1**, 69 (1951)

[67] W. G. Richards. *J. Mass Spectrom. Ion Phys.* **2**, 419 (1969)

[68] M. F. Guest and V. R. Saunders. *Mol. Phys.* **29**, 873 (1975)

[69] J. M. Foster and S. F. Boys. *Rev. Mod. Phys.* **32**, 303 (1960)

[70] T. H. Dunning. *J. Chem. Phys.* **53**, 2823 (1970)

[71] T. H. Dunning. *J. Chem. Phys.* **55**, 716 (1971)

[72] W. Küchle, M. Dolg, H. Stoll and H. Preuss. *Molecular Physics* **74**, 1245 (1991)

[73] D. E. Woon and J. T. H. Dunning. *The Journal of Chemical Physics* **98(2)**, 1358 (1993)

[74] R. A. Kendall, T. H. D. Jr. and R. J. Harrison. *J. Chem. Phys.* **96**, 6796 (1992)

[75] J. C. Slater. *Advance Quantum Chemistry* **6**, 1 (1971)

[76] A. D. Becke. *J. Chem. Phys.* **98**, 5648 (1993)

[77] C. Lee, W. Yang and R. G. Parr. *Phys. Rev.* **37**, 785 (1988)

[78] C. Moller and M. Plesset. *Phys. Rev.* **46**, 618 (1934)

[79] E. Schrödinger. *Annalen der Physik* **80**, 437 (1926)

[80] J. W. S. Rayleigh. Theory of Sound, 2nd edition Vol. I (London: Macmillan, 1894)

[81] N. P. Machara and B. S. Ault. *J. Phys. Chem.* **63**, 1705 (1985)

[82] U. P. Agarwal, A. J. Barnes and W. J. O. Thomas. *Can. J. Chem.* **63**, 1705 (1985)

[83] L. M. Nxumalo and T. A. Ford. *Journal of Molecular Structure* **656**, 303 (2003)

[84] M. V. Ghosh. *Research report, University of Southampton* (2003)

[85] F. Boberg, G. Winter and J. Moss. *Annalen der Chimie* 8 (1958)

[86] G. C. Hayward and P. J. Hendra. *J. Chem. Soc. (A)* 1760 (1969)

[87] H. F. Askew, P. N. Gates and A. S. Muir. *J. Raman Spectroscopy* **22**, 265 (1991)

[88] G. B. M. Vaughan, A. J. Mora, A. N. Fitch, P. N. Gates and A. S. Muir. *J. Chem. Soc., Dalton Trans.* **1**, 79 (1999)

[89] A. J. Barnes, H. E. Hallam and G. F. Scrimshamw. *Trans. Faraday Soc.* **65**, 3159 (1969)

[90] M. J. Frisch, G. W. Trucks, H. B. Schlegel, G. E. Scuseria, M. A. Robb, J. R. Cheeseman, J. A. Montgomery, Jr., T. Vreven, K. N. Kudin, J. C. Burant, J. M. Millam, S. S. Iyengar, J. Tomasi, V. Barone, B. Mennucci, M. Cossi, G. Scalmani, N. Rega, G. A. Petersson, H. Nakatsuji, M. Hada, M. Ehara, K. Toyota, R. Fukuda, J. Hasegawa, M. Ishida, T. Nakajima, Y. Honda, O. Kitao, H. Nakai, M. Klene, X. Li, J. E. Knox, H. P. Hratchian, J. B. Cross, V. Bakken, C. Adamo, J. Jaramillo, R. Gomperts, R. E. Stratmann, O. Yazyev, A. J. Austin, R. Cammi, C. Pomelli, J. W. Ochterski, P. Y. Ayala, K. Morokuma, G. A. Voth, P. Salvador, J. J. Dannenberg, V. G. Zakrzewski, S. Dapprich, A. D. Daniels, M. C. Strain, O. Farkas, D. K. Malick, A. D. Rabuck, K. Raghavachari, J. B. Foresman, J. V. Ortiz, Q. Cui, A. G. Baboul, S. Clifford, J. Cioslowski, B. B. Stefanov, G. Liu, A. Liashenko, P. Piskorz, I. Komaromi, R. L. Martin, D. J. Fox, T. Keith, M. A. Al-Laham, C. Y. Peng, A. Nanayakkara, M. Challacombe, P. M. W. Gill, B. Johnson, W. Chen, M. W. Wong, C. Gonzalez and J. A. Pople. 'Gaussian 03, Revision C.02'. Gaussian, Inc., Wallingford, CT, 2004

[91] K. Kimura, S. Katsumata, Y. Achiba, T. Yanazaki and S. Iwata. Handbook of HeI photoelectron spectra of Fundamental organic molecules (Japan Scientific Societies Press, Tokyo, Halsted Press, New York)

[92] S. Dunlavey, J. Dyke and A. Morris. *J. Elec. Spec. and Rel. Phen.* **12**, 259 (1977)

[93] F. L. Greenwood. *J. Org. Chem.* **30(9)**, 3109 (1965)

[94] L. A. Hull and I. C. H. J. Heicklen. *J. Am. Chem. Soc.* **94(14)**, 4856 (1972)

[95] C. K. Kohlmiller and L. Andrews. *J. Am. Chem. Soc.* **103(10)**, 2578 (1981)

[96] J. Z. Gillies, C. W. Gillies, R. D. Suenram and F. J. Lovas. *J. Am. Chem. Soc.* **110(24)**, 7991 (1988)

[97] V. Sablinskas, F. Hegelund, J. Ceponkus, R. Bariseviciute, V. Aleksa and B. Nelander. *J. Phys. Chem. A* **109(39)**, 8719 (2005)

[98] M. D. Hoops and B. S. Ault. *J. Am. Chem. Soc.* **131(8)**, 2853 (2009)

[99] J. M. Anglada, R. Crehuet and J. M. Bofill. *Chem. Eur. J.* **5(6)**, 1809 (1999)

[100] W.-T. Chan and I. P. Hamilton. *J. Chem. Phys.* **118**, 1688 (2003)

[101] M. F. A. Hendrickx and C. Vinckier. *J. Phys. Chem. A* **107(38)**, 7574 (2003)

[102] I. Ljubić and A. Sabljić. *J. Phys. Chem. A* **106(18)**, 4745 (2002)

[103] L. Golob. Ph.D. thesis, University of Southampton (1975)

[104] J. M. Dyke, L. Golob, N. Joonathan, A. Morris and M. Okuda. *J. Chem. Soc. Faraday Trans.* **20(2)**, 1828 (1974)

[105] R. J. McNeal and G. R. Cook. *J. Chem. Phys.* **45**, 3469 (1966)

[106] H. van Lonkhuyzen and C. A. de Lange. *J. Electron Spectrosc. Relat. Phenom.* **27**, 255 (1982)

[107] K. Becker, W. Grothand and U. Schurath. *Chem. Phys. Lett.* **8**, 259 (1971)

[108] G. Marston. *Chem. Soc. Rev.* **25**, 33 (1996)

[109] R. P. Wayne. *Research on Chemical Intermediates* **20(3-5)**, 395 (1994)

[110] M. A. A. Clyne and B. A. T. R. P. Wayne. *Nature* **199**, 1057 (1963)

[111] N. Jonathan, A. Morris, M. Okuda, K. J. Ross and D. J. Smith. *J. Chem. Soc., Faraday Trans. 2* **70**, 1810 (1974)

[112] B. J. Cocksey, J. H. D. Eland and C. J. Danby. *J. Chem. Soc. B* 790 (1971)

[113] R. A. J. J. Pitts and R. Steer. *J. Chem. Phys.* **52**, 1603 (1970)

[114] E. Grosjean, J. B. de Andrade and D. Grosjean. *Environ. Sci. Technol.* **30(3)**, 975 (1996)

[115] R. D. Ashford and E. A. Ogryzlo. *J. Am. Chem. Soc.* **97(13)**, 3604 (1975)